공학박사학위논문

SYNTHESIS AND APPLICATION OF ION IMPRINTED AND SELECTIVE ADSORBENTS FOR CONTAMINANT REMOVAL FROM AQUEOUS SOLUTIONS

수중 오염물질의 제거를 위한 이온 각인 및 선택적 흡착제의 합성 및 적용

2018 년 8 월

서울대학교 대학원

생태조경·지역시스템공학부

지역시스템공학전공

강 진 규

SYNTHESIS AND APPLICATION OF ION IMPRINTED AND SELECTIVE ADSORBENTS FOR CONTAMINANT REMOVAL FROM AQUEOUS SOLUTIONS

A DISSERTATION
SUBMITTED TO THE DEPARTMENT OF LANDSCAPE ARCHITECTURE AND RURAL SYSTEMS ENGINEERING
AND THE COMMITTEE ON GRADUATE STUDIES OF
SEOUL NATIONAL UNIVERSITY
IN PARTIAL FULFILLMENT OF THE REQUIREMENTS
FOR THE DEGREE OF

DOCTOR OF PHILOSOPHY

By
JIN-KYU KANG
AUGUST, 2018

SYNTHESIS AND APPLICATION OF ION IMPRINTED AND SELECTIVE ADSORBENTS FOR CONTAMINANT REMOVAL FROM AQUEOUS SOLUTIONS

수중오염물질의 제거를 위한 이온 각인 및
선택적 흡착제의 합성 및 적용

지도교수 김 성 배

이 논문을 공학박사 학위논문으로 제출함

2018 년 8 월

서울대학교 대학원
생태조경·지역시스템공학부 지역시스템공학전공

강 진 규

강진규의 공학박사 학위논문을 인준함

2018 년 8 월

위 원 장 이 인 복 (인)
부위원장 김 성 배 (인)
위 원 박 성 직 (인)
위 원 이 창 구 (인)
위 원 송 인 홍 (인)

I certify that I have read this dissertation and that in my opinion it is fully adequate, in scope and quality, as dissertation for the degree of Doctor of Philosophy.

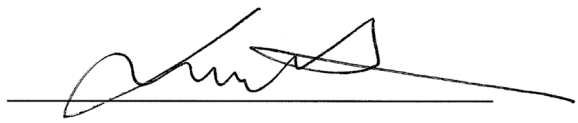

Chairman

I certify that I have read this dissertation and that in my opinion it is fully adequate, in scope and quality, as dissertation for the degree of Doctor of Philosophy.

Vice-Chairman

I certify that I have read this dissertation and that in my opinion it is fully adequate, in scope and quality, as dissertation for the degree of Doctor of Philosophy.

Seong-Jik Park

I certify that I have read this dissertation and that in my opinion it is fully adequate, in scope and quality, as dissertation for the degree of Doctor of Philosophy.

Changgu Lee

I certify that I have read this dissertation and that in my opinion it is fully adequate, in scope and quality, as dissertation for the degree of Doctor of Philosophy.

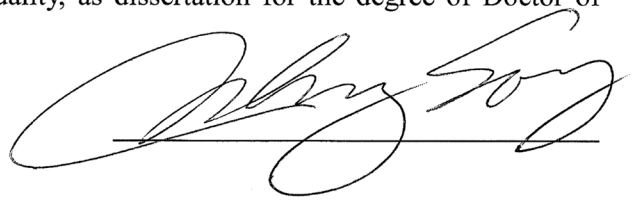

ABSTRACT

This dissertation deals with the synthetization, characterization, and evaluation of selective Cu(II) ion removal by Cu(II) imprinted mesoporous silica SBA-15 and Cu(II) imprinted silica gel, and selective nitrate removal by nitrate selectivity enhanced quaternary ammonium functionalized mesoporous silica SBA-15 and nitrate selectivity enhanced quaternary ammonium functionalized silica gel.

Surface-imprinted poly(ethyleneimine) (PEI) grafted mesoporous silica SBA-15 (Cu-imprinted PEI-SBA-15) was synthesized and characterized for selective Cu(II) sorption from aqueous solutions. To enhance Cu(II) selectivity of Cu-imprinted PEI-SBA-15, Cu(II) loading on PEI-SBA-15 was increased through Cu(II) sorption under high-molar-concentration ratios of chloride (Cl^-) and Cu(II) ions. Then, selective Cu(II) sorption sites were increased through imprinting processes (crosslinking and elution) on Cu-loaded PEI-SBA-15. Selectivity experiments were performed using Cu-imprinted PEI-SBA-15 prepared at various [Cl^-]/[Cu(II)] ratios, ranging from 2 to 1000. In multinary solutions containing divalent ions such as Cu(II), Pb(II), Zn(II),

Ni(II), and Co(II), Cu(II), selectivity was highest (79.62) at a $[Cl^-]/[Cu(II)]$ ratio of 500; the relative Cu(II) selectivity for Cu-imprinted PEI-SBA-15 over PEI-SBA-15 was 29.24. In multinary solutions containing Cu(II) and other trivalent and tetravalent ions such as Al(III), Cr(III), and Zr(IV), the Cu(II) selectivity was also highest (3.40) at a $[Cl^-]/[Cu(II)]$ ratio of 500; the relative Cu(II) selectivity was 3.96. In this study, it is demonstrated that the Cu(II) selectivity of surface-imprinted SBA-15 could be enhanced through its preparation under high $[Cl^-]/[Cu(II)]$ ratios.

Cu(II) surface-imprinted PEI coated silica gel (Cu-PEI-silica) was synthesized and characterized for selective Cu(II) sorption from aqueous solutions. To imprint Cu(II) on coated PEI, Cu(II) loading process was added into PEI-coated silica gel preparation processes. From the Cu(II) batch test, Cu-PEI-silica gel showed much higher Cu(II) sorption capacity (352.540 mg/g) than PEI-silica gel (30.727 mg/g). In multinary solutions containing divalent ions, such as Cu(II), Pb(II), Zn(II), Ni(II), and Co(II), the relative Cu(II) selectivity for Cu-PEI-silica gel over PEI-silica gel was 5.17. In multinary solutions containing Cu(II) along with trivalent and tetravalent ions, such as Al(III), Cr(III), and Zr(IV), the

relative Cu(II) selectivity was 3.06. In this study, it is demonstrated that the Cu(II) selectivity and Cu(II) sorption capacity were enhanced via Cu(II) surface imprinting process.

Quaternary ammonium functionalized mesoporous silica SBA-15 with various length of alkyl chain were synthesized and characterized for selective nitrate sorption from aqueous solutions. The results of nitrate batch test indicate that the quaternary ammonium functionalized SBA-15 which contain the longer alkyl chain length have the slower sorption kinetics. On the other hand, nitrate sorption capacity was not related to alkyl chain length. From the result of competing anion effect tests, it was observed that the adsorbents with longer alkyl chain removed nitrate more selectively against other competing anions than the adsorbents with shorter alkyl chain. Nitrate has highest hydration energy among all other competing anions. In addition, longer alkyl chain quaternary ammonium functionalized silica gel has less hydrated environment Among various competing anions. Therefore, nitrate can be removed more selectively by adsorbents with longer alkyl chain. It was observed that phosphate had the greatest effect on nitrate removal of the adsorbents, whereas chloride had the least. In this study, various quaternary ammonium functionalized

mesoporous silica were prepared well and the effect of alkyl chain length on nitrate selectivity via competing anion tests was demonstrated.

Quaternary ammonium functionalized silica gel with dimethyloctyl alkyl chain (C8Q-silica gel) and dimehtyldodecyl alkyl chain (C12Q-slica gel) were synthesized and characterized for selective nitrate sorption from aqueous solutions. From the nitrate batch test and column tests, C12Q-slica gel was chosen as a more proper adsorbent for selective nitrate removal. From the column experiments, the effect of initial nitrate concentration, flow rate, bed depth were examined. As a results, Bohart-Adams and bed depth service time models are considered as proper models to explain and estimate the nitrate removal in flow through conditions. From the artificial groundwater flow through tests, C12Q-silica gel removed nitrate selectively even in bicarbonate-added conditions. After the 2 times of regeneration of C12Q silica gel, the breakthrough curves from the column experiments was mostly overlapped with previous curves. In this study, quaternary ammonium functionalized silica gel were prepared well and its characteristics in flow through conditions were examined.

From the results, selectivity enhanced adsorbents were prepared and its selective removal characteristics were examined. Furthermore, applicability of the selective adsorbents were confirmed in water treatment. It is considered that results from this study are contributable for selectivity enhanced water treatment process.

Keywords: Selective adsorbent, Ion imprinting, Surface ion imprinting, Quaternary ammonium functionalized, Alkyl chain length, Selective removal, Copper, Nitrate

***Student Number*: 2013-30343**

CONTENTS

List of Tables

List of Figures

Chapter 1 Introduction

1.1 Background

Water is the most important molecule for life on earth. Pure and uncontaminated water is the basic requirement for all living organisms. However, water contamination threats have been increasing from industries, agricultural activities, municipal wastewater, and environmental changes (Singh et al., 2018). Therefore, water treatment is essential and continuously required technology to supply clean water.

Techniques for water treatment have been advanced from boiling, filtration, straining, and coagulation to precipitation, incineration, flocculation, ion exchange, reverse osmosis, membrane filtration, electrochemical reduction/oxidation, electrodeionization, photo electrochemistry, advanced oxidation processes, and biological methods. But, those methods have several drawbacks like low removal efficiency, high production of sewage sludge, non-cost-and-energy efficiency, generation of toxic by-products which requires an additional treatment (Raval et al., 2016; Singh et al., 2018). Among the various physico chemical processes, adsorption has advantages such as flexibility in term of operation, feasibility in term of production of high quality product, economically viability in the context of initial capital cost and chemicals requirement as well as effectiveness in term of treating pollutants at low concentrations (Raval et al., 2016). In the aqueous phase, adsorption is a

process that occurs when a liquid solute accumulate on the surface of a solid (adsorbent), forming a molecular or atomic film (adsorbate) (Singh et al., 2018). Therefore, application of adsorption usually means application of adsorbent in water treatment. However, main mechanism for the contaminants uptake on adsorbents have been expanded from adsorption to ion exchange, ligand exchange, partition, surface precipitation, structural incorporation for extension of adsorbents' applicability. The introduction of those mechanisms on adsorbent enhanced applicability and effectiveness on removal of various contaminants in aqueous solutions. One or more mechanisms can be applied to prepare advanced adsorbents than typical adsorbents. Meaning of 'advanced' is sorption capacity increased or removable contaminants broadened or selective removable. Sorption capacity increased or removable contaminants broadened adsorbents may be removable almost contaminants in aqueous solutions. However, from the characteristics of contaminants, there has removal selectivity between similar contaminants. From that removal selectivity, sorption capacity increased or removable contaminants broadened adsorbents hard to remove selectivity low contaminants. Therefore, selective removability enhancement has been increased and it applied material called as selective adsorbent. To prepare selective adsorbents, imprinting technology commonly used.

Imprinting technology started from molecular-imprinting technology (MIT). MIT for preparing polymeric materials is capable of high molecular recognition (SenGupta, 1995; Jiang et al., 2006). As a MIT, Molecular imprinted polymers are synthesized by polymerization of functional monomers in the presence of template and excess of cross-linker. The imprinted molecule is leached out after polymerization and leaved the memory of the analyte as Fig.1.1. (a) (Zhang et al., 2007).

Ion-imprinting technology (IIT) is an advanced technology to selectively recognize target ions in place of molecule in aqueous media using ion-imprinted materials (Vatanpour et al., 2011; Fu et al., 2015). Polymerization imprinting techniques have been used to prepare ion-imprinted polymers via polymerization of functional monomers around template ions. After polymerization, the template ions are extracted from a polymer matrix through an elution process to generate binding cavities for target ions as Fig.1.1 (b) (Rao et al., 2006; Shakerian et al., 2016). However, ion-imprinted polymers have several drawbacks, including incomplete removal of template ions, formation of diffusion barriers, low binding capacity, slow mass transfer, and slow binding kinetics (Branger et al., 2013).

Surface imprinting technology (SIT) have been advanced to overcome these problems. During the preparation of ion-imprinted materials, binding cavities

are formed on or near the surface of a support matrix through an imprinting process as Fig.1.1. (c) (Branger et al., 2013; Fu et al., 2015). In SIT, silica particles are preferred as a support matrix due to their physico-chemical stability, thermal resistance, and high reusability (Fang et al., 2005; Guo et al., 2013). Organic functionalities, such as organosilanes and polyamines, are grafted on the silica particles to synthesize ion-imprinted materials (Markowitz et al., 2001; Jiang et al., 2006; Guo et al., 2009; Fan et al., 2014b).

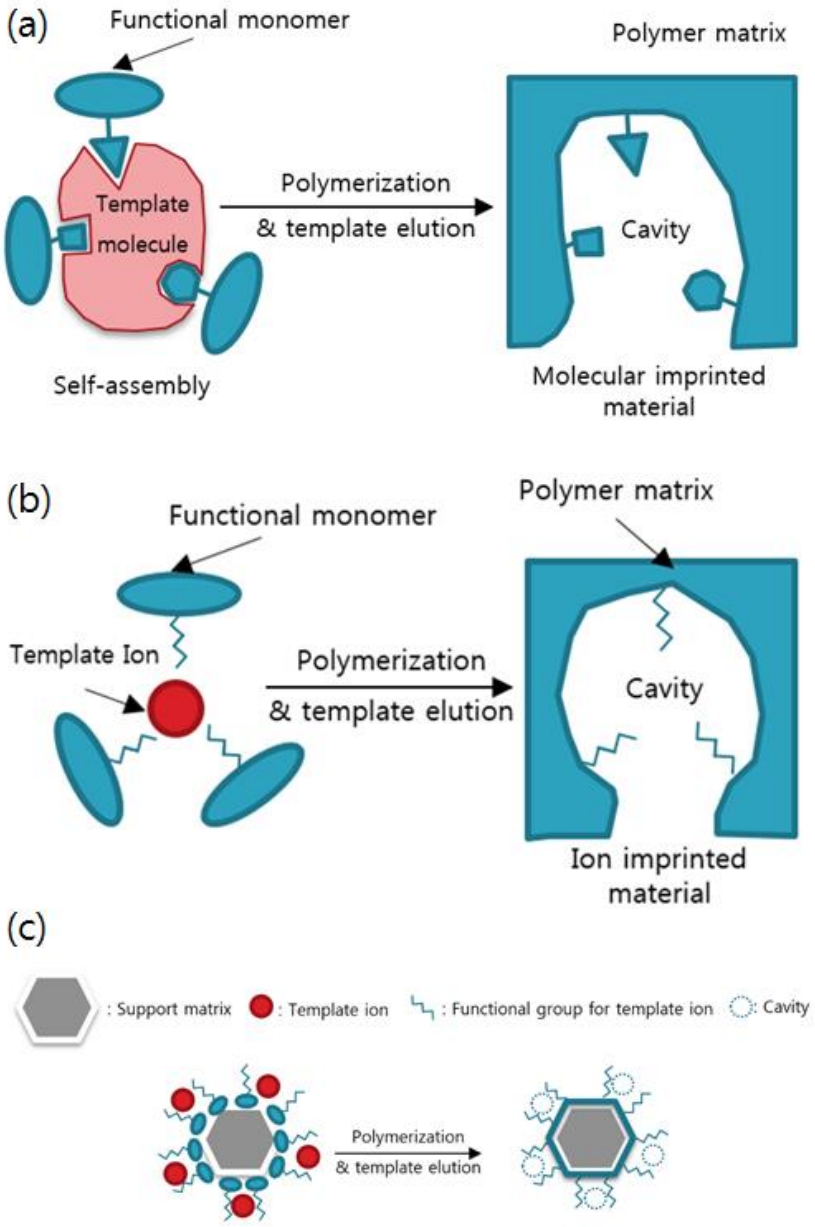

Figure 1.1. Preparation of imprinted material; (a) Molecular imprinted, (b) Ion imprinted, (c) surface ion imprinted

Not only imprinting technology, but also alkyl chain length intention is used for selective removal of specific ions. Alkyl chain length intention mostly used on quaternary ammonium functionalized material for nitrate removal from nitrate's low selectivity over other anions. It is known that alkyl chain length highly effective on nitrate selectivity over other anions like HCO_3^-, Cl^-, PO_4^{3-}, SO_4^{2-} (SenGupta, 1995). To remove nitrate in aqueous conditions, type1 strong base resins are mostly commercialized material (Fig. 1.4). Commonly used strong base resins for nitrate removal are quaternary ammonium functionalized polymer forms of styrene containing some divinyl benzene like Ionac SR6, Purolite A-520E, Amberlite IRA 400, and Indion NSSR resin as Fig.1.4 (SenGupta, 1995; Chabani et al., 2006; Milmile et al., 2011).

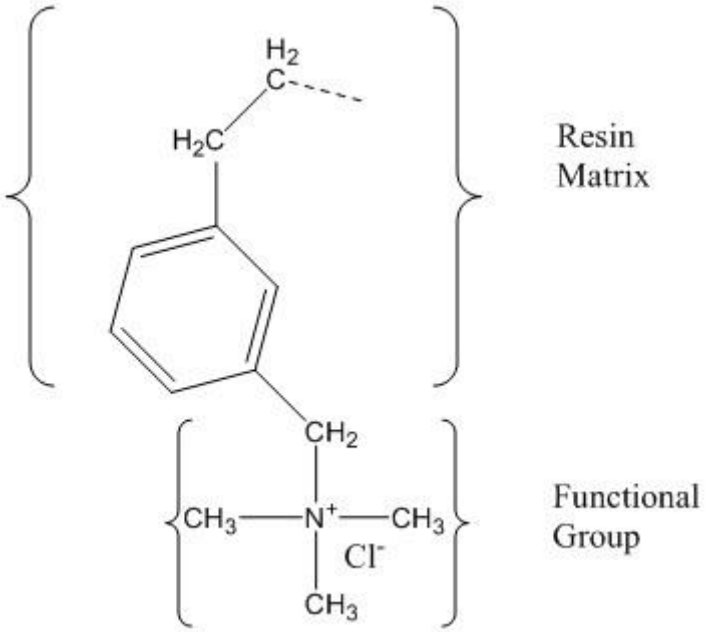

Figure 1.2. Type1 SB resin (commonly used form for nitrate removal, (SenGupta, 1995))

In this dissertation, SIT based Copper (Cu(II)) ion imprinting were performed. Because, Cu(II) is an indispensable trace element for life and plays an important role in various biological processes. It serves as a catalytic cofactor for a variety of metalloenzymes (Xu et al., 2018). Cu(II) is also used widely in industries, such as mining, paint manufacturing, electroplating, steel production, electronics, and finishing processing. Copper-containing industrial wastewater is discharged primarily as a form of cupric ion (Cu^{2+}) into water environments, causing serious environmental and health problems. High Cu(II) concentration in soils causes delay in flowering and fruiting and low seed set. It is also toxic to fish life even at low concentration (Faghihian and Asghari, 2013).Cu(II) is known as harmful to organs such as kidneys and livers, and carcinogenic heavy metal ion (Agrawal et al., 2009; Monier et al., 2015). The maximum allowable level of copper in drinking water has set to 1.3 mg/L by World Health Organization (WHO) and The United States Environmental Protection Agency (EPA) (Monier et al., 2015; Xu et al., 2018). These days, Cu(II) ions are mostly removed by using membrane, chemical precipitation, ion exchange, neutralization, filtration and adsorption. Among these methods, adsorption is an eye-catching and promising technology for Cu(II) ion removal due to its high efficiency and selectivity, and low cost (Liu et al., 2016). From the pros of adsorption, SIT applied adsorbent is considered as proper material for Cu(II) selective removal in aqueous conditions.

Alkyl chain intention for selective removal of nitrate also performed. Because, as mention above, nitrate has low selectivity but also has high effectivity on environment. Nitrate is a major nutrient for plant growth and nitrogenous fertilizers applied to agricultural lands over the worldwide (Loganathan et al., 2014). From the excessive usage and disposal of agricultural fertilizers, septic tank systems, and animal waste disposal, chance for nitrate introduction into the surface water and ground water has been increasing (Milmile et al., 2011; Mazarji et al., 2017). Nitrate is a main factor of the eutrophication of water body and eutrophication stimulates the growth of algae and aquatic plants which can endanger fish and other aquatic life and water quality (Loganathan et al., 2014). In addition, excessive nitrate contained drinking water can cause severe methamoglobinemia ‘blue baby’ syndrome in infants (Milmile et al., 2011; Hamoudi and Belkacemi, 2013) and stomach cancer in adults (Chiu et al., 2007). From those reasons, World Health Organisation limits the recommended maximum concentration for nitrate in drinking water as 50 mg/L (Kilpimaa et al., 2015).

1.2 Objectives

This dissertation deals with the synthetization, characterization, and evaluation of Cu(II) imprinted materials and nitrate selectivity enhanced quaternary ammonium functionalized materials.

In chapter 3, Selectivity enhancement of ion imprinted material were performed via target ion loading increasing method.

In chapter 4, simplified method developed for synthesis of surface ion imprinted adsorbent to overcome low productivity of imprinted material.

In chapter 5, alkyl chain length intended quaternary ammonium functionalized adsorbents synthesized for selective nitrate removal.

In chapter 6, Applicability enhanced quaternary ammonium functionalized adsorbents were synthesized and characterized for selective nitrate removal.

Overall flow of this dissertation are presented in Fig. 1.3.

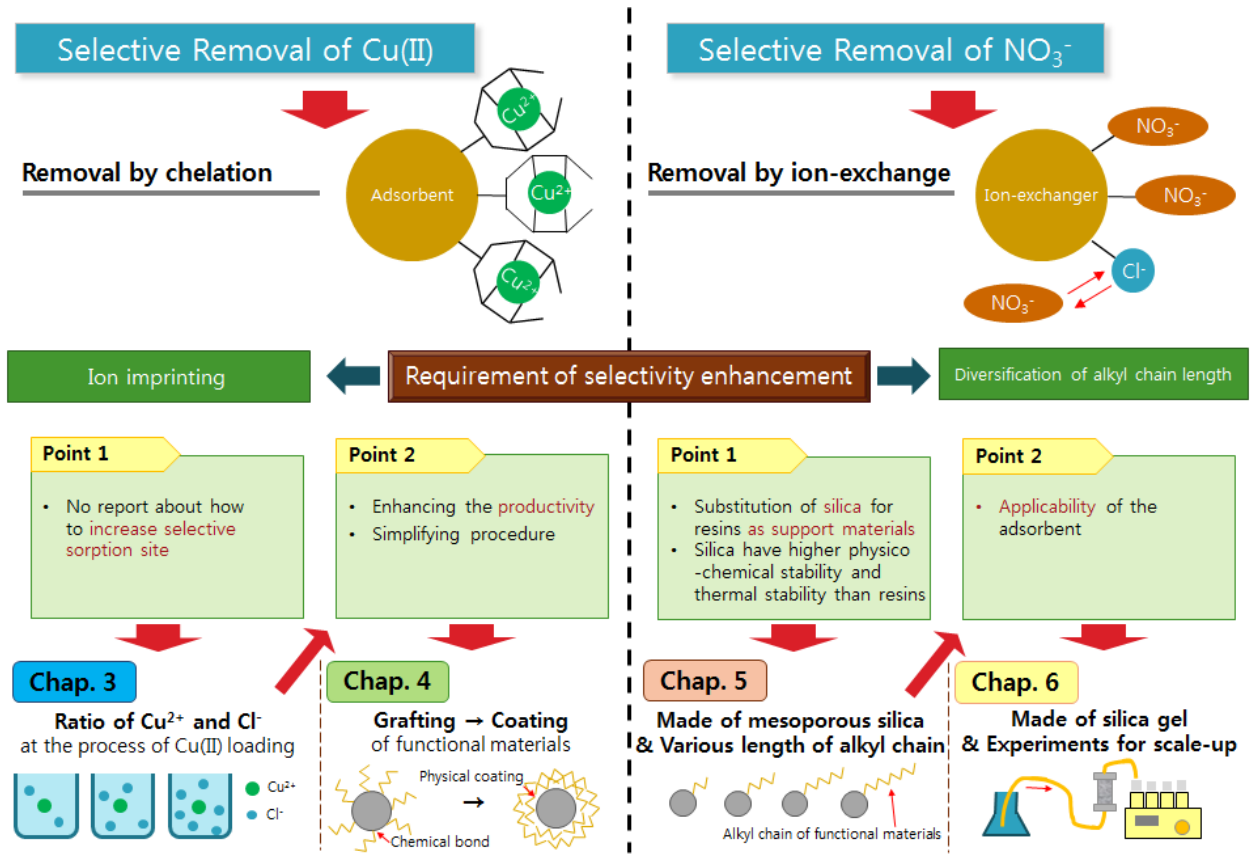

Figure 1.3. Schematic flow and relationships between all chapters

Chapter 2 Literature Review

2.1 Surface ion imprinting

Many researchers have investigated various way for surface ion imprinting on various support materials. Surface ion imprinting can be classified into 3 categories; surface ion imprinting through functionalization, surface ion imprinting through polymerization, and surface ion imprinting through polymer grafting (Fig. 2.1).

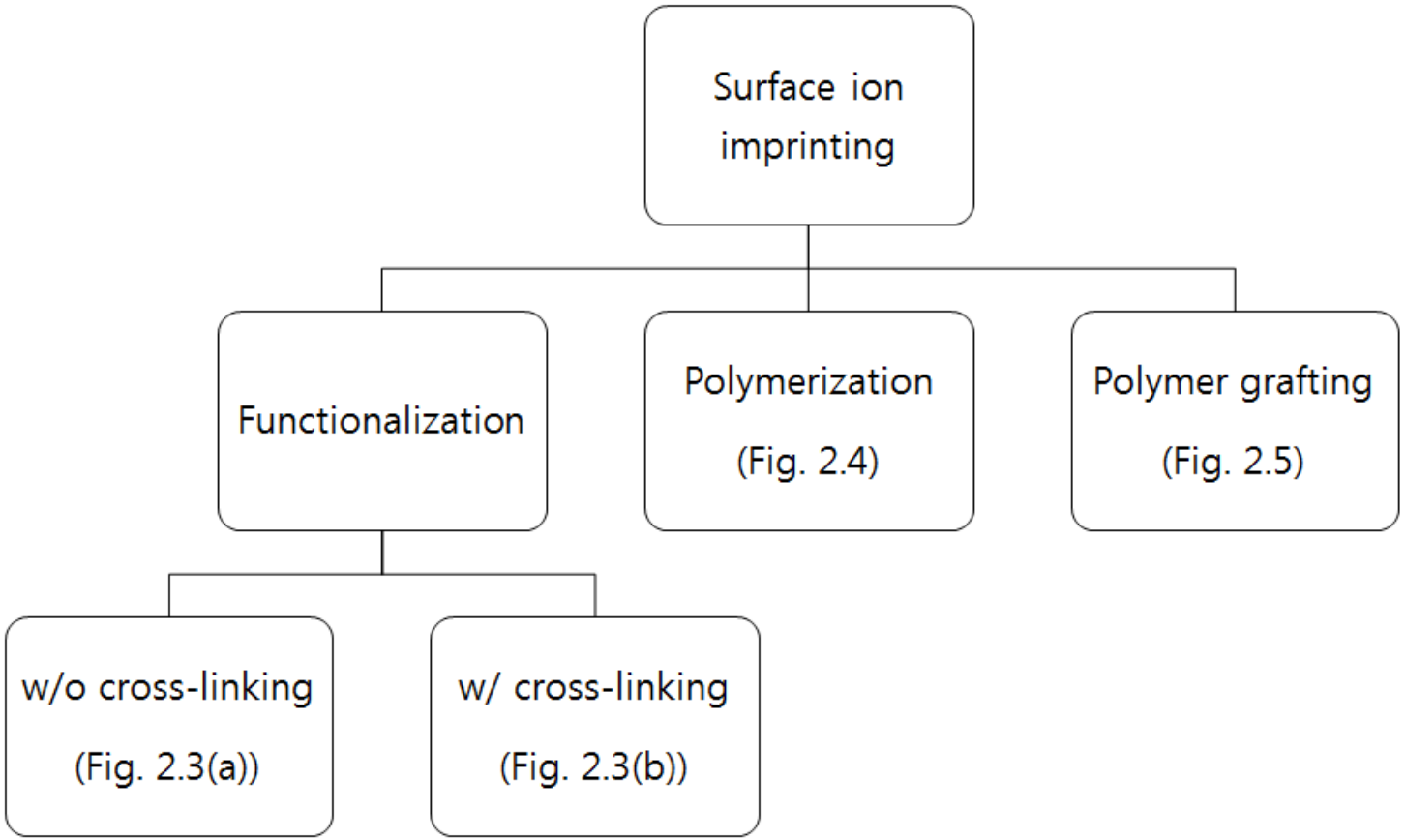

Figure 2.1. Categories of surface ion imprinting methods

Fig. 2.3 and Table 2.1-2 represented researches about surface ion imprinting through functionalization to selectively remove heavy metals. Silica gel or mesoporous silica is mostly preferred support material from its characteristics as mentioned in 1.1. In addition, silane coupling agents are mostly used functional monomers for surface ion imprinting through functionalization from its ease to functionalize silica surface with various functionalities. The general structure of silane coupling agents can be represented as Fig. 2.2. The X represents the hydrolyzable groups that are typically chloro, ethoxy, or methoxy groups. The organofunctional group, R, can have a variety of functionalities (Blum, 2016).

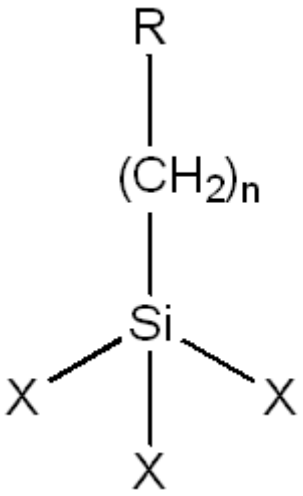

Figure 2.2. Structure of silane coupling agents

Surface ion imprinting through functionalization is performed as following procedures. Firstly, prepare proper support material; when support material is silica gel, activation is required. After that, load (complex) template metal ion (object metal ion) on functional monomers (mostly, silane coupling agents). Then, Graft template metal ion loaded functional monomers on support material surface. Case, cross-link between functional monomer to fix template metal ion loaded sites. However, many researches did not performed cross-linking procedure (Table 2.1). Because, functional monomers (silane coupling agents) are grafted not only with surfaces of support material, but also with near functional monomers (Ren et al., 2014). Therefore, grafted functional monomers with template ion may have selective cavities. But there has also some case performed cross-link between functional monomer (Table 2.2). Then, elute template ion by using acid solution or chelate agent solution (some researchers used basic solution). Template eluted sites (cavity) are required to be neutralized for sorption of template ion by complex. Therefore, neutralization is also performed. After neutralization, surface ion imprinted material is prepared.

Fig. 2.4 and Table 2.3 represented researches about surface ion imprinting through polymerization to selectively remove heavy metals. In this method, silica gel or mesoporous silica are also preferred as support material. Polymer

grafting method is similar with MIT. In the preparation of MIT, Ethylene glycol dimethacrylate (EGDMA) and Trimethylolpropane Trimethacrylate (TRIM) are the most commonly employed cross-linker (Vasapollo et al., 2011). In the preparation of SIT through polymer grafting, EGDMA is mostly used cross-linker (Table 2.3-4). Meaning of cross-linker is different from cross-linker at SIT through functionalization. Cross-linker acts as a monomer for polymer matrix in SIT through polymer grafting. Unlike this, cross-linker added to fix the template loaded sites for selective cavity in SIT through functionalization. In this thesis, 'cross-linker' is replaced with 'matrix monomer' in SIT through polymer grafting. To polymerize EGDMA matrix monomer, initiator is required. azo N-N'-bis isobutyronitrile (AIBN) is mostly used initiator (Vasapollo et al., 2011). To load (complex) template metal ion in matrix, proper functional group have be immobilized in polymer matrix. In the MIT and SIT through polymer grafting, immobilized functional group is called functional monomer.

From those elements, surface ion imprinting through polymerization is performed as following procedures. Firstly, prepare proper support material. After that, load (complex) template metal ion (object metal ion) on monomer. Then, immobilize template metal ion loaded monomer on matrix monomer. After that, polymerize template metal ion loaded monomer loaded matrix

monomer with initiator on support material. Then, elute template ion and neutralized template-eluted resultant. After neutralization, surface ion imprinted material is prepared.

Fig. 2.5 and Table 2.4 represented researches about surface ion imprinting through polymer grafting to selective remove heavy metals. This method is simplest method among SITs. Surface ion imprinting through polymer grafting is performed as following procedures. Firstly, prepare proper support material. Then, graft polymer on support material. After that, load (complex) template metal ion (object metal ion) into polymer on support material. Then, cross-link polymer to fix template metal ion loaded sites. In this method, cross-linking procedure is essential. Then, elute template ion and neutralized template-eluted resultant. After neutralization, surface ion imprinted material is prepared.

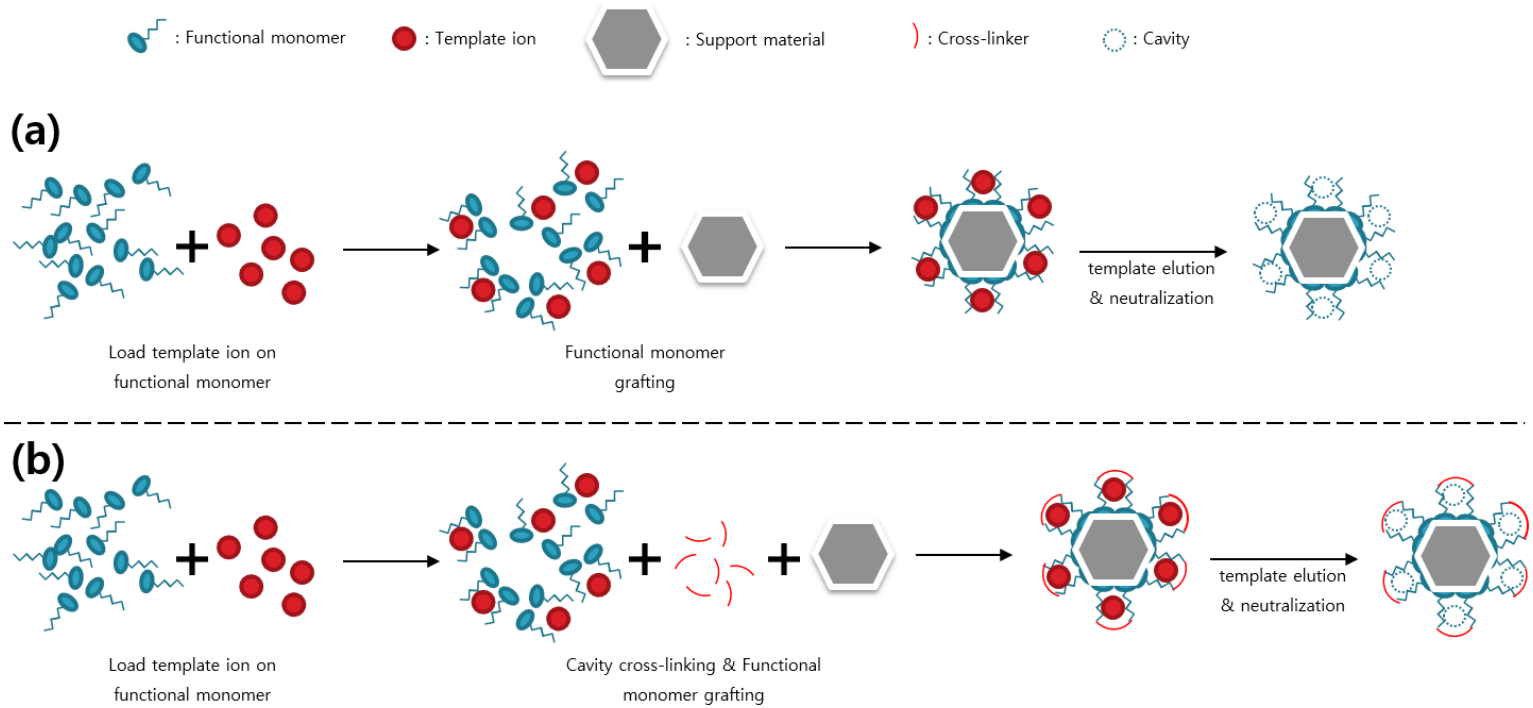

Figure 2.3. Procedure of surface ion imprinting through functionalization on support material; (a) without cross-linking, (b) with cross-linking

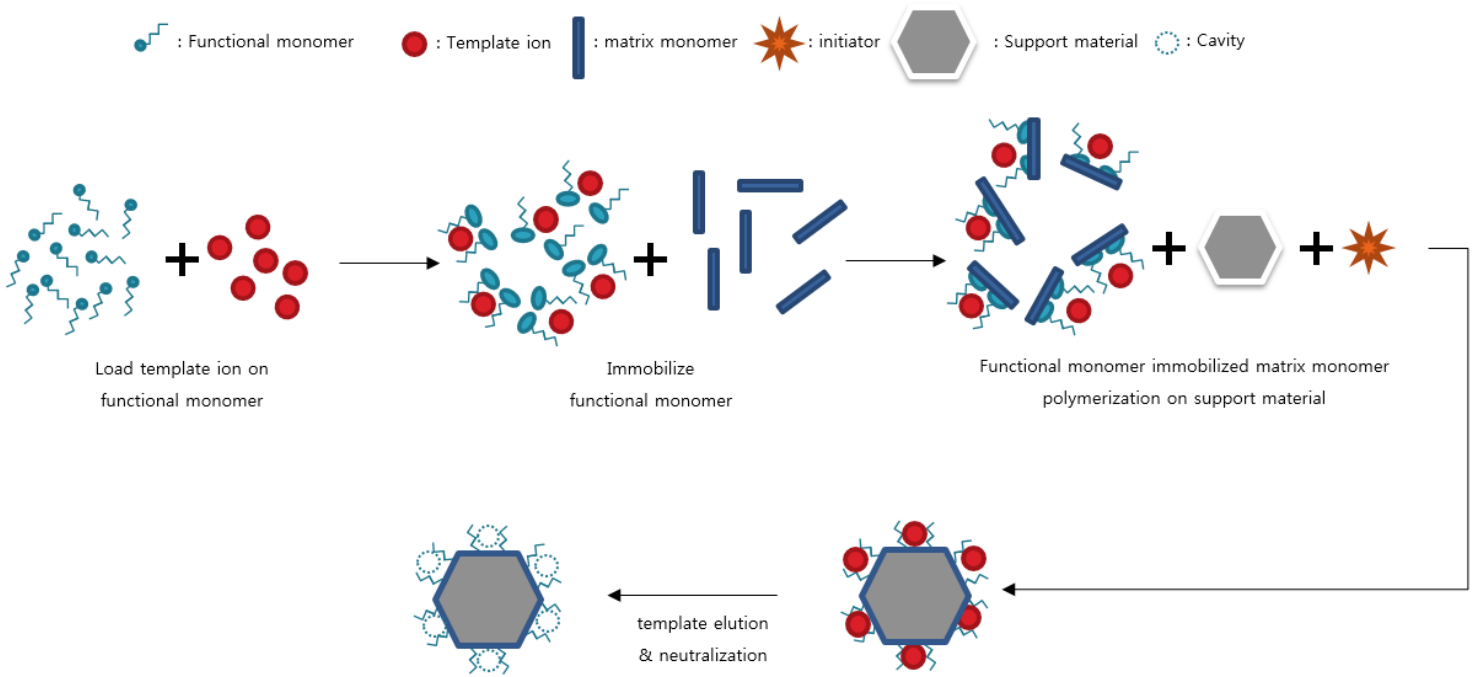

Figure 2.4. Procedure of surface ion imprinting through polymerization on support material

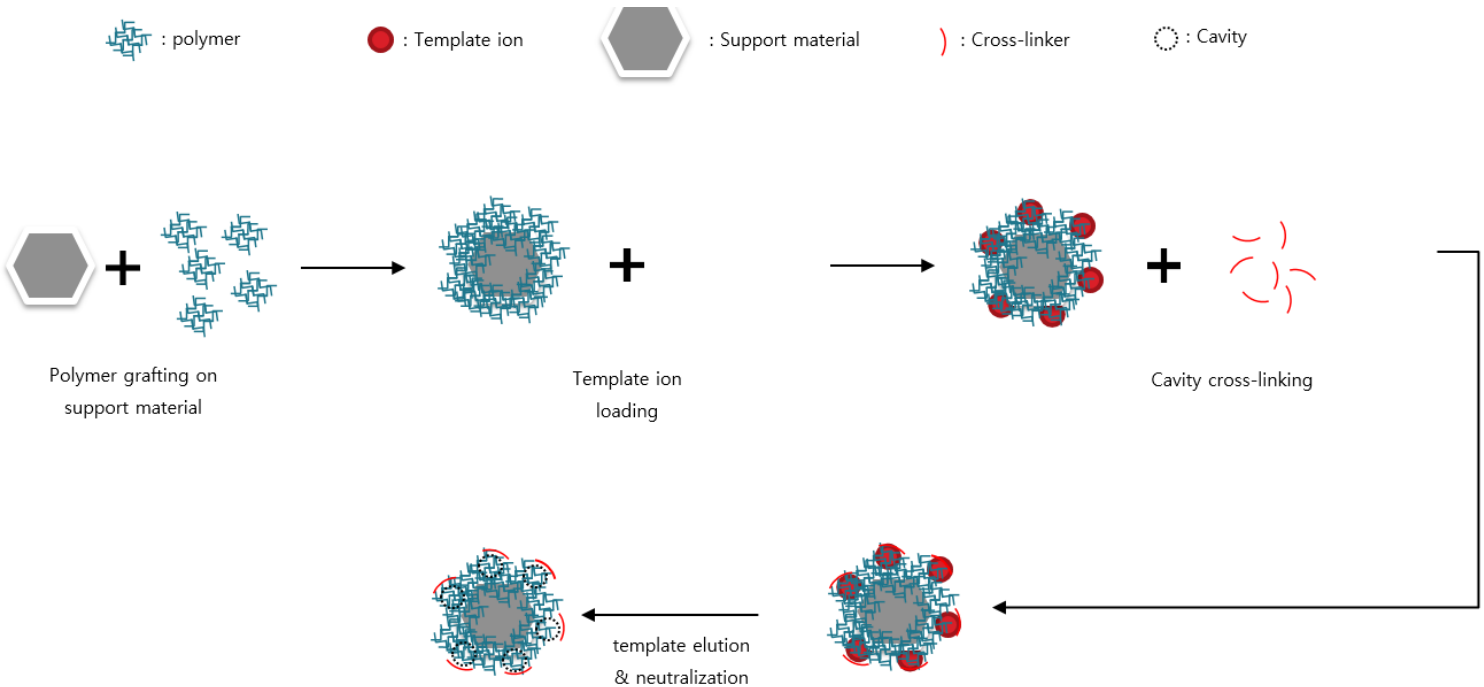

Figure 2.5. Procedure of surface ion imprinting through polymer grafting to support material

Table 2.1. Previous studies for surface ion imprinting through functionalization on support material without cross-linking

Author	Title	Target ion	Abstract
He et al. (2018)	Design and fabrication of highly ordered ion imprinted SBA-15 and MCM-41 mesoporous organosilicas for efficient removal of Ni2+ from different properties of wastewaters	Ni(II)	Ni complexed Iminodiacetic acid immobilized (3-Glycidyloxypropyl)trimethoxysilane or Ni complexed 3-(γ-aminoethylamino)-propyltrimethoxysilane were grafted on mesoporous silica. After that, Ni(II) elution and neutralization were performed to prepare Ni(II) imprinted mesoporous silica. Ni(II) selectivity were calculated as 43.1, 12.4, 46.4, 22.6, and 34.7 or 36.9, 34.4, 18.8, 28.1, and 26.9 over Ca(II), Mg(II), Cu(II), Zn(II), and Fe(III) from binary solution
Cui et al. (2017)	Novel Pb(II) ion-imprinted materials based on bis-pyrazolyl functionalized mesoporous silica for the selective removal of Pb(II) in water samples	Pb(II)	Pb(II) complexed 4-(di (1H-pyrazol-1-yl) methyl) phenol were immobilized on 3-(triethoxysilyl)-propyl-isocyanate grafted mesoporous silica. After that, Pb(II) elution and neutralization were performed to prepare Cu(II) imprinted mesoporous silica. Pb(II) selectivity were calculated as 132.68, 38.76, 63.13, 44.77, 576.61, 63.07, and 104.25 over Cd(II), Co(II), Cu(II), Hg(II), Mg(II), Mn(II), and Zn(II) from multinary solution
Song et al. (2017)	Effective and selective adsorption of As(III) via imprinted magnetic Fe3O4/HTCC composite nanoparticles	As(III)	Ar(III) complexed glycidyl trimethyl ammonium chloride modified chitosan was cross-linked with formaldehyde and grafted on Fe_3O_4. From competing ions test, As(III) imprinted material showed slightly higher As(III) removal rate than non-imprinted material
Ren et al. (2014)	Preparation of zirconium oxy ion-imprinted particle for the selective separation of trace zirconium ion from water	Zr(IV)	Zr(IV) complexed 3-aminopropyltriethoxysilane were grafted on synthesized silica with tetraethyl orthosilicate (TEOS). After that, Zr(IV) elution and neutralization were performed to prepare Zr(IV) imprinted silica. Zr(IV) selective removal test over Pb(II) were performed.
Fan et al. (2014a)	Selective adsorption of antimony(III) from aqueous solution by ion-imprinted organic–inorganic hybrid sorbent: Kinetics, isotherms and thermodynamics	Sb(III)	Sb(III) complexed γ-chloropropyltrimethoxysilane was grafted on silicate TEOS. Sb(III) elution and neutralization were performed to prepare Sb(III) imprinted silica. Sb(III) selectivity were calculated as 28.89, 34.80, and 30.59 over Zn(II), Ni(II), and Fe(II), from multinary solution
Fan et al. (2014a)	Selective removal of antimony(III) from aqueous solution using antimony(III)-imprinted organic–inorganic hybrid sorbents by	Sb(III)	Sb(III) complexed 3-Iodopropyltrimethoxysilane were grafted on silica. Sb(III) elution and neutralization were performed to prepare Sb(III) imprinted silica. From

	combination of surface imprinting technique with sol–gel process		the batch test, relative Sb(III) selectivity were calculated as 13.2, 10.4, and 11.8 over Cr(III), Fe(III), and As(III), from binary solution
Guo et al. (2014)	Magnetic ion-imprinted and –SH functionalized polymer for selectiveremoval of Pb(II) from aqueous samples	Pb(II)	Silica were coated on Fe_3O_4 using tetraethyl orthosilicate (Fe_3O_4@SiO_2). Pb (II) complexed 3-mercaptopropyltrimethoxysilane were grafted on Fe_3O_4@SiO_2. After that, Pb(II) elution and neutralization were performed to prepare Pb(II) imprinted Fe_3O_4@SiO_2. From the batch test, relative Pb(II) selectivity were calculated as 2.25, 1.72 and 1.97 over Cu(II), Zn(II), and Co(II), from binary solution
Meng et al. (2014)	An ion-imprinted functionalized SBA-15 adsorbent synthesized bysurface imprinting technique via reversible addition–fragmentationchain transfer polymerization for selective removal of Ce(III) fromaqueous solution	Ce(III)	Ce(III) ion imprinted SBA-15 was prepared by surface imprinting technique with reversible addition-fragmentation chain transfer polymerization. Ce(III) selectivity were calculated as 5.64, 3.40, 14.44, 8.54, 11.81 and 6.11 over Co(II), Pb(II), Sr(II), Cu(II), Ca(II), and Fe(III)
Ren et al. (2013)	Selective recognition of molybdenum(VI) from water by Mo(VI) oxy ion-imprinted particle as an adsorbent	Mo(VI)	Amino-silica were prepared using 3-aminopropyltriethoxysilane and nano-silica. Mo(VI) complexed isonicotinic acid were grafted on amino-silica. Mo(VI) elution was performed to prepare Mo(VI) imprinted silica. Mo(VI) imprinted silica shows more Mo(VI) selective sorption characteristics than Mo(VI) non imprinted silica.
Zhang and Hu (2012)	Cadmium (II) imprinted 3-mercaptopropyltrimethoxysilane coated stir bar for selective extraction of trace cadmium from environmental water samples followed by inductively coupled plasma mass spectrometry detection	Cd(II)	Tetramethoxysilane were coated on magnetic bar. After that, Cd(II) complexed 3-mercaptopropyltrimethoxysilane were grafted on tetramethoxysilane were coated on magnetic bar.
Fan et al. (2012a)	Selective Removal of Arsenic(V) from Aqueous Solution Using A Surface-Ion-Imprinted Amine-Functionalized Silica Gel Sorbent	As(V)	As(V) complexed 3-(2-Aminoethylamino)propyltrimethoxysilane was grafted on activated silica gel. AS(V) elution and neutralization were performed to prepare As(V) imprinted silica gel. From the batch test, relative As(V) selectivity were calculated as 4.13, 4.33, 4.18, 4.02, and 5.67 over Cu(II), Pb(II), Cd(II), NI(II), and P(V), from binary solution
Li et al. (2011a)	Application of imprinted functionalized silica gel sorbent for selective removal of cadmium (II) from industial wastewaters	Cd(II)	Cd(II) complexed 3-Mercaptopropyltrimethoxysilane were grafted on activated silica gel. After that, Cd(II) elution and neutralization were performed to prepare Cd(II) imprinted silica gel. From the batch test, relative Cd(II) selectivity were calculated as 27.35, 18.46, 5.91 and 4.08 over Co(II), Ni(II), Zn(II), and Cu(II), from binary solution

Zheng et al. (2011)	Highly selective determination of rhodium(III) using silica gel surface-imprinted solid-phase extraction	Rh(III)	Rh(III) complexed 3-aminopropyltrimethoxysilane were grafted on activated silica gel. After that, Rh(III) elution and neutralization were performed to prepare Rh(III) imprinted silica gel. From the batch test, relative Rh(III) selectivity were calculated as 26.7, 39.0, 29.2 28.1, and 43.7 over Ru(III), Au(III), Pt(IV), Ir(IV), and Pd(II), from multinary solution
Luo et al. (2011)	Novel Cu (II) magnetic ion imprinted materials prepared by surface imprinted technique combined with a sol–gel process	Cu(II)	Cu(II) complexed 3-aminopropyltriethoxysilane was grafted on SiO_2 coated Fe_3O_4. Cu(II) elution and neutralization were performed to prepare Cu(II) imprinted SiO_2 coated Fe_3O_4. Cu(II) selectivity were calculated as 29.16 and 38.15 over Zn(II) and Ni(II)
Liu et al. (2011b)	Selective adsorption behavior of Pb(II) by mesoporous silica SBA-15-supported Pb(II)-imprinted polymer based on surface molecularly imprinting technique	Pb(II)	Pb(II) complexed chitosan were grafted on SBA-15 by using KH-560. Pb(II) elution and neutralization were performed to prepare Pb(II) imprinted SBA-15. From the batch test, relative Pb(II) selectivity were calculated as 12.67, 422.56, 13.88, 12.30, 17.02, 36.56, and 20.63 over Cr(III), Co(II), Cu(II), Hg(II), Mg(II), Ni(II), and Zn(II), from multinary solution
Wu et al. (2010)	Synthesis of ion-imprinted mesoporous silica gel sorbent for selective adsorption of copper ions in aqueous media	Cu(II)	Cu(II) complexed pyridine-2-carboxaldehyde were immobilized on N-[3-(trimethoxy-silyl)propyl]ethylenediamine grafted silica gel. After that, Cu(II) elution and neutralization were performed to prepare Cu(II) imprinted silica gel. Cu(II) selectivity were calculated as 12.3 and 17.7 over Zn(II) and Cd(II) from binary solution
Li et al. (2009)	An ion-imprinted polymer supported by attapulgite with a chitosan incorporated sol–gel process for selective separation of Ce(III)	Ce(III)	Ce(III) complexed chitosan were grafted on attapulgite by using KH-560. Ce(III) elution and neutralization were performed to prepare Ce(III) imprinted attapulgite. From the batch test, relative Ce(III) selectivity were calculated as 3.23, 6.60, 3.53, 5.12, 5.51, 8.73, 1.98, and 6.50 over Fe(III), Cd(II), Cs(I), Cu(II), Ni(II), Pb(II), Sr(II), and Zn(II), from multinary solution
Guo et al. (2009)	On-line Selective Solid-Phase Extraction of Copper with a Surface Ion Imprinted Silica Gel Sorbent	Cu(II)	Chloropropyl functionalized silica gel was prepared by γ-chloropropyltrimethoxysilane and activated silica gel. Cu(II) complexed diethylenetriamine were grafted on chloropropyl functionalized silica gel. Rh(III) elution and neutralization were performed to prepare Cu(II) imprinted silica gel. Cu(II) selectivity were calculated as 28.89, 34.80, and 30.59 over Zn(II), Ni(II), and Fe(II), from multinary solution
Wang et al. (2009)	Ion-imprinted thiol-functionalized silica gel sorbent for selective separation of mercury ions	Hg(II)	Hg(II) complexed 3-Mercaptopropyltrimethoxysilane were grafted on activated silica gel. After that, Cd(II) elution and neutralization were performed to prepare Hg(II) imprinted silica gel. From the batch test, relative Hg(II) selectivity were calculated as 982 over Cd(II) from binary solution

Zhu et al. (2009)	Selective solid-phase extraction of lead(II) from biological and natural water samples using surface-grafted lead(II)-imprinted polymers	Pb(II)	Pb(II) complexed 3-aminopropyltriethoxysilane were grafted on activated silica gel. After that, Pb(II) elution and neutralization were performed to prepare Pb(II) imprinted silica gel. Pb(II) selectivity were calculated as 450 over Cd(II) from binary solution
Dey et al. (2009)	Removal of Toxic/Heavy Metal Ions Using Ion-Imprinted Aminofunctionalized Silica Gel	Fe(III), Cr(III)	Fe(III) or Cr(III) complexed 3-aminopropyltriethoxysilane were grafted on activated silica gel. After that, Fe(III) or Cr(III) elution and neutralization were performed to prepare Fe(III) or Cr(III) imprinted silica gel.
He et al. (2008)	Determination of chromium(III) and total chromium in natural waters using a surface ion-imprinted silica gel as selective adsorbent	Cr(III)	Cr(III) complexed 3-aminopropyltrimethoxysilane were grafted on activated silica gel with tetraethyl orthosilicate (TEOS). After that, Cr(III) elution and neutralization were performed to prepare Cr(III) imprinted silica gel. From the batch test, relative Cr(III) selectivity were calculated as 377, 21.4, 15.4, 27.7, 26.4, and 31.9 over Co(II), Au(III), Ni(II), Cu(II), Zn(II), and Cr(VI), from binary solution. Furthermore, the usability for Cr(III) determination and speciation were performed.
Chang et al. (2008)	Silica gel surface-imprinted solid-phase extraction of Zr(IV) from aqueous solutions	Zr(IV)	Zr(IV) complexed 3-aminopropyltriethoxysilane were grafted on activated silica gel. After that, Zr(IV) elution and neutralization were performed to prepare Zr(IV) imprinted silica gel. Zr(IV) selectivity were calculated as 134, 120, and 138 over Ti(IV), Y(III), and Nb(V) from multinary solution
Zheng et al. (2007)	Highly selective determination of palladium(II) after preconcentration using Pd(II)-imprinted functionalized silica gel sorbent prepared by a surface imprinting technique	Pd(II)	Pd(II) complexed 3-aminopropyltriethoxysilane were grafted on activated silica gel. After that, Pb(II) elution and neutralization were performed to prepare Pd(II) imprinted silica gel. Pd(II) selectivity were calculated as 133, 87.5, 65.5, 103, 89, 51, and 60 over Zn(II), Fe(II), Au(III), Ru(III), Rh(III), Pt(IV), and Ir(III) from multinary solution
Chang et al. (2007)	Solid-phase extraction of iron(III) with an ion-imprinted functionalized silica gel sorbent prepared by a surface imprinting technique	Fe(III)	Fe(III) complexed 3-aminopropyltriethoxysilane were grafted on activated silica gel. After that, Fe(III) elution and neutralization were performed to prepare Fe(III) imprinted silica gel. Fe(II) selectivity were calculated as 451.0 over Cr(III) from binary solution
Zhang et al. (2007)	A new ion-imprinted silica gel sorbent for on-line selective solid-phase extraction of dysprosium(III) with detection by inductively coupled plasma-atomic emission spectrometry	Dy(III)	3-aminopropyltrimethoxysilane were grafted on activated silica gel. After that, Dy(III) complexed thenoyltrifluoroacetone were cross-linked on 3-aminopropyltrimethoxysilane silica gel by using formaldehyde. The resultants were eluted and neutralized to prepare Dy(III) imprinted silica gel. From the batch test, relative Dy(III) selectivity were calculated as 6.52, 7.67, and 6.45 over La(III), Nd(III), and Gd(III), from binary solution

Jiang et al. (2006)	Selective solid-phase extraction of nickel(II) using a surface-imprinted silica gel sorbent	Ni(II)	Ni(II) complexed 3-aminopropyltrimethoxysilane were grafted on activated silica gel. After that, Ni(II) elution and neutralization were performed to prepare Ni(II) imprinted silica gel. From the batch test, relative Ni(II) selectivity were calculated as 45.99, 32.83, 43.79 and 28.36 over Cu(II), Co(II), Zn(II), and Pb(II), from binary solution
Fang et al. (2005)	An ion-imprinted functionalized silica gel sorbent prepared by a surface imprinting technique combined with a sol-gel process for selective solid-phase extraction of cadmium(II)	Cd(II)	Cd(II) complexed 3-Mercaptopropyltrimethoxysilane were grafted on activated silica gel. After that, Cd(II) elution and neutralization were performed to prepare Cd(II) imprinted silica gel. From the batch test, relative Cd(II) selectivity over Pb(II) was calculated as 3.11 -3.15.

Table 2.2. Previous studies for surface ion imprinting through functionalization on support material with cross-linking

Author	Title	Target ion	Abstract
Monier et al. (2018)	Preparation of ruthenium (III) ion-imprinted beads based on 2-pyridylthiourea modified chitosan	Ru(III)	Ru(III) complexed 2-pyridyl isothuicyanate grafted chitosan were cross-linked with ephichlorohydrin. After that, Ru(III) elution and neutralization were performed to prepare Pb(II) imprinted chitosan resin. From the batch test, Ru(III) selectivity were calculated as 7.40, 5.47, 7.81, 10.24, 8.36, 6.70, 10.76, 11.69, and 12.37 over Pd(II), Pt(IV), Co(II), Fe(III), Ni(II), Cu(II), Mn(II), Zn(II), and Ca(II), from mulinary solution
Monier et al. (2016)	Ion-imprinted modified chitosan resin for selective removal of Pd(II) ions	Pd(II)	Pd(II) complexed 2-aminobenzaldehyde grafted chitosan were cross-linked with glyoxal. After that, Pb(II) elution and neutralization were performed to prepare Pb(II) imprinted chitosan resin. From the batch test, Pd(II) selectivity were calculated as 1.75, 2.73, 3.12, and 5.85 over Cu(II), Ni(II),Co(II), and Mn(II), from mulinary solution
Gao et al. (2013)	Preparation of chromate anion surface-imprinted material IIP-PVI/SiO2 based on polyvinylimidazole-grafted particles PVI/SiO2 and its ionic recognition characteristic	Cr(VI)	Cr(VI) complexed polyvinylimidazole grafted on silica gel. After that, 1,6-dibromohexane used to cross-link Cr(VI) complexed sites. Finally, Cr(VI) elution and neutralization were performed to prepare Cr(VI) imprinted silica gel. Cr(VI) selectivity were calculated as 7.78 over PO_4^{3-} from binary solution
Fan and Sun (2012)	Selective Removal of Iron from Aqueous Solution using Ion Imprinted Cyanato-Functionalized Silica Gel Sorbents	Fe(III)	Fe(III) complexed 3-thiocyanatopropyltriethoxysilane grafted on silica gel. After that, epichlorohydrin used to cross-link Fe(III) complexed sites. Finally, Fe(III) elution and neutralization were performed to prepare Fe(III) imprinted silica gel. Fe(III) selectivity were calculated as 17.33, 35.14, 48.68, and 14.63 over Co(II), Pb(II), Cd(II), and Ni(II) from binary solution
Fan et al. (2012b)	An ion-imprinted amino-functionalized silica gel sorbent prepared by hydrothermal assisted surface imprinting technique for selective removal of cadmium (II) from aqueous solution	Cd(II)	Cd(II) complexed 3-[2-(2-aminoethylamino)ethylamino]propyl-trimethoxysilane grafted on silica gel. After that, epichlorohydrin used to cross-link Cd(II) complexed sites. Finally, Cd(II) elution and neutralization were performed to prepare Cd(II) imprinted silica gel. Cd(II) selectivity were calculated as 2.220, 2.603, 2.486, 2.419, and 2.259 over Co(II), Ni(II), Cu(II), Pb(II), and Zn(II) from binary solution

Li et al. (2011b)	Cd(II)-imprinted polymer sorbents prepared by combination of surface imprinting technique with hydrothermal assisted sol–gel process for selective removal of cadmium(II) from aqueous solution	Cd(II)	Cd(II) complexed 3-thiocyanatopropyltriethoxysilane grafted on silica gel. After that, epichlorohydrin used to cross-link Cd(II) complexed sites. Finally, Cd(II) elution and neutralization were performed to prepare Cd(II) imprinted silica gel. Cd(II) selectivity were calculated as 3.539, 3.639, 2.438, and 1.704 over Co(II), Cu(II), Pb(II), and Zn(II) from binary solution

Table 2.3. Previous studies for surface ion imprinting through polymerization on support material

Author	Title	Target ion	Abstract
Li et al. (2018)	A novel In(III) ion-imprinted polymer (IIP) for selective extraction of In(III) ions from aqueous solutions	In(III)	In(III) complexed vinylphosphonic acid and allyl mercaptan immobilized ethylene glycol dimethacrylate polymer were grafted on silica gel. After that, In(III) elution and neutralization were performed to prepare In(III) imprinted silica gel. In(III) selectivity were calculated as 41, 212, 37, and 69 over Cu(II), Pb(II), Zn(II), and Fe(II) from binary solution.
Liang et al. (2017)	Fast and selective removal of Cr(VI) from aqueous solutions by a novel magnetic Cr(VI) ion-imprinted polymer	Cr(VI)	Cr(VI) complexed 4-vinyl pyridine immobilized 2-hydroxyethyl methacrylate and ethylene glycol dimethacrylate polymer were grafted on graphene oxide include silica coated Fe_3O_4. After that, Cr(VI) elution and neutralization were performed to prepare Cr(VI) imprinted graphene oxide. Cr(VI) selectivity were calculated as 177.03, 208.04, 46.48, 171.59, 12.91, and 16.37 over Cu(II), Cd(II), Cr(III), Ni(II), SO_4^{2-}, and NO_3^- from multinary solution.
Dahaghin et al. (2017)	A novel magnetic ion imprinted polymer as a selective magnetic solid phase for separation of trace lead(II) ions from agricultural products, and optimization using a Box–Behnken design	Pb(II)	Pb(II) complexed imidazole and 4-vinylpyridine immobilized ethylene glycol dimethacrylate polymer were grafted on silica coated Fe_3O_4. After that, Pb(II) elution and neutralization were performed to prepare Pb(II) imprinted silica coated Fe_3O_4.
Taghizadeh and Hassanpour (2017)	Selective adsorption of Cr(VI) ions from aqueous solutions using a Cr(VI)-imprinted polymer supported by magnetic multiwall carbon nanotubes	Cr(VI)	Cr(VI) complexed 2-hydroxyethyl methacrylate and 4-vinylpyridine immobilized ethylene glycol dimethacrylate polymer were grafted on silica coated Fe_3O_4 impregnated multiwall carbon nanotubes. After that, Cr(VI) elution and neutralization were performed to prepare Cr(VI) imprinted silica coated Fe_3O_4 impregnated multiwall carbon nanotubes. Cr(VI) selectivity were calculated as 2, 1.3, 5.56, 16.39, and 12.32 over SO_4^{2-}, NO_3^-, F^-, Ni(II), and Cu(II) from binary solution.
Kang et al. (2016)	A novel magnetic and hydrophilic ion-imprinted polymer as a selective sorbent for the removal of cobalt ions from industrial wastewater	Co(II)	Co(II) complexed 1-vinylimidazole immobilized ethylene glycol dimethacrylate polymer were grafted on silica coated Fe_3O_4. After that, Co(II) elution and neutralization were performed to prepare Co(III) imprinted silica coated Fe_3O_4. Co(II) selectivity were calculated as 1.33, 2.51, 1.29, and 1.41 over Cu(II), Cd(II), Zn(II), and Pb(II) from multinary solution.

Gao et al. (2015)	Preparation of Fe(III) ion surface-imprinted material for removing Fe(III) impurity from lanthanide ion solutions	Fe(III)	Fe(III) complexed p-styrenesulfonate immobilized N,N'-Methylenebisacrylamide polymer were grafted on silica. After that, Fe(III) elution and neutralization were performed to prepare Fe(III) imprinted silica. Fe(III) selectivity were calculated as 5.77 over La(III) from binary solution.
Li et al. (2015a)	Synthesis and application of a surface-grafted In (III) ion-imprinted polymer for selective separation and pre-concentration of indium (III) ion from aqueous solution	In(III)	In(III) complexed vinylphosphonic acid immobilized ethylene glycol dimethacrylate polymer were grafted on silica gel. After that, In(III) elution and neutralization were performed to prepare In(III) imprinted silica gel. In(III) selectivity were calculated as 189.17, 67.94, 886.63, and 2479.71 over Cu(II), Pb(II), Zn(II), and Fe(II) from binary solution.
Li et al. (2015b)	Synthesis and characterization of a surface-grafted Cd(II)ion-imprinted polymer for selective separation of Cd(II) ion from aqueous solution	Cd(II)	Cd(II) complexed allyl thiourea immobilized ethylene glycol dimethacrylate polymer were grafted on silica gel. After that, Cd(II) elution and neutralization were performed to prepare Cd(II) imprinted silica gel. Cd(II) selectivity were calculated as 2.86, 18.64, 15.41, 20.82, and 6.27 over Cu(II), Ni(II), Zn(II), Pb(II), and Co(II) from binary solution.
Monier et al. (2015)	Surface ion-imprinted amino-functionalized cellulosic cotton fibers for selective extraction of Cu(II) ions	Cu(II)	Cu(II) complexed o-nitrobenzaldehyde immobilized polyacrylonitrile polymer were grafted on cotton fiber. After that, glutaraldehyde cross-link Cu(II) complexed sites. Finally, Cu(II) elution and neutralization were performed to prepare Cu(II) imprinted cotton fiber. Cu(II) selectivity were calculated as 50.37, 45.84, 57.52, and 79.27 over Co(II), Ni(II), Zn(II), and Cd(II) from multinary solution.
Milja et al. (2011)	Synthesis of surface imprinted nanospheres for selective removal of uranium from simulants of Sambhar salt lake and ground water	U(VI)	U(VI) complexed 4-vinyl pyridine and 2-hydroxy ethyl methacrylate immobilized ethylene glycol dimethacrylate polymer were grafted on silica. After that, U(VI) elution and neutralization were performed to prepare U(VI) imprinted silica. U(VI) selectivity were calculated as 140, 2500, 18, 170, 950, 100, and 110 over Ca(II), Mg(II), Cu(II), Zn(II), Fe(III), Co(II), and Ni(II) from multinary solution.
Lin et al. (2010)	Selective solid-phase extraction of trace thorium(IV) using surface-grafted Th(IV)-imprinted polymers with pyrazole derivative	Th(IV)	Th(IV) complexed pyrazole derivative 1-phenyl-3-methylthio-4-cyano-5-acrylicacidcarbamoyl-pyrazole immobilized ethylene glycol dimethacrylate polymer were grafted on silica gel. After that, Th(IV) elution and neutralization were performed to prepare Th(IV) imprinted silica gel. Th(IV) selectivity were calculated as 124.6, 156.6, 19.7, and 12.9 over Ce(III), La(III), U(VI), and Zr(IV) from binary solution.

Lin et al. (2010)	Selective preconcentration of trace thorium from aqueous solutions with Th(IV)-imprinted polymers prepared by a surface-grafted technique	Th(IV)	Th(IV) complexed methacrylic acid immobilized ethylene glycol dimethacrylate polymer were grafted on silica gel. After that, Th(IV) elution and neutralization were performed to prepare Th(IV) imprinted silica gel. Th(IV) selectivity were calculated as 24.7, 128.3, 143.6, and 18.2 over U(VI), Ce(III), La(III), and Zr(IV) from multinary solution.
He et al. (2007)	Synthesis and applications of surface-grafted Th(IV)-imprinted polymers for selective solid-phase extraction of thorium(IV)	Th(IV)	Th(IV) complexed N-(o-carboxyphenyl)maleamic acid immobilized ethylene glycol dimethacrylate polymer were grafted on silica gel. After that, Th(IV) elution and neutralization were performed to prepare Th(IV) imprinted silica gel. Th(IV) selectivity were calculated as 2212, 1976, 615.0, 154.7, and 69.4 over La(III), Ce(III), Nd(III), U(VI), and Zr(IV) from multinary solution

Table 2.4. Previous studies for surface ion imprinting through polymer grafting to support material

Author	Title	Target ion	Abstract
Monier and Abdel-Latif (2013a)	Synthesis and characterization of ion-imprinted chelating fibers based on PET for selective removal of Hg2+	Hg(II)	Hg(II) complexed thiosemicarbazide immobilized polyacrylonitrile polymer were grafted on poly(ethylene terephthalate). After that, formaldehyde used to cross-link Hg(II) complexed sites. Finally, Hg(II) elution and neutralization were performed to prepare Hg(II) imprinted poly(ethylene terephthalate). Hg(II) selectivity were calculated as 32.11, 19.78, 21.55, 119.22, and 83.23 over Cu(II), Cd(II), Pb(II), Ni(II), and Fe(III) from multinary solution
Monier and Abdel-Latif (2013b)	Synthesis and characterization of ion-imprinted resin based on carboxymethyl cellulose for selective removal of UO_2^{2+}	U(VI)	U(VI) complexed salicylaldehyde immobilized polyacrylonitrile polymer were grafted on carboxymethyl cellulose microsphere. After that, formaldehyde used to cross-link U(VI) complexed sites. Finally, U(VI) elution and neutralization were performed to prepare U(VI) imprinted carboxymethyl cellulose microsphere. U(VI) selectivity were calculated as 50.27, 34.51, 21.55, 82.54, and 42.14 over V(VI), Fe(III), Mn(II), Co(II), and Cu(II) from multinary solution
Wang et al. (2013b)	Effective removal of Fe(II) impurity from rare earth solutionusing surface imprinted polymer	Fe(II)	Cu(II) complexed polyethyleneimine grafted on silica gel. After that, Ethylene glycol diglycidyl ether used to cross-link Fe(II) complexed sites. Finally, Fe(II) elution and neutralization were performed to prepare Fe(II) imprinted silica gel. Fe(II) selectivity were calculated as 25.57, and 20.63 over Ce(III) and Pr(III) from binary solution
Liu et al. (2011a)	Selective Adsorption of Co(II) by Mesoporous Silica SBA-15-Supported Surface Ion Imprinted Polymer: Kinetics, Isotherms, and Thermodynamics Studies	Co(II)	Co(II) complexed polyethyleneimine grafted on SBA-15. After that, epichlorohydrin used to cross-link Co(II) complexed sites. Finally, Co(II) elution and neutralization were performed to prepare Co(II) imprinted SBA-15. Co(II) selectivity were calculated as 7.33, 8.66, 8.63, 37.06, and 8.22 over Pb(II), Cu(II), Zn(II), Sr(II), and Ni(II) from multinary solution
An and Gao (2009)	Adsorption characteristics of Cr(III) ionic imprinting polyamine on silica gel surface	Cr(III)	Cr(III) complexed polyethyleneimine grafted on silica gel. After that, epichlorohydrin used to cross-link Cr(III) complexed sites. Finally, Cr(III) elution and neutralization were performed to prepare Cr(III) imprinted silica gel. Cr(III) selectivity were calculated as 11.23, and 21.00 over Zn(II) and Pb(II) from binary solution

Gao et al. (2007)	Novel surface ionic imprinting materials prepared via couple grafting of polymer and ionic imprinting on surfaces of silica gel particles	Cu(II)	Cu(II) complexed polyethyleneimine grafted on silica gel. After that, epichlorohydrin used to cross-link Cu(II) complexed sites. Finally, Cu(II) elution and neutralization were performed to prepare Cu(II) imprinted silica gel. Cu(II) selectivity were calculated as 71.05, and 88.22 over Cr(III) and Pb(II) from binary solution

Among various heavy metals, Cu(II) imprinting has been tried continuously. Several researchers have synthesized Cu(II)-imprinted silica using diethylenetriamine (Guo et al., 2009; Ding et al., 2012), [3-(2-aminoethylamino)propyl] trimethoxysilane (Dai et al., 2000; Makote and Dai, 2001), N-[3-(trimethoxysilyl)propyl] ethylenediamine (Wu et al., 2010), poly(allylamine) (Fan et al., 2014b), N,N'-bis (4-hydroxysalicylidene) ethylene-1,2-diamine (Faghihian and Asghari, 2013), and oligomers (Bi et al., 2007), as organic functionalities for selective sorption of Cu(II) from aqueous solutions. Most of these researchers did not use a crosslinker to fix Cu(II) complex sites on the silica during the imprinting process (Table 2.5). Studies related to grafting PEI on silica particles and using a crosslinker during imprinting to produce Cu(II)-imprinted silica are limited. Only one study, reported by Gao et al. (2007), prepared ion-imprinted silica gels through grafting of PEI onto the surfaces of silica particles and ionic imprinting with epichlorohydrin as a crosslinker. They performed batch experiments in binary solutions containing Cu(II)/Zn(II) and Cu(II)/Ni(II) to examine the selective Cu(II) removal by imprinted silica gels.

Table 2.5. Previous studies for Cu(II) ion imprinting

Support material	Imprinting Technique	Bridge	Organic functionality provider	Cross-linker to fix complex site	Reference
Silica forming on copper complex	Polymerize silica-precursor with Copper complex	-	[3-(2-Aminoethylamino)propyl]trimethoxysilane (AAPTS)	-	Dai et al. (2000)
Silica forming on copper complex	Polymerize silica-precursor with Copper complex	-	AAPTS	-	Makote and Dai (2001)
Silica gel	Anchor the copper complex on bridge functionalized silica	(3-Aminopropyl)triethoxysilane (APES), glutaraldehyde	Glycine, diglycine, triglycine oligomers		Bi et al. (2007)
Silica gel (120-160 mesh)	Anchor the copper complex on bridge functionalized silica and cross-link to fix complex site	3-chloropropyl-trimethoxy silane (CPS)	Poly(ethyleneimine) (PEI)	Epichlorohydrin (ECH)	Gao et al. (2007)
Silica gel (80-120 mesh)	Anchor the copper complex on bridge functionalized silica	CPS	Diethylenetriamine (DETA)	-	Guo et al. (2009)
Mesoporous silica	Anchor the copper complex on bridge functionalized silica	N-[3-(Trimethoxysilyl)propyl]ethylenediamine (TPED)	TPED, 2-Pyridinecarboxaldehyde	-	Wu et al. (2010)
SiO_2 coated Fe_3O_4	Anchor the copper complex SiO_2 coated Fe_3O_4	-	3-aminopropyltriethoxysilane		Luo et al. (2011)
Silica gel (60-100 mesh)	Anchor the copper complex on bridge functionalized silica	CPS	DETA	-	Ding et al. (2012)
Silica gel (5 – 40 µm)	Anchor the copper complex on bridge functionalized silica	CPS	N,N'-bis(4-hydroxysalicylidene)ethylene-1,2-diamine	-	Faghihian and Asghari (2013)
Silica gel (40-80 mesh)	Chelate the copper on functionalized silica and cross-linking to fix complex site	CPS	Poly(allylamine)	ECH	Fan et al. (2014b)
Cotton fiber	Cu(II) complexed o-nitrobenzaldehyde immobilized polyacrylonitrile polymer were grafted on cotton fiber and glutaraldehyde used to fix complex site	polyacrylonitrile polymer	o-nitrobenzaldehyde	glutaraldehyde	Monier et al. (2015)
Mesoporous silica SBA-15	Anchor the copper complex on bridge functionalized silica and cross-link to fix complex site	CPS	PEI	Ethylene glycol diglycidyl ether (EGDE)	This study

2.2 Nitrate removal technology

Nitrate has low tendency for precipitation and adsorption from its high stability and solubility. These characteristics make hard to remove nitrate from water using conventional water treatment technology (Islam et al., 2010). To remove nitrate in aqueous condition, reduction, electrocoagulation, membrane filtration, ligand exchange, ion exchange are feasible methods. Few studies below represented nitrate removal examples by using various mechanisms (Fig 2.6).

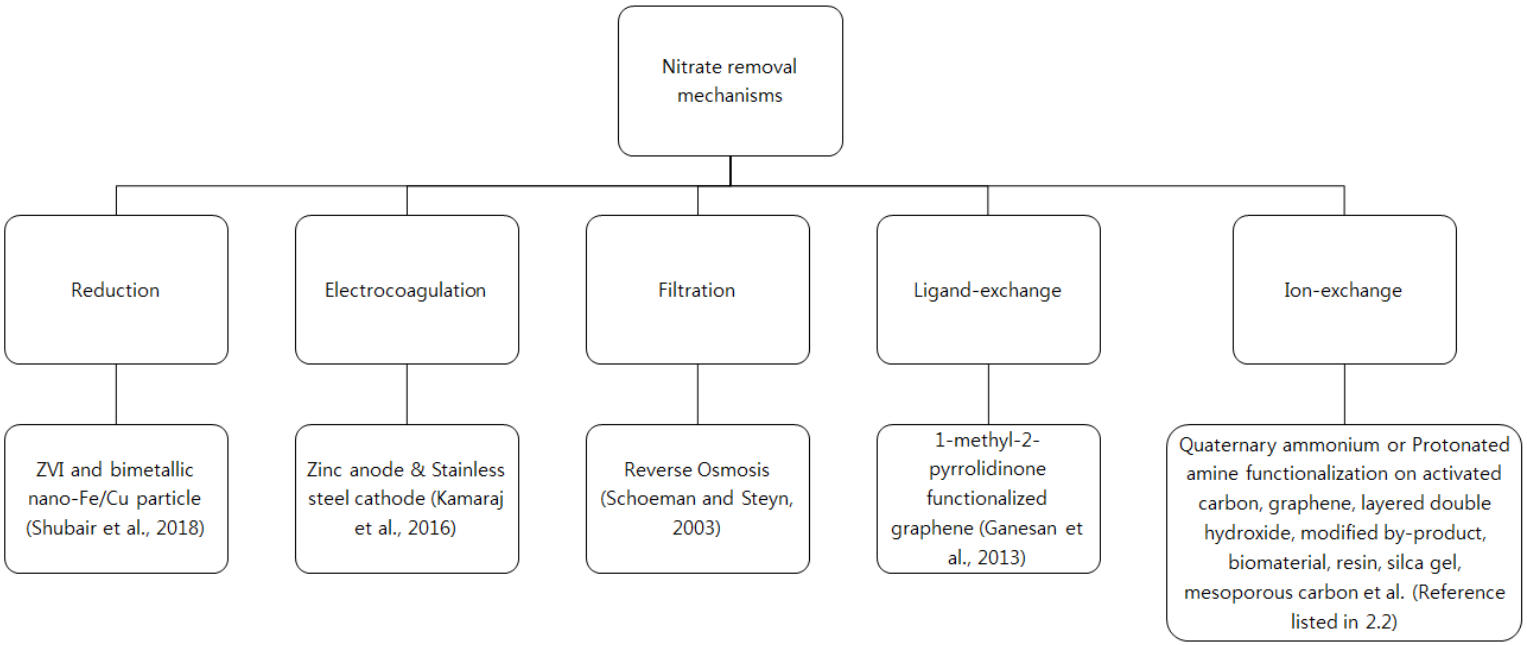

Figure 2.6. Applied mechanisms and examples for nitrate removal

Shubair et al. (2018) studied the nitrate removal in porous media using nanoscale zero valent iron and bimetallic nano-Fe/Cu particles by reduction in a packed with sand column. The main mechanism of nitrate removal by nanoscale zero valent iron and bimetallic nano-Fe/Cu particles was the nitrate reduction. Nitrate was removed as NH_4^+-N and NO_2-N form.

Kamaraj et al. (2016) studied the nitrate removal by electrocoagulation process using zinc and stainless steel as anode and cathode. From the electrocoagulation process, Zn was oxidized as Zn^{2+}, and Zn^{2+} reacted with $2H_2O$ to from $Zn(OH)_2$. $Zn(OH)_2$ acted as nitrate adsorbent. Sorption capacity was calculated as 1.747 mg/g from Langmuir model.

Schoeman and Steyn (2003) studied the application of reverse osmosis at nitrate removal in a rural area in South Africa. From results, not only nitrate but also other ions were effectively removed.

Ganesan et al. (2013) prepared graphene by a liquid phase exfoliation and functionalized with 1-methyl-2-pyrrolidinone. Even pH_{PZC} of prepared graphene was 5.7, optimum pH of nitrate removal was 7. This phenomenon can be explained as the main mechanism of nitrate removal by graphene is ligand-exchange reactions (anion is displaced with OH group on graphene surface). Sorption reaction was considered as endothermic and sorption capacity was calculated as 847.81 mg/g at 343 K from Langmuir model.

From few kinds of nitrate removal methods, ion-exchange is most feasible from an economic standpoint (Ganesan et al., 2013). To remove nitrate in aqueous solution by ion exchange, various materials (activated carbon, graphene, layered double hydroxide, modified by-product, biomaterial, resin, silica gel, mesoporous silica, etc.,) has been adopted as support material or functional material. Surface activation or amine protonation or quaternization is required to adopt various material into nitrate removal by ion exchange.

Some researchers studied the nitrate removal using activated carbon or biochar materials. Öztürk and Bektaş (2004) studied the nitrate removal characteristics of sepiolite, activated sepiolite, slag, and powdered activated carbon. From the results, slag did not show any effective nitrate sorption characteristics. From sepiolite, activated sepiolite, and powdered activated carbon, activated sepiolite was the fastest, highest, and selective one. This tendency is considered as effect of activation with hydrochloric acid. Positively charged surface of sepiolite by activation makes ion-exchange as the main mechanism of the nitrate removal. Demiral and Gündüzoğlu (2010) prepared activated carbon from sugar beet bagasse. The prepared activated carbon had 1826 m^2/g of surface area and 27.55 mg/g of sorption capacity from Langmuir model. Kilpimaa et al. (2015) physically activated the carbon residue from the biogasification process. Sorption capacity was calculated as

11.198 mg/g from Langmuir model. Mazarji et al. (2017) modified commercial granular activated carbon with sodium hydroxide followed by a cationic surfactant. From its modification, modified granular activated carbon showed 21.51 mg/g of sorption capacity from Langmuir model. Divband Hafshejani et al. (2016) examined the potential of modified sugarcane bagasse biochar for the removal of nitrate in aqueous solution. Modified sugarcane bagasse biochar's point of zero charge (pH_{PZC}) was measured as 5.35. From the pH_{PZC}, its nitrate sorption was maximized at pH 4.64. Sorption capacity was calculated as 28.21 mg/g from Langmuir model. From the effect of competing anion experiment, inhibition effect on nitrate removal as following order; $CO_3^{2-} > PO_4^{3-} > SO_4^{2-} > Cl^-$.

There has some reports that the application of modified graphene on nitrate removal. Rashidi Nodeh et al. (2017) synthesized nanosized lanthanum hydrous doped on magnetic graphene nanocomposite. Lathanium was hardly leached when pH is over 4. Sorption capacity was calculated as 277 mg/g from Langmuir model.

Some researchers reported the nitrate removal characteristics of alumina. Bhatnagar et al. (2010) studied the nitrate sorption characteristics of nano-alumina. Nano-alumina showed 4.57 mg/g of sorption capacity from Langmuir model. From the effect of competing anion results, Cl^- was the

mostly affected on nitrate sorption than F^-, SO_4^{2-}, CO_3^{2-}, and PO_4^{3-}. Golie and Upadhyayula (2016) prepared chitosan/alumina composite. Prepared chitosan/alumina composite were acidified to protonate amine group. Continuous fixed-bed column study were performed with acidified chitosan/alumina composite.

Some researchers reported the nitrate removal characteristics of layered double hydroxide (LDH). Islam and Patel (2009) investigated the ability of Mg-Al-Cl hydrotalcite-like compound for the removal of nitrate. Nitrate percent removal was 78.6 % when initial concentration was 10 mg/L and adsorbent dose was 3 g/L. From the effect of competing anion experiment, inhibition effect on nitrate removal as following order; $CO_3^{2-} > PO_4^{3-} > Cl^- > SO_4^{2-}$. Even its high nitrate sorption capacity, Mg-Al-Cl hydrotalcite could be easily regenerated (less than 2 %). Islam and Patel (2010) synthesized Zn-Al-Cl LDH by co-precipitation. Nitrate percent removal was 85.5 % when initial concentration was 10 mg/L and adsorbent dose was 3 g/L. Competing anion results and regeneration characteristics are familiar with Islam and Patel (2009). Islam and Patel (2011) synthesized Ca-Al-Cl hydrotalcite-like compound by co-precipitation. Nitrate percent removal was 84.6 % when initial concentration was 10 mg/L and adsorbent dose was 3.5 g/L. Competing anion results and regeneration characteristics are also familiar with Islam and

Patel (2009). Ivánová et al. (2018) synthesized Mg-Al-CO_3 LDH by two co-precipitation. From the results, LDH prepared by calcination of slow co-precipitation at low supersaturation was more effective in comparison with LDH prepared by calcination of quickly co-precipitation at high supersaturation. At the initial concentration of nitrate was 130 mg/L, the removal percent of nitrate were 73.9 %, 94.7 %, 98.7 %, and 99.2 % when dose = 5, 10, 15, and 20 g/L.

There were also some reports that the application of modified by-product or biomaterial on nitrate removal. Chatterjee and Woo (2009) investigated the adsorption of nitrate on chitosan hydrogel. By increasing pH, nitrate sorption capacity gradually decreased. This is considered as protonated amine group on chitosan acts as nitrate sorption site by electrostatic interaction in low pH. Sorption capacity was calculated as 92.1 mg/g from Sips model at pH 5. de Lima et al. (2012) functionalized coconut shell with 3-chloride 2-hydroypropyltrimethylammonium chloride. Quaternary ammonium functionalized coconut shell showed nitrate sorption capacity as 33.7 mg/g from Langmuir model. From reuse test, quaternary ammonium functionalized coconut shell had poor reusability. Olgun et al. (2013) investigated the nitrate removal through boron waste and heat-treated boron waste. Boron waste is mainly composed of ulexite, zeolite, colemanite, and some clays. From pH_{PZC}

of heat-treated boron waste was about 6, nitrate sorption capacity was gradually decreased by increasing of solution pH. Heat-treated boron waste showed maximized sorption capacity at calcination temperature 400 ^{o}C and pH 3 as 62.62 mg/g of sorption capacity from Langmuir model. Islam et al. (2010) prepared hydroxyapatite from eggshell by sol-gel method. Nitrate percent removal was 96 % when initial concentration was 100 mg/L and adsorbent dose was 3 g/L. From the effect of competing anion experiment, inhibition effect on nitrate removal as following order; $Cl^{-} > CO_3^{2-} > SO_4^{2-} > PO_4^{3-}$. Katal et al. (2012) synthesized anionic sorbent from rice husk with dimethylamine. Nitrate percent removal was 94.3 % when initial concentration was 50 mg/L and adsorbent dose was 4 g/L. From the effect of competing anion experiment, inhibition effect on nitrate removal as following order; $CO_3^{2-} > Cl^{-} > PO_4^{3-} > SO_4^{2-}$. Xu et al. (2013) synthesized biomaterial based resins from virgin wheat stalk and cotton stalk. In the preparation, quaternary ammonium functionalization process was contained. Prepared biomaterial based resins nitrate sorption capacity as 33.35 – 50.24 mg/g from Langmuir model. Sowmya and Meenakshi (2013) prepared glutaraldehyde cross-linked chitosan beads and quaternized with glycidyl trimethyl ammonium chloride. Sorption capacity was calculated as 27.048 mg/g from Langmuir model. Sowmya and Meenakshi (2014) synthesized chitosan-melamine-glutaraldehyde terpolymer and quaternized with glycidyl trimethyl

ammonium chloride. Sorption capacity was calculated as 97.5 mg/g from Langmuir model. Jóźwiak et al. (2017) cross-linked chitosan hydrogel with sodium citrate or epichlorohydrin. Cross-linked with epichlorohydrin one showed higher nitrate sorption capacity than sodium citrate cross-linked. Sorption was maximized at pH 3 able to protonate amine on chitosan. Sorption capacity was calculated as 13.09 mg/g from Langmuir model.

Resin is also commonly used support material for nitrate removal as basic functionalization. Commonly used strong base resins for nitrate removal are polymerized forms of styrene containing some divinyl benzene like Ionac SR6, Purolite A-520E, Amberlite IRA 400, and Indion NSSR resin (SenGupta, 1995; Chabani et al., 2006; Milmile et al., 2011). Banu and Meenakshi (2017) quaternized melamine formaldehyde resin with triethylamine. Sorption capacity was calculated as 124.16 mg/g from Langmuir model. From the effect of competing anion experiment, inhibition effect on nitrate removal as following order; $SO_4^{2-} > Cl^- > HCO_3^-$.

Mesoporous silica and silica gel also considered as a support material. Hamoudi and Belkacemi (2013) amine functionalized mesoporous silica MCM-48 with 3-aminopropyltriethoxysilane. Before apply amine functionalized mesoporous silica MCM-48 into nitrate removal, acidification performed with HCl to protonate amine group. Sorption capacity was

calculated as 45 mg/g from Langmuir model. Dioum and Hamoudi (2014) functionalized SBA-15 with aminopropyltriethoxysilane or N-((trimethoxysilyl)propyl)-N,N,N-trimethylammonium as amine functionalized SBA-15 or quaternary ammonium functionalized SBA-15. Amine functionalized SBA-15 was acidified to protonate amine as ammonium moieties. Sorption capacity was calculated as 46 and 55 mg/g from Langmuir model. Wu et al. (2016) quaternized chloromethylated cross-linked polystyrene with 3-chloro-2-hydroxypropyltrimethylammonium chloride. From the effect of competing anion experiment, inhibition effect on nitrate removal as following order; SO_4^{2-} > HCO_3^- > Cl^-. Lau and Yeong (2016) aminated MCM-41 with 3-[2-(2-aminoethylamino) ethylamino] propyl trimethoxysilane. Amine functionalized SBA-15 was acidified to protonate amine as ammonium moieties. When initial nitrate concentration about 15 mg/L and dose = 0.5 g/L, nitrate removal achieved up to 70 %.

Among various support materials, mesoporous materials are most considerable from its large surface area, high pore volume, and high thermal stability (Lau and Yeong, 2016). Furthermore, mesoporous silica and silica gel have high resistance to chemicals and high temperature, easy of functionalization for both outer and inner surface (Hanafi-Bojd et al., 2015; He et al., 2018). In addition, alkyl chain length highly effective on nitrate

selectivity over other anions like HCO_3^-, Cl^-, PO_4^{3-}, SO_4^{2-} (SenGupta, 1995). However, there was no report about the nitrate removal effect of the alkyl chain length of quaternary ammonium functionalized on silica material.

In this thesis, various kinds of quaternized mesoporous silica or silica gel were prepared which has various length of alkyl chain. The morphology and functional group of the quaternary ammonium functionalized mesoporous silica or silica gel were characterized via scanning electron microscope (SEM), Fourier-transform infrared (FTIR) spectroscopy, and X-ray photoelectron spectroscopy (XPS). Latterly, nitrate sorption tests were conducted to identify the effect of alkyl chain length for nitrate removal.

Chapter 3 Enhancement of selective Cu(II) sorption through preparation of surface-imprinted mesoporous silica SBA-15 under high molar concentration ratios of chloride and copper ions

In this chapter, (ethyleneimine) (PEI)-grafted mesoporous silica SBA-15 (Cu-imprinted PEI-SBA-15) were prepared for selective Cu(II) sorption from aqueous solutions. To enhance the Cu(II) selectivity of Cu-imprinted PEI-SBA-15, Cu(II) loading on PEI-SBA-15 was increased via Cu(II) sorption under high-molar-concentration ratios of chloride (Cl) and Cu(II) ions. Then, selective Cu(II) sorption sites were increased through imprinting processes (crosslinking and elution) on Cu-loaded PEI-SBA-15. Selective experiments were performed using Cu-imprinted PEI-SBA-15 prepared at various $[Cl^-]/[Cu(II)]$ ratios, ranging from 2 to 1000. In multinary solutions containing divalent ions, such as Cu(II), Pb(II), Zn(II), Ni(II), and Co(II), Cu(II) selectivity was highest (79.62) at a $[Cl^-]/[Cu(II)]$ ratio of 500; the relative Cu(II) selectivity for Cu-imprinted PEI-SBA-15 over PEI-SBA-15 was 29.24. In multinary solutions containing Cu(II) along with trivalent and tetravalent ions, such as Al(III), Cr(III), and Zr(IV), the Cu(II) selectivity was also highest (3.40) at a ratio of 500; the relative Cu(II) selectivity was 3.96. In this study, we demonstrated that the Cu(II) selectivity of surface-imprinted SBA-15 could be enhanced through its preparation under high $[Cl^-]/[Cu(II)]$ ratios.

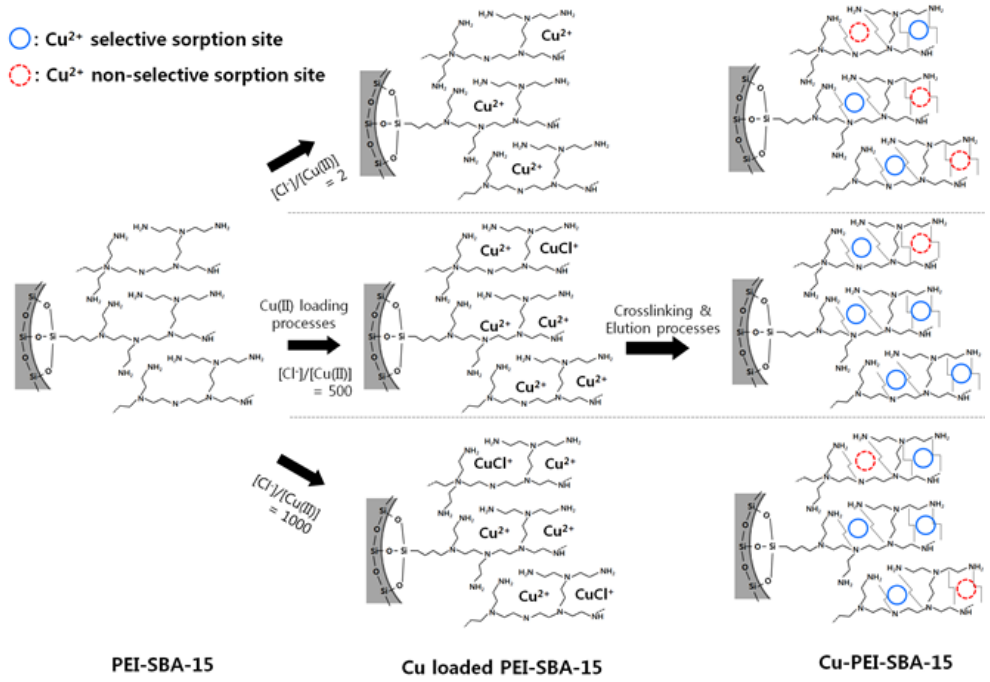

Figure 3.1. Graphical abstract of chapter 3

3.1. Materials and Methods

3.1.1. Preparation of PEI-SBA-15

All chemicals used in the experiments were purchased from Sigma Aldrich (Saint Louis, MO, USA) unless stated otherwise. A schematic diagram of the synthesis of PEI-SBA-15 is shown in Fig. 3.2. Prior to the preparation of PEI-SBA-15, mesoporous silica SBA-15 was synthesized following the method from Liu et al. (2009). A mixture solution containing 16 mL of deionized water, 20 mL of 2 M hydrochloric acid (HCl, 36.0%, Duksan Pure Chemicals, Seoul, Republic of Korea), 10 mL of absolute ethyl alcohol (EtOH, 99.9%, Samduk Lab-Science, Guri, Republic of Korea), 1.2 g of poly(ethylene glycol)-block-poly(propylene glycol)-block-poly(ethylene glycol) (P123), and 0.2 g of cetyltrimethylammonium bromide surfactant (CTAB, ≥ 99%) was prepared. The mixture solution was stirred at room temperature for 45 min to form micelle rods. Then, 4 mL of tetraethylorthosilicate (TEOS, ≥ 99%) was added as a silica precursor to the solution. After 45 min of crystallization through stirring, a white precipitate was obtained. The white precipitate was filtered through a 0.45-μm membrane filter and washed with 2 L of deionized water to remove unreacted reactants and neutralize pH. The washed precipitate was dried in a desiccator overnight and then calcined at 600°C for 6 h to remove

the remaining surfactant. After cooling, SBA-15 particles were obtained through fragmentation with a mortar and pestle.

Based on the SBA-15 particles, PEI-SBA-15 was prepared following the method modified from Wang et al. (2013b). 3-chloropropyl-SBA-15 (CP-SBA-15) was prepared through reacting 5 g of SBA-15 with 100 mL of (3-chloropropyl)trimethoxysliane (≥97%) at 80°C for 6 h, to which 1 mL of deionized water was added intermittently. CP-SBA-15 was filtered and dried at 60°C overnight. After cooling, CP-SBA-15 particles were obtained through fragmentation with a mortar and pestle. To prepare PEI-SBA-15, 50 mL of poly(ethyleneimine) (PEI) solution (50% in H_2O) and 1 g of CP-SBA-15 were stirred at 90°C for 6 h. After the reaction, PEI-SBA-15 was filtered, washed with deionized water, and dried at 60°C overnight. After cooling, PEI-SBA-15 particles were obtained through fragmentation with a mortar and pestle.

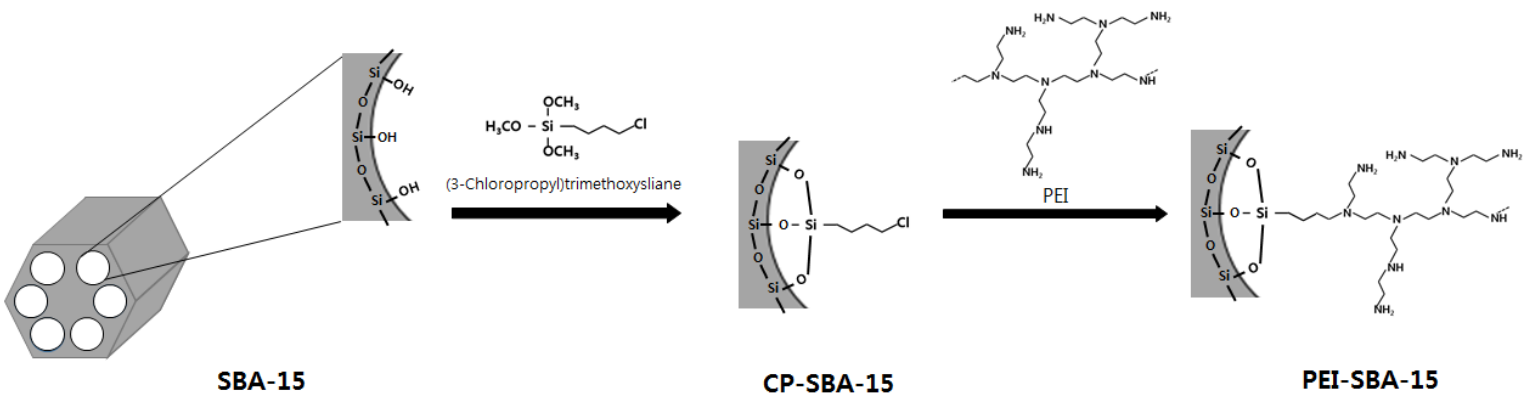

Figure 3.2. PEI-SBA-15 preparation

3.1.2. Preparation of Cu-imprinted PEI-SBA-15

Cu-imprinted PEI-SBA-15 (Cu-PEI-SBA-15) was prepared following a method modified from Wang et al. (2013b). A schematic diagram for the synthesis of Cu-PEI-SBA-15 is presented in Fig. 3.3. Prior to the preparation of Cu-imprinted PEI-SBA-15, Cu(II) ions were loaded onto PEI-SBA-15 at a fixed Cu(II) concentration of 1000 μM and molar $[Cl^-]/[Cu(II)]$ concentration ratios of 2, 50, 100, 200, 500, and 1000. Cu(II) loading on the PEI-SBA-15 was conducted by adding 1 g of PEI-SBA-15 into a 1-L solution of NaCl and Cu(II) ions under vigorous stirring for 6 h at 30°C. Cu-loaded PEI-SBA-15 was filtered and dried at 60°C overnight.

To prepare Cu-imprinted PEI-SBA-15, 1 g of Cu-loaded PEI-SBA-15 and 0.25 g of ethylene glycol diglycidyl ether (EGDE, Tokyo Chemical Industry Co., Tokyo, Japan) as a crosslinker were added into 50 mL of absolute ethanol and reacted at 25°C for 4 h under continuous stirring. After the reaction, particles were washed with 1 L of 0.1 M HCl solution to remove the template Cu(II) ions and unreacted EGDE and then washed with deionized water to neutralize the pH. The particles were filtered and dried at 60°C for overnight. After cooling, Cu-imprinted PEI-SBA-15 was obtained through fragmentation with a mortar and pestle.

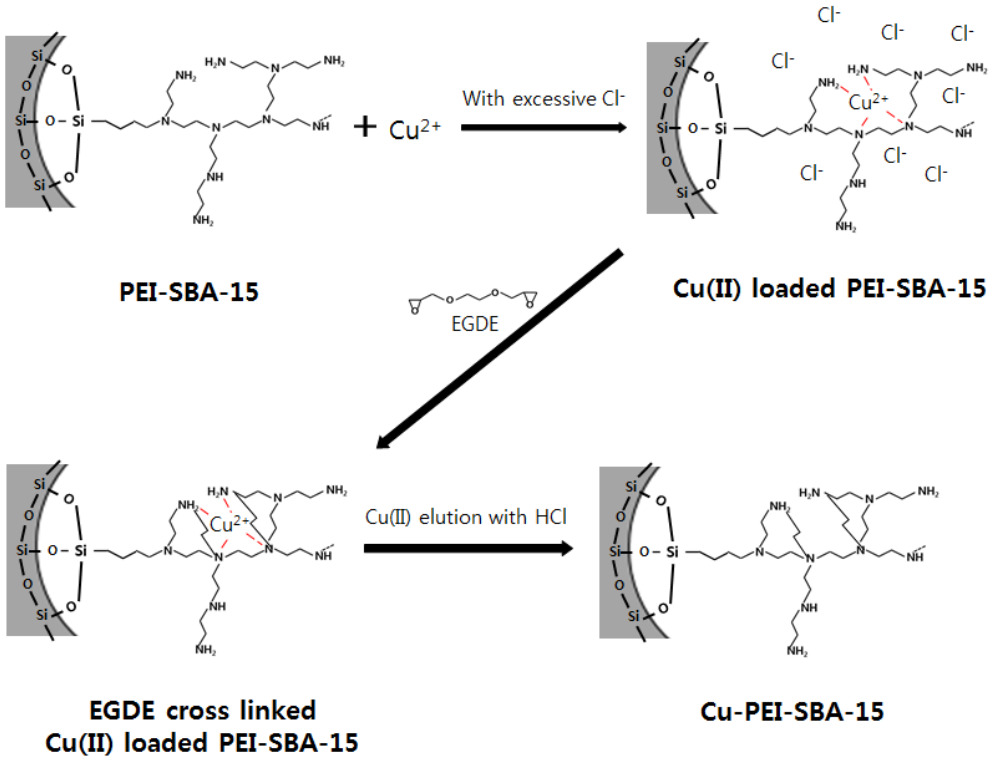

Figure 3.3. Cu-imprinted PEI-SBA-15 preparation

3.1.3. Characterization of PEI-SBA-15 and Cu-imprinted PEI-SBA-15

PEI-SBA-15 and Cu-imprinted PEI-SBA-15 were characterized using several techniques. Field-emission scanning electron microscopy (FE-SEM, Supra 55VP, Carl Zeiss, Oberkochen, Germany) and energy-dispersive X-ray spectroscopy (EDX, AURIGA, Carl Zeiss) were used to analyze the surface morphology and elemental composition. Fourier-transform infrared (FTIR) spectroscopy (Nicolet 6700, Thermo Fisher Scientific, Waltham, MA, USA) was used to analyze the effect of PEI impregnation and ion imprinting on PEI-SBA-15 and Cu-PEI-SBA-15. X-ray photoelectron spectroscopy (XPS, AXIS HSi, Kratos Analytical, Shimadzu, Japan) scans with Al Kα radiation ($h\nu$ = 1253.6 eV) was used to analyze the chemical bonding and elements of PEI-SBA-15 and Cu-imprinted PEI-SBA-15.

3.1.4. Cu(II) selectivity experiments

Cu(II) sorption experiments were performed under batch conditions to characterize PEI-SBA-15 and Cu-PEI-SBA-15 in Cu(II) sorption. The desired concentration of Cu(II) solution was prepared by diluting a stock solution (0.1

M), which was prepared from the copper(II) chloride dihydrate ($CuCl_2 \cdot 2H_2O$, EP grade, Duksan Pure Chemicals). All of the batch experiments were performed at 30°C in triplicate.

pH experiments were performed with 50 mL polypropylene conical tubes containing 30 mL solutions of PEI-SBA-15 (adsorbent dose = 1 g/L) and Cu(II) ions (initial concentration = 1000 μM), which were shaken in a shaking incubator at 120 rpm. Then, 0.1 M NaOH and 0.1 M HCl solutions were used to adjust the pH of the solution from 2 to 5. After reaction for 24 h, the samples were collected and filtered through a 0.45-μm membrane filter. The Cu(II) concentration was analyzed using inductively coupled plasma optical emission spectrometry (iCAP 7200 ICP-OES Duo, Thermo Fisher Scientific, Waltham, MA, USA). The Cu(II) sorption capacity (q, μmol/g) can be calculated with the following equation:

$$q = \frac{C_i - C_f}{C_a} \tag{3.1}$$

where C_i is the Cu(II) concentration in the aqueous phase before sorption reaction, C_f is the Cu(II) concentration in the aqueous phase after sorption reaction, and C_a is the adsorbent dose.

Cu(II) selectivity experiments were performed in multinary solutions containing binary metals, including Cu(II), Pb(II), Zn(II), Ni(II), and Co(II).

The multinary metal solutions (each metal concentration = 200 μM) were prepared with $CuCl_2 \cdot 2H_2O$, lead (II) chloride ($PbCl_2$, ≥ 98%), zinc (II) chloride ($ZnCl_2$, ≥ 98%), nickel (II) chloride hexahydrate ($NiCl_2 \cdot 6H_2O$, ≥ 96%), and cobalt (II) chloride hexahydrate ($CoCl_2 \cdot 6H_2O$, ≥ 95%). The solution pH was adjusted to 5 with 0.1 M HCl and 0.1 M NaOH solutions. Cu(II) selectivity experiments were performed under batch conditions (adsorbent dose = 1 g/L). First, 30 mg of each adsorbent (PEI-SBA-15 and Cu-imprinted PEI-SBA-15) was added to 50-mL conical tubes, containing 30 mL of the multinary metal solution. The solutions were shaken in a shaking incubator for 6 h at 120 rpm. After reaction, the samples were collected and filtered through the membrane filter. The metal concentration was analyzed using ICP-OES. Following the same procedures as for the divalent metal ions, Cu(II) selectivity experiments were conducted in multinary solutions containing Cu(II) ions along with trivalent/tetravalent metal ions (Cr(III), Al(III), and Zr(IV)). The multinary metal solutions (each metal concentration = 200 μM) were prepared with $CuCl_2 \cdot 2H_2O$, chromium (III) chloride hexahydrate ($CrCl_3 \cdot 6H_2O$, 96%), aluminum (III) chloride hexahydrate ($AlCl_3 \cdot 6H_2O$, 99%), and zirconium (IV) chloride ($ZrCl_4$, ≥99.5%).

From the selectivity experiments, the distribution coefficients for metal ions (k_d) can be determined using the following equations:

$$k_{d,copper} = \frac{q_{Cu}}{C_f^{Cu}} \quad (3.2)$$

$$k_{d,metals} = \frac{\sum q_{metal}}{\sum C_f^{metal}} \quad (3.3)$$

Based on the distribution coefficients, the Cu(II) selectivity (α) and relative Cu(II) selectivity (α') can be calculated using the following relationships:

$$\alpha = \frac{k_{d,copper}}{k_{d,metals}} \quad (3.4)$$

$$\alpha' = \frac{\alpha_{Cu-PEI-SBA-15}}{\alpha_{PEI-SBA-15}} \quad (3.5)$$

Cu(II) sorption to Cu-imprinted PEI-SBA-15 was performed as a function of reaction time (initial Cu(II) concentration of 1000 μM, adsorbent dose = 1 g/L). Additionally, Cu(II) sorption to Cu-imprinted PEI-SBA-15 was performed as a function of initial Cu(II) concentration (reaction time = 24 h, adsorbent dose = 1 g/L). All parameters in the models were obtained using SigmaPlot 10.0 program (Systat Software, Inc. San Jose, CA, USA). The model parameter values were determined by non-linear regression using error functions, such as the determination coefficient (R^2), chi-square coefficient (χ^2), and the sum of the absolute errors (SAE):

$$R^2 = \frac{\sum_{i=1}^{m}(y_c - \bar{y_e})_i^2}{\sum_{i=1}^{m}(y_c - \bar{y_e})_i^2 + \sum_{i=1}^{m}(y_c - y_e)_i^2} \quad (3.6)$$

$$\chi^2 = \sum_{i=1}^{m}\left[\frac{(y_e - y_c)^2}{y_c}\right]_i \quad (3.7)$$

$$SSE = \sum_{i=1}^{m}(y_e - y_c)_i^2 \quad (3.8)$$

3.2. Results and Discussion

3.2.1. Characteristics of PEI-SBA-15 and Cu-imprinted PEI-SBA-15

FE-SEM images and EDX patterns are shown in Fig. 3.4. FE-SEM images showed the smooth PEI-coated surface of PEI-SBA-15 (Fig. 3.4a) and the Cu-loaded surface of Cu-loaded PEI-SBA-15 (Fig. 3.4b). The surface of Cu-imprinted PEI-SBA-15 (Fig. 3.4c) was similar to that of PEI-SBA-15 because Cu(II) ions were removed from the surface of Cu-loaded PEI-SBA-15 during the imprinting process (crosslinking and elution). EDX patterns demonstrated the N peaks (Kα = 0.392 keV, Kβ = 0.400 keV) of PEI on PEI-SBA-15 (Fig. 3.4d), Cu-loaded PEI-SBA-15 (Fig. 3.4e), and Cu-imprinted PEI-SBA-15 (Fig.

3.4f), along with the Cu peak (Lα = 0.930 keV) on Cu-loaded PEI-SBA-15 (Fig. 3.4e). After the imprinting processes, the Cu(II) peak disappeared from Cu-imprinted PEI-SBA-15 (Fig. 3.4f).

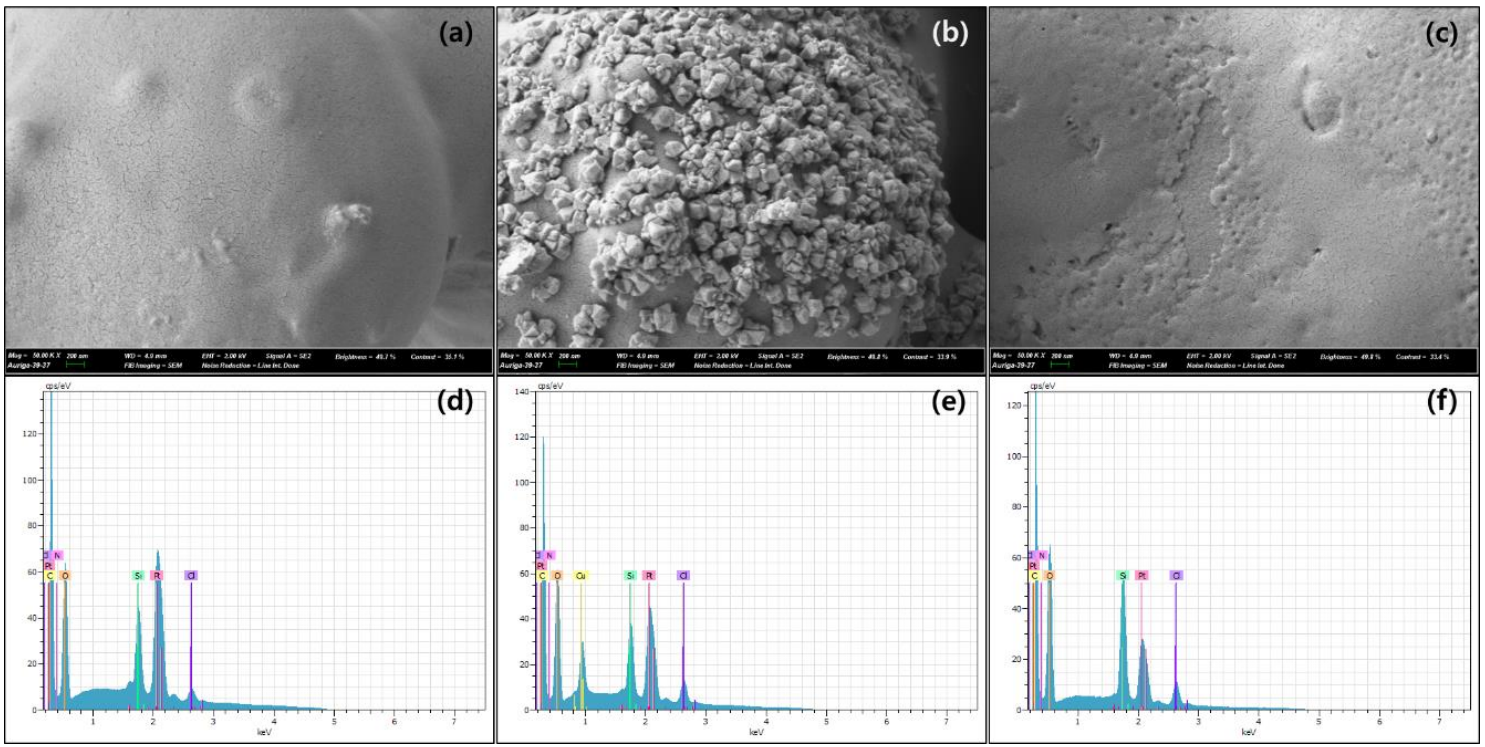

Figure 3.4. Field-emission scanning electron microscopy images (bar = 200 nm) and energy dispersive X-ray spectroscopy patterns of (a) PEI-SBA-15, (b) Cu-loaded PEI-SBA-15, and (c) Cu-imprinted PEI-SBA-15

FTIR spectra are presented in Fig. 3.5. In the spectra of SBA-15 (Fig. 3.5a), the peaks at 1049.51 and 805.51 cm^{-1} were attributed to stretching of siloxane (Si-O-Si) (Liu et al., 2011a). In the spectra of PEI-SBA-15 (Fig. 3.5b), new peaks to stretching of C-H (2937.32 cm^{-1}) and C-N (1439.44 cm^{-1}) appeared, indicating that PEI was well functionalized on the surface of SBA-15 (Shabanian et al., 2015). Even after cross-linking EGDE and loading Cu(II) on PEI-SBA-15, the spectra of Cu-loaded PEI-SBA-15 (Fig. 3.5c) had similar peaks to those of PEI-SBA-15. This result could be attributed to the fact that the characteristic peaks of EGDE were contributed from stretching of C-H at 2866 cm^{-1} and C-O-C at 1065 cm^{-1}, which are hindered by C-H stretch of PEI and Si-O-Si stretch of SBA-15 (Peng et al., 2014). The FTIR spectrum of Cu-imprinted PEI-SBA-15 (data not shown) was similar to that of PEI-SBA-15.

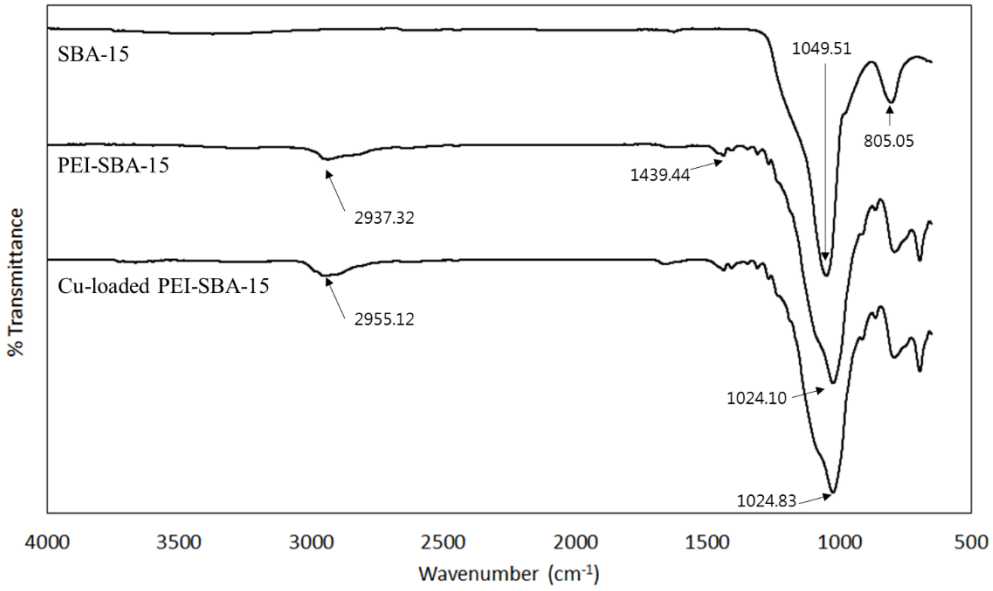

Figure 3.5. Fourier transform infrared spectroscopy measurements of SBA-15, PEI-SBA-15, and Cu-loaded PEI-SBA-15

XPS spectra are presented in Fig. 3.6. In wide scans of PEI-SBA-15, Cu-loaded PEI-SBA-15, and Cu-imprinted PEI-SBA-15, the peaks at the binding energies of 102 and 153 eV were attributed to Si 2p and Si 2s, respectively, whereas those at 284 and 532 eV were attributed to C 1s and O 1s, respectively. The peak of N 1s appeared due to functionalization of PEI on the surfaces of SBA-15. Additionally, the peak of Cl 1s was related to the use of (3-chloropropyl) trimethoxysliane as a bridge during the preparation of PEI-SBA-15. In a wide scan of Cu-loaded PEI-SBA-15, a Cu 2p peak appeared at 932 eV, whereas Cu 2p1/2 and Cu 2p3/2 peaks appeared at 953 and 933 eV, respectively, in a high-resolution scan of the Cu 2p region. However, the Cu 2p peak disappeared in a wide scan of Cu-imprinted PEI-SBA-15 due to the imprinting process. In high-resolution scans of Si 2p and O 1s regions, the peaks at 103.5 eV (Si 2p) and 533.0 eV (O 1s) were assigned to silicon dioxide (SiO_2); they are the characteristic peaks of SBA-15 (He et al., 1992). In the C 1s spectrum, the peaks of 285.2 and 286.6 eV were attributed to C-C and C-N bonds, respectively, from PEI (Yun et al., 2014). In the N 1s spectrum, three deconvoluted peaks could be assigned to N in tertiary amines (398.7 eV), -NH (400.0 eV), and -NH_2 in PEI (400.9 eV) (Wang and Li, 2015). The C 1s and N 1s spectra of PEI-SBA-15 demonstrated that PEI was well grafted onto the surfaces of SBA-15. In the N 1s spectrum of Cu-loaded PEI-SBA-15, a new peak, observed at 401.6 eV, could be assigned to Cu(II)-amine complexes,

which appeared due to chelation between Cu(II) ions and amine groups (Wang and Li, 2015).

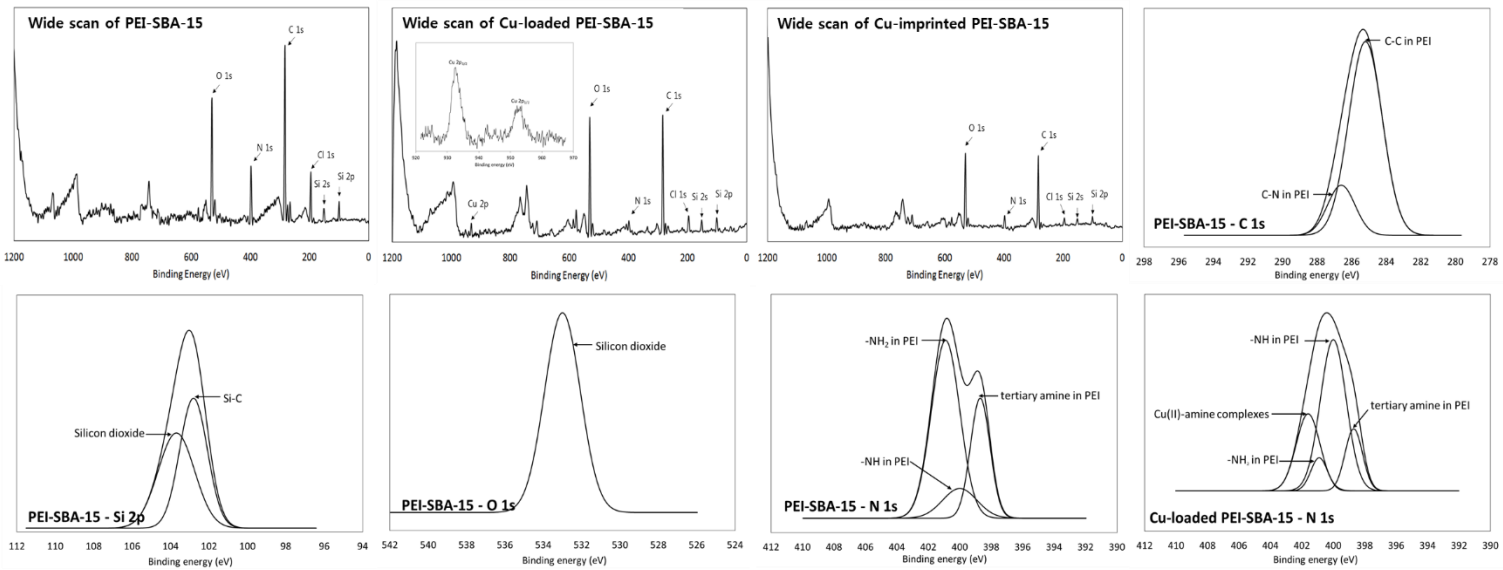

Figure 3.6. X-ray photoelectron spectroscopy spectra of PEI-SBA-15, Cu-loaded PEI-SBA-15, and Cu-imprinted PEI-SBA-15

3.2.2. Characteristics of PEI-SBA-15 and Cu-PEI-SBA-15 in Cu(II) selectivity

3.2.2.1. Cu(II) selectivity of PEI-SBA-15

Cu(II) sorption to PEI-SBA-15 at solution pH ranging from 2 to 5 is presented in Fig. 3.7. The maximum Cu(II) sorption was achieved at pH 5, with the Cu(II) sorption capacity of 83.71 μmol/g under the given experimental conditions. At pH 2 and 3, Cu(II) sorption to PEI-SBA-15 was negligible because the amine groups on PEI were well protonated into ammonium groups (Goon et al., 2010):

$$-NH_2 + H^+ \leftrightarrow -NH_3^+ \quad (3.9)$$

The formation of ammonium groups can prevent chelation between Cu(II) ions and amine groups. Also, electrostatic interaction becomes unfavorable because both Cu(II) ions and ammonium groups are positively charged (Wu et al., 2013). At pH 5, Cu(II) sorption to PEI-SBA-15 becomes favorable, occurring through chelation and electrostatic interactions (Banerjee and Chen, 2007). The chelating reaction of PEI with Cu(II) ions occurs as follows:

$$-NH_2 + Cu^{2+} \rightarrow -NH_2Cu^{2+} \quad (3.10)$$

At pH 5, the amine groups on PEI can be partially converted to deprotonated amine groups:

$$-NH_2 + OH^- \leftrightarrow -NH_2OH^- \quad (3.11)$$

Thus, Cu(II) ions can also be adsorbed on deprotonated moieties of amine groups via electrostatic interactions:

$$-NH_2OH^- + Cu^{2+} \leftrightarrow -NH_2OH^- \cdots Cu^{2+} \quad (3.12)$$

Based on these pH experiments, further Cu(II) sorption experiments were conducted at pH 5.

Selectivity experimental results of PEI-SBA-15 in multinary solutions containing divalent metal ions are provided in Table 3.1. Among the divalent ions in multinary solutions, Cu(II) showed the highest sorption capacity, of 40.79 μmol/g. This result could be explained by the Irving−Williams series, which refers to the relative stabilities of metal complexes formed by transition metal ions (Kandanapitiye et al., 2015). According to the Irving–Williams series, Cu(II) has higher metal complex stability than other divalent metal ions (Henry et al., 2004). The Cu(II) selectivity values were in the range of 1.19 to 22.79, with the highest value for Cu(II)/Pb(II). Overall, the Cu(II) selectivity for Cu(II)/Me(II) was calculated to be 2.81. Note that 'Me(II)' indicates all divalent ions in multinary solutions excluding Cu(II) ions.

Selectivity experimental results of PEI-SBA-15 in multinary solutions containing trivalent/tetravalent metal ions are presented in Table 3.2. The Cu(II) sorption capacity was 11.04 μmol/g, which was slightly higher than those of Cr(III) and Zr(IV), but lower than that of Al(III). The Cu(II) selectivity values were in the range of 0.57 to 1.19, with the highest value for Cu(II)/Zr(IV). The Cu(II) selectivity for Cu(II)/Me(III-IV) was determined to be 0.86 (Me(III-IV) = all trivalent and tetravalent ions in multinary solutions), indicating that Cu(II) sorption to PEI-SBA-15 was not selective in the presence of trivalent or tetravalent ions. It is known that the charge to radius ratio (Z/r) is directly related to the sorption capacity of cationic metal ions (Wu and Zhou, 2009; Da'na and Sayari, 2012). The Z/r ratio of Cu(II) is 2.74, which is lower than those of trivalent and tetravalent ions (Cr(III) = 4.84, Al(III) = 5.66, and Zr(IV) = 5.56).

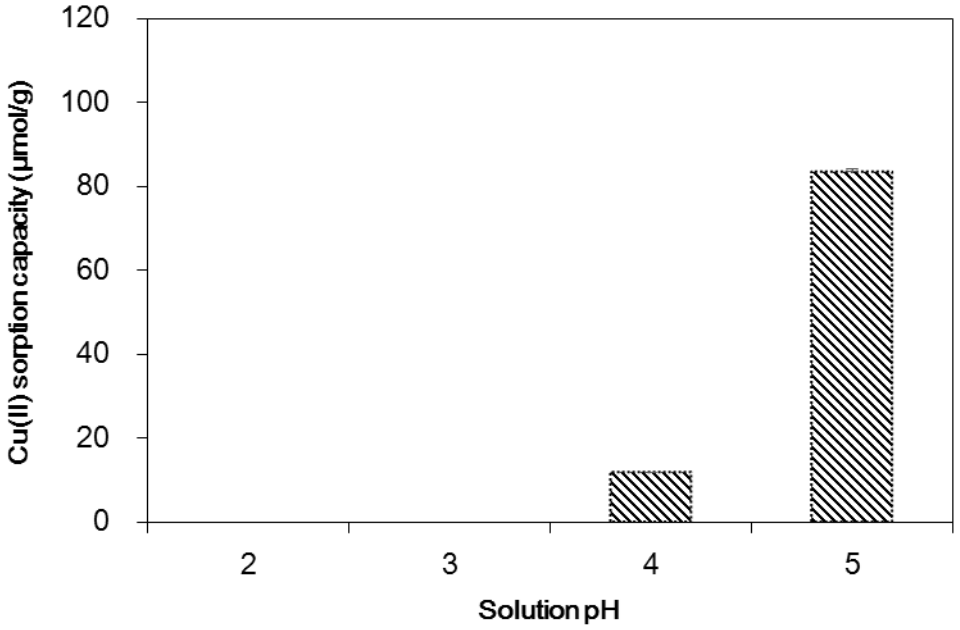

Figure 3.7. Cu(II) sorption to PEI-SBA-15 at solution pH ranging from 2 to 5

Table 3.1. Comparison of Cu(II) selectivity between PEI-SBA-15 and Cu-imprinted PEI-SBA-15 in multinary solutions containing divalent ions

Metal ion	PEI-SBA-15			Cu-imprinted PEI-SBA-15*			
	q (μmol/g)	k_d (L/g)	α	q (μmol/g)	k_d (L/g)	α	α'
Cu(II)	40.788±0.309	0.256±0.002	-	42.514±4.132	0.271±0.033	-	-
Pb(II)	2.223±2.223	0.011±0.011	22.79	2.703±2.703	0.014±0.014	19.70	0.86
Zn(II)	24.321±2.357	0.139±0.015	1.85	0±0	0±0	∞	∞
Ni(II)	14.372±0.068	0.077±0.000	3.31	0±0	0±0	∞	∞
Co(II)	26.027±0.509	0.150±0.003	1.19	0±0	0±0	∞	∞

* Note that the values were obtained from the experiments using Cu-imprinted poly(ethyleneimine)-grafted mesoporous silica SBA-15 (Cu-imprinted PEI-SBA-15) prepared at a [Cl-]/[Cu(II)] ratio of 500.

Table 3.2. Comparison of Cu(II) selectivity between PEI-SBA-15 and Cu-imprinted PEI- SBA-15 in multinary solutions containing trivalent/tetralent ions

Metal ion	PEI-SBA-15			Cu-imprinted PEI-SBA-15*			
	q (μmol/g)	k_d (L/g)	α	q (μmol/g)	k_d (L/g)	α	α'
Cu(II)	11.043±2.527	0.059±0.014	-	56.712±0.088	0.396±0.001	-	-
Al(III)	18.694±8.022	0.105±0.049	0.57	41.671±3.208	0.264±0.026	1.50	2.63
Cr(III)	10.13±9.333	0.056±0.052	1.10	8.251±2.626	0.043±0.014	9.20	8.36
Zr(IV)	9.383±9.044	0.052±0.050	1.19	12.644±2.669	0.068±0.015	5.87	4.93

Note that the values were obtained from the experiments using Cu-imprinted PEI-SBA-15 prepared at a $[Cl^-]/[Cu(II)]$ ratio of 500.

3.2.2.2. Enhancement of Cu(II) loading on PEI-SBA-15

The effect of the [Cl^-]/[Cu(II)] ratio on Cu(II) loading on the PEI-SBA-15 is presented in Table 3.3. The Cu(II) loading on the PEI-SBA-15 was enhanced as the [Cl^-]/[Cu(II)] ratio increased. At a ratio of 2, the Cu(II) loading capacity was 76.66 μmol/g. At ratios of 200 and 500, Cu(II) loading capacity increased to 154.05 and 140.25 μmol/g, respectively. This trend could be explained based on the following equilibrium constant (K_{eq}) and separation factors ($\alpha_{Cu/H}$), which were modified from Sengupta and Zhu (1992):

$$K_{eq} = \frac{\left[\overline{PEI\text{-}Cu^{2+}}\right][H^+]}{\left[\overline{PEI\text{-}H}\right][Cu^{2+}][Cl^-]} \qquad (3.13)$$

$$\alpha_{Cu/H} = \frac{\left[\overline{PEI\text{-}Cu^{2+}}\right][H^+]}{\left[\overline{PEI\text{-}H}\right][Cu^{2+}]} \qquad (3.14)$$

where $\left[\overline{PEI\text{-}Cu^{2+}}\right]$ and $\left[\overline{PEI\text{-}H}\right]$ are the molar concentrations of Cu(II) and H^+ on PEI, respectively. $[H^+]$, $[Cu^{2+}]$, and $[Cl^-]$ are the molar concentrations of the ion species in the aqueous phase. Combining Eq. (3.11) and Eq. (3.12), we have

$$\alpha_{Cu/H} = K_{eq}[Cl^-] \qquad (3.15)$$

According to Eq. (3.10), the Cu(II) loading on PEI-SBA-15 can be enhanced with an increase in [Cl^-] concentration because K_{eq} is constant.

Compared with [Cl^-]/[Cu(II)] ratios of 200 and 500, however, the Cu(II) loading capacity decreased by a ratio of 1000. This trend could be attributed to the proportion of $CuCl^+$ in Cu(II) ion species increasing as the ratio increased. According to a calculation with visual MINTEQ (ver. 3.1, KTH, Sweden) in Fig. 3.6, 88.7% of Cu(II) exists as Cu^{2+} at a ratio of 200, whereas 10.5% was in the form of $CuCl^+$. At a ratio of 1000, 61.0% of Cu(II) exists as Cu^{2+}, whereas 34.7% was in the form of $CuCl^+$. Compared with Cu^{2+}, $CuCl^+$ has lower electrostatic attraction with PEI, resulting in the lower Cu(II) loading on the PEI-SBA-15 at higher [Cl^-]/[Cu(II)] ratios. Similar findings were reported by Chanda and Rempel (1997), who examined the effects of [Cl^-]/[Cr(III)] ratio on the sorption Cr(III) on PEI-coated silica. They showed that Cr(III) loading on PEI-coated silica increased as the [Cl^-]/[Cr(III)] ratio increased from 0 to 100 and then decreased slightly with an increase of the ratio from 100 to 500.

Table 3.3. Effect of [Cl^-]/[Cu(II)] ratio on Cu(II) loading on PEI-SBA-15

[Cl^-]/[Cu(II)]	2	50	100	200	500	1000
Cu(II) loading (μmol/g)	76.66±0.63	80.10±10.25	126.41±4.71	154.05±14.64	140.25±11.08	134.35±13.55

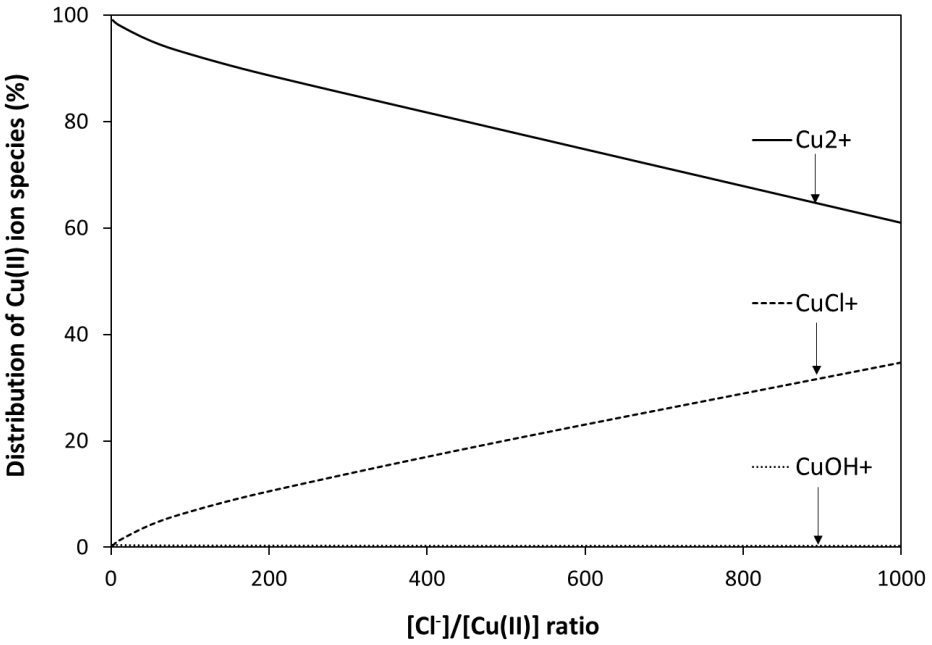

Figure 3.8. Effect of $[Cl^-]/[Cu(II)]$ ratio on the distribution of Cu(II) ion species calculated using visual MINTEQ

3.2.2.3. Enhancement of Cu(II) selectivity in Cu-imprinted PEI-SBA-15

Selectivity experimental results of Cu-imprinted PEI-SBA-15, which were prepared under various synthetic conditions ($[Cl^-]/[Cu(II)]$ ratio ranging from 2 to 1000), are presented in Fig. 3.9. In the multinary solutions containing divalent ions, the Cu(II) sorption tended to increase with an increase of the $[Cl^-]/[Cu(II)]$ ratio from 2 to 500 and then decreased at a ratio of 1000 (Fig. 3.9a). At ratios of 2–500, the sorption of Zn(II), Ni(II), and Co(II) was negligible. Under the given experimental conditions (molar concentrations of divalent ions = 200 μM; pH = 5), the Cu(II) sorption capacity was highest at a ratio of 500. The Cu(II) selectivity (Cu(II)/Me(II)) increased with an increase of the ratio, from 2 to 500. At a ratio of 500, Cu(II) sorption to Cu-imprinted PEI-SBA-15 was highest (42.51 μmol/g) among the divalent ions. The Cu(II) selectivity was 19.70 for Cu(II)/Pb(II) and unlimited for Cu(II)/Zn(II), Cu(II)/Ni(II), and Cu(II)/Co(II) (Table 1). Overall, the Cu(II) selectivity for Cu(II)/Me(II) was calculated to be 79.62, indicating that Cu(II) selectivity improved greatly in Cu-imprinted PEI-SBA-15.

In the multinary solutions containing Cu(II) along with trivalent/tetravalent ions, the Cu(II) sorption increased with an increase in the ratio from 2 to 500 and then dropped at a ratio of 1000 (Fig. 3.9b). Under the given experimental

conditions (molar concentrations of trivalent/tetravalent ions = 200 μM; pH = 5), the Cu(II) sorption capacity was highest at a ratio of 500. The Cu(II) selectivity (Cu(II)/Me(III/IV)) also increased with an increase in the ratio from 2 to 500. At a ratio of 500, Cu(II) sorption to Cu-imprinted PEI-SBA-15 was highest (56.71 μmol/g) among the metal ions. The Cu(II) selectivities for Cu(II)/Al(III), Cu(II)/Cr(III), and Cu(II)/Zr(IV) were 1.50, 9.12, and 5.87, respectively (Table 2). Overall, the Cu(II) selectivity for Cu(II)/Me(III-IV) was determined to be 3.40, indicating that Cu(II) sorption to Cu-imprinted PEI-SBA-15 was selective in the presence of trivalent and tetravalent ions.

The Cu(II) selectivity of Cu-imprinted PEI-SBA-15 could be enhanced through its preparation under high $[Cl^-]/[Cu(II)]$ ratios. In the multinary solution conditions, the selective Cu(II) removal of Cu-imprinted PEI-SBA-15, prepared at a ratio of 500, was far higher than that of non-imprinted PEI-SBA-15. In the presence of divalent ions, the relative selectivity values (α') for Cu(II)/Zn(II), Cu(II)/Ni(II), and Cu(II)/Co(II) were unlimited, whereas the relative selectivity for Cu(II)/Pb(II) was 0.86 (Table 1). Overall, the relative selectivity (α') for Cu(II) in the multinary solution containing divalent ions was 29.24. The relative Cu(II) selectivity of Cu(II)-imprinted silica in binary solution (Cu(II)/Ni(II) = 31.65–50.32, Cu(II)/Zn(II) = 20.57–240) reported in the literature is presented in Table 4. In solutions of trivalent and tetravalent

ions, the relative selectivity values (α') for Cu(II)/Al(III), Cu(II)/Cr(III), and Cu(II)/Zr(IV) were 2.63, 8.36, and 4.93, respectively (Table 2). Overall, the relative selectivity (α') for Cu(II) in the multinary solution containing trivalent and tetravalent ions was 3.96.

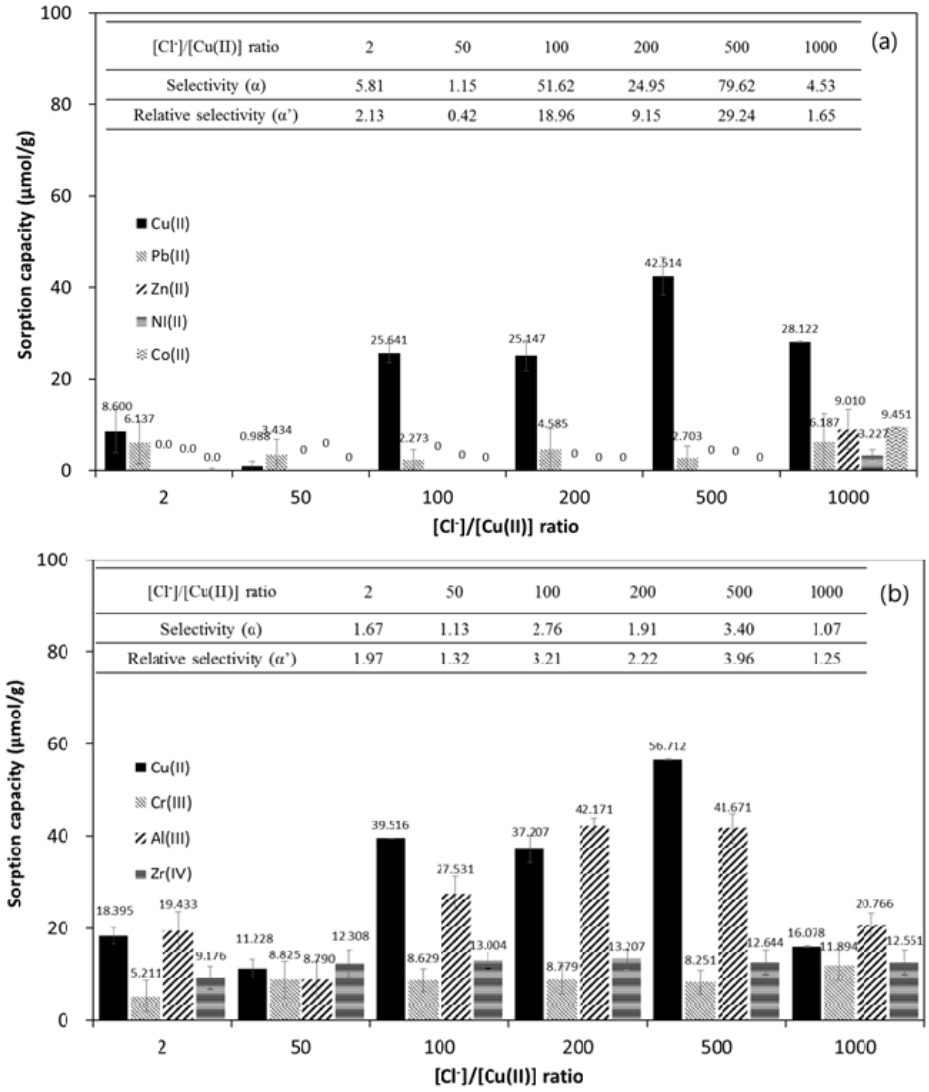

Figure 3.9. Cu(II) selectivity experiments of Cu-imprinted PEI-SBA-15 prepared under various synthetic conditions ([Cl$^-$]/[Cu(II)] ratio from 2 to 1000): (a) Cu(II) sorption capacity and selectivity in divalent ions and (b) Cu(II) sorption capacity and selectivity in trivalent and tetravalent ions.

3.2.2.4. Kinetic and equilibrium sorption model analyses

Cu-imprinted PEI-SBA-15 prepared at a ratio of 500 was used for Cu(II) sorption experiments. The data from effect of contact time on copper removal of PEI-SBA-15 experiment was fitted (Fig. 3.10a) to the following nonlinear equations of pseudo first-order, pseudo second-order, and Elovich kinetic models (Sen Gupta and Bhattacharyya, 2011):

$$\mathrm{q}_t = q_e[1 - \exp(-k_1 t)] \qquad (3.16)$$

$$q_t = \frac{k_2 {q_e}^2 t}{1 + k_2 q_e t} \qquad (3.17)$$

$$q_t = \frac{1}{\beta}\ln(\alpha \cdot \beta) + \frac{1}{\beta}\ln(t) \qquad (3.18)$$

where q_t is the amount of adsorbed copper per unit mass of absorbent at time t (μmol/g), and q_e is the amount of adsorbed copper per unit mass of absorbent at equilibrium (μmol/g). k_1 is the pseudo first-order rate constant (1/h), k_2 is the pseudo second-order rate constant (g/μmol·h), α is the initial adsorption rate constant (μmol/g·h), and β is the Elovich adsorption constant (g/μmol).

The kinetic model parameters are provided in Table 3.4. Cu(II) sorption to Cu-imprinted PEI-SBA-15 was a relatively fast process, reaching an equilibrium at 6 h of reaction time. A pseudo second-order model provided the

best fit to the kinetic data, with parameter values of q_e = 99.78 μmol/g and k_2 = 0.01 g/μmol/h.

The Cu(II) sorption data as a function of initial Cu(II) concentration in Cu-imprinted PEI-SBA-15 (Fig. 3.10b) were analyzed by equilibrium isotherm models, including the Langmuir, Freundlich, and Redlich–Peterson models (Foo and Hameed, 2010):

$$q_e = \frac{Q_m K_L C_e}{1 + K_L C_e} \qquad (3.19)$$

$$q_e = K_F {C_e}^n \qquad (3.20)$$

$$q_e = \frac{K_R C_e}{1 + a_R C_e^g} \qquad (3.21)$$

where Q_m is the maximum mass of adsorbed copper per unit mass of adsorbent (removal capacity, μmol /g), and C_e is the concentration of copper in the aqueous solution at equilibrium (μmol/L). K_L is the Langmuir constant related to the binding energy (L/g), K_F is the distribution coefficient (L/ μmol), n is the Freundlich constant, K_R is the Redlich-Peterson constant, a_R is the Redlich–Peterson constant related to the affinity of the binding sites, and g is the Redlich–Peterson constant related to the adsorption intensity.

The equilibrium model parameters are provided in Table 3.5. The Redlich–Peterson model gave the best fit to the equilibrium data with parameter values of g = 0.977, K_R = 0.059 L/g, and a_R = 1.08E-4 L/μmol. The maximum Cu(II) sorption capacity was determined to be 675.23 μmol/g from the Langmuir model.

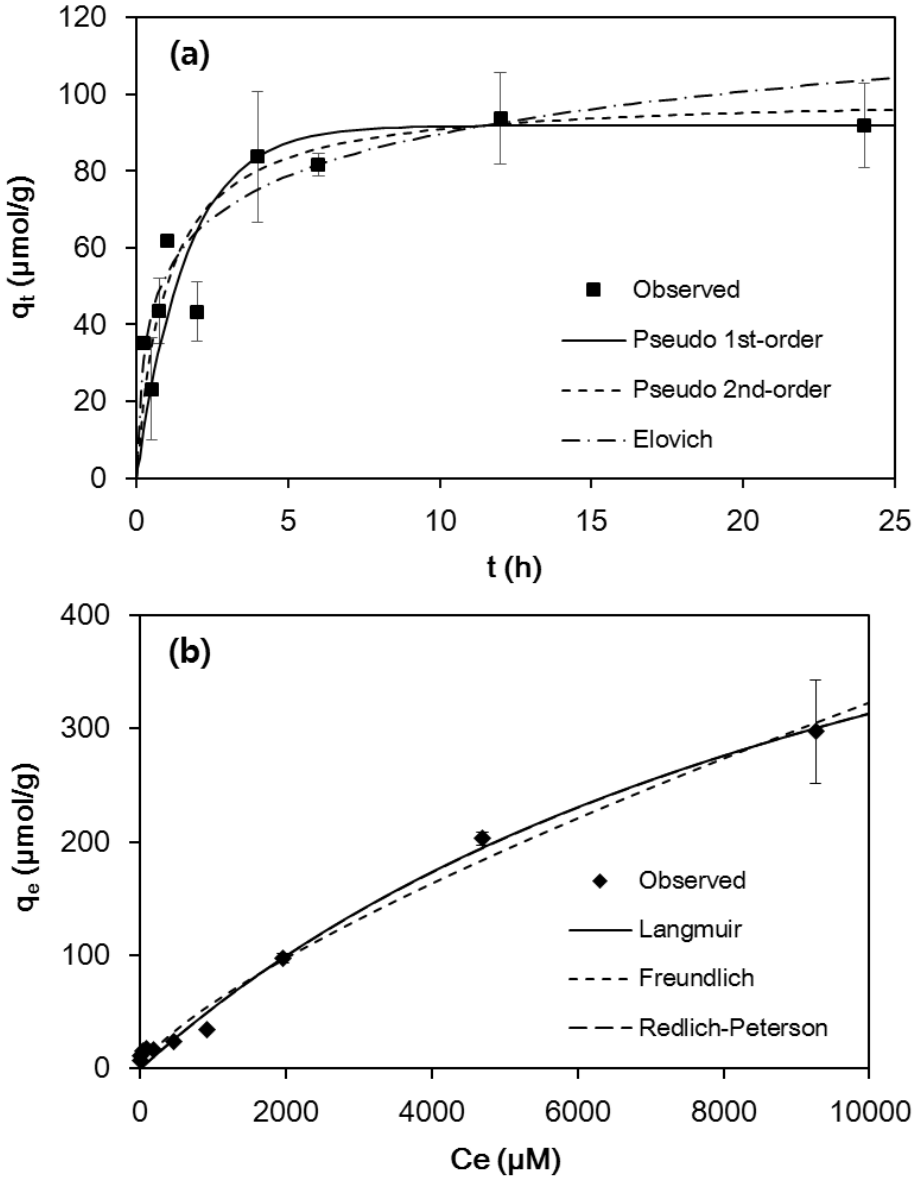

Figure 3.10. Cu(II) sorption to Cu-imprinted PEI-SBA-15: (a) kinetic sorption model analysis and (b) equilibrium isotherm model analysis.

Table 3.4. Kinetic model parameters

Adsorbent	Pseudo first order					Pseudo second order						Elovich				
	q_e (μmol/g)	k_1 (1/h)	R^2	χ^2	SSE	q_e (μmol/g)	k_2 (g/μmol/h)	h	R^2	χ^2	SSE	α (μmol/g/h)	β (g/μmol)	R^2	χ^2	SSE
Cu-PEI-SBA-15	84.0	0.892	0.832	1.6E+3	3.5E+1	91.4	0.014	119.7	0.838	6.1E+5	7.5E+3	574.5	0.072	0.663	2.0E+3	3.9E+1

Table 3.5. Equilibrium isotherm model parameters

Adsorbent	Freundlich						Langmuir					Redlich-Peterson						
	K_F (L/g)	n	q_m (μmol/g)	R^2	χ^2	SSE	Q_m (μmol/g)	K_L (L/mmol)	R^2	χ^2	SSE	K_R (L/g)	a_R (1μ/mol)	K_R/a_R (μmol/g)	g	R^2	χ^2	SSE
Cu-PEI-SBA-15	2.424	0.474	550.783	0.914	74.69	7677	321.832	1.88.E-04	0.943	69.96	5074	0.031	6.03E-7	5.2E+4	2.654	0.968	0.08	3E-3

Chapter 4 Synthesis and characterization of Cu-imprinted PEI coated silica gel via surface imprinting

In this chapter, Cu(II) imprinted PEI coated silica gel (Cu-PEI-silica gel) were prepared for selective Cu(II) sorption from aqueous solutions. To enhance the productivity of Cu-imprinted material, Cu(II) imprinting were perfomed through PEI coating on silica gel (PEI-silica gel). Then, selective Cu(II) sorption sites were increased through imprinting processes (crosslinking and elution) on Cu-loaded PEI-silica gel. Selective experiments were performed using PEI-silica gel and Cu-PEI-silica gel. In multinary solutions containing divalent ions, such as Cu(II), Pb(II), Zn(II), Ni(II), and Co(II), the Cu(II) selectivities were ∞, 46.79, 11.55, and 28.85 over Pb(II), Zn(II), Ni(II), and Co(II); the relative Cu(II) selectivities for Cu-PEI-silica gel over PEI-silica gel were ∞, 4.38, 3.37, and 3.06. In multinary solutions containing Cu(II) along with trivalent and tetravalent ions, such as Al(III), Cr(III), and Zr(IV), the Cu(II) selectivities were 0.73, 3.58, and ∞ over Al(III), Cr(III), and Zr(IV); the relative Cu(II) selectivities for Cu-PEI-silica gel over PEI-silica gel were 2.17, 5.56, and 1. In this study, we demonstrated that the Cu(II) imprinted material well prepared with polymer coating procedure.

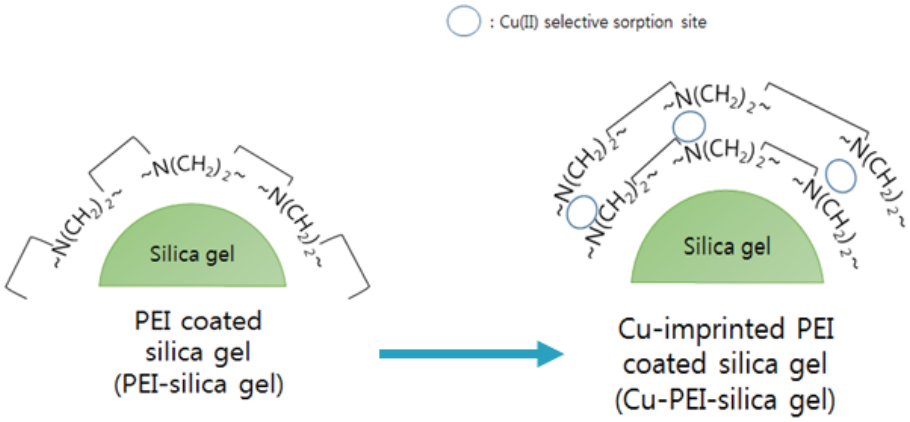

Figure 4.1. Graphical abstract of chapter 4

4.1. Materials and Methods

4.1.1. Synthesis of Cu-imprinted PEI coated silica gel

Schematic diagram of PEI-silica gel and Cu-PEI-silica gel preparation are shown at Fig. 4.2-3. All chemicals used in the experiments were purchased from Sigma Aldrich (Saint Louis, MO, USA) unless stated otherwise. Cu(II) imprinted PEI coated silica gel preparation method oriented from the method of PEI coated silica gel preparation (Chanda and Rempel, 1995). Firstly, 200 g of silica gel (35-60 mesh) was poured into 500 mL of 4% $CuCl_2 \cdot 2H_2O$ solution. Silica gel contained $CuCl_2 \cdot 2H_2O$ solution was evaporated using rotary evaporator (HS-2005V, Hanshin, Korea) to prepare Cu(II) coated silica gel. 40 g of PEI solution (50% in H_2O) was poured and agitated in 400 mL of isopropanol to prepare PEI/isopropanol solution with peddle stir. 100 g of Cu(II) coated silica gel was added into the PEI/isopropanol solution and agitated for 3 h to coat PEI on Cu(II) coated silica surface by making PEI-Cu(II) complex. 0.1 mole of $CuCl_2 \cdot 2H_2O$ was added into the upper resultant to load Cu(II) on the amine group of PEI and agitated for 3 h. The resultant was decanted off and washed with isopropanol to remove unreacted PEI and Cu(II). To cross-link and fix the Cu(II) adsorbed sites, 400 mL of 10 % glutaraldehyde in isopropanol was poured and reacted into the upper resultant for overnight by agitation. Prepared Cu(II) loaded Cu-imprinted PEI coated

silica gel washed with isopropanol for several times to remove unreacted glutaraldehyde. To elute loaded Cu(II), the upper resultant reacted with 5 L of 0.1 HCl twice. Cu(II) imprinted PEI coated silica was washed with DI water to neutralize protonated PEI. The resultant was filtered and dried at 60°C for overnight. After cooling, Cu-imprinted PEI coated silica gel (Cu-PEI-silica gel) was obtained. The non-imprinted PEI coated silica gel (PEI-silica gel) was also prepared without addition of 0.1 mole of $CuCl_2 \cdot 2H_2O$.

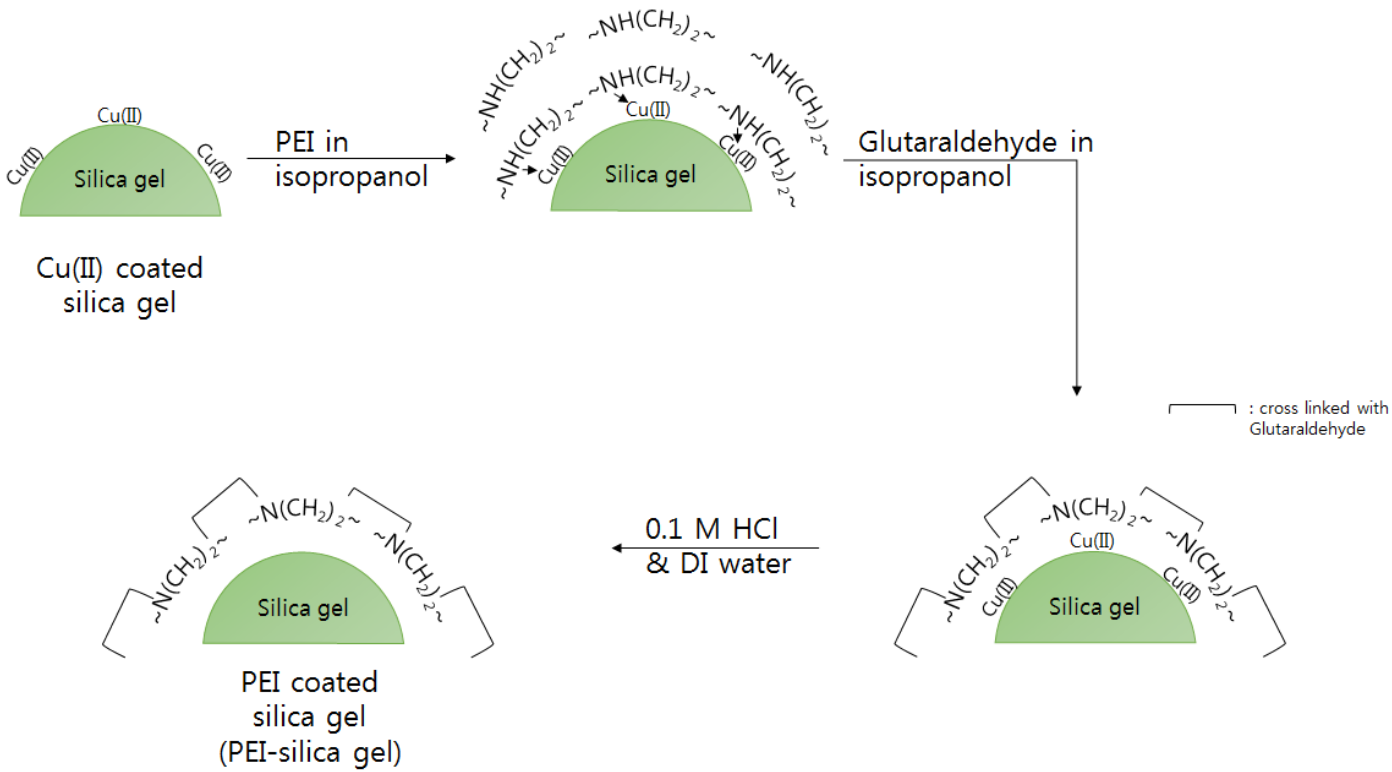

Figure 4.2. Schematic diagram of PEI-silica gel preparation

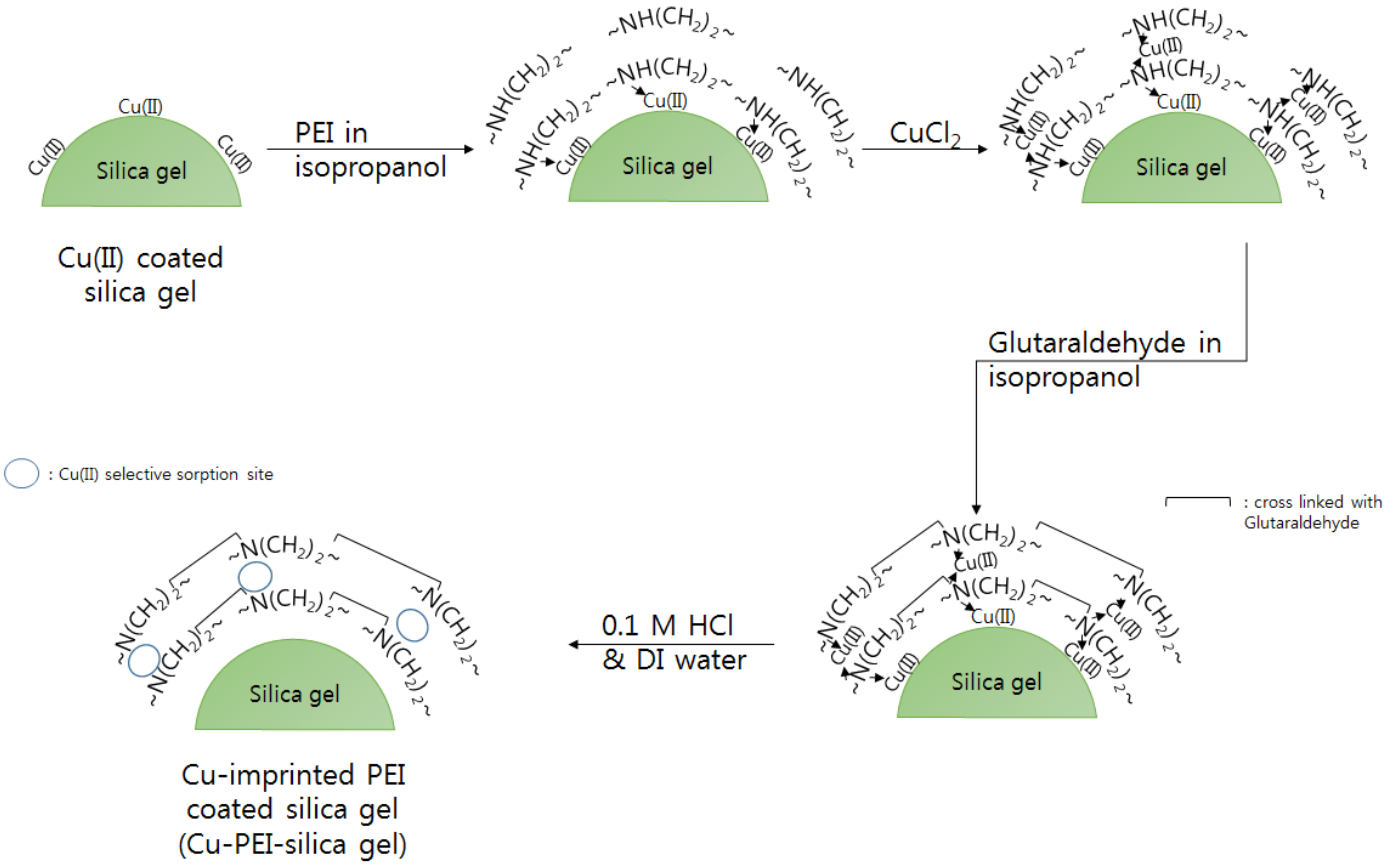

Figure 4.3. Schematic diagram of Cu-PEI-silica gel preparation

4.1.2. Characterization of PEI coated silica gel and Cu-imprinted PEI coated silica gel

PEI-silica gel and Cu-PEI-silica gel were characterized using several techniques. Field-emission scanning electron microscopy (FE-SEM, Supra 55VP, Carl Zeiss, Oberkochen, Germany) and energy-dispersive X-ray spectroscopy (EDX, AURIGA, Carl Zeiss) were used to analyze the surface morphology and elemental composition. Fourier-transform infrared (FTIR) spectroscopy (Nicolet 6700, Thermo Fisher Scientific, Waltham, MA, USA) was used to analyze the effect of PEI coating and ion imprinting on PEI-silica gel and Cu-PEI-silica gel.

4.1.3. Cu(II) selectivity experiments

Cu(II) sorption experiments were performed under batch conditions to characterize PEI-silica gel and Cu-PEI-silica gel in Cu(II) sorption. The desired concentration of Cu(II) solution was prepared by diluting a stock solution (0.1 M), which was prepared from the copper(II) chloride dihydrate ($CuCl_2 \cdot 2H_2O$, EP grade, Duksan Pure Chemicals). All of the batch experiments were performed at 30°C in triplicate.

pH experiments were performed with 50 mL polypropylene conical tubes containing 30 mL solutions of PEI-silica gel or Cu-PEI-silica gel (adsorbent dose = 3 g/L) and Cu(II) ions (initial concentration = 1000 μM), which were shaken in a shaking incubator at 120 rpm. Then, 0.1 M NaOH and 0.1 M HCl solutions were used to adjust the pH of the solution from 2 to 5. After reaction for 24 h, the samples were collected and filtered through a 0.45-μm membrane filter. The Cu(II) concentration was analyzed using inductively coupled plasma optical emission spectrometry (iCAP 7200 ICP-OES Duo, Thermo Fisher Scientific, Waltham, MA, USA). The Cu(II) sorption capacity (q, μmol/g) can be calculated with the following equation:

$$q = \frac{C_i - C_f}{C_a} \tag{4.1}$$

where C_i is the Cu(II) concentration in the aqueous phase before sorption reaction, C_f is the Cu(II) concentration in the aqueous phase after sorption reaction, and C_a is the adsorbent dose.

Cu(II) sorption to PEI-silica gel and Cu-PEI-silica gel were performed as a function of reaction time (initial Cu(II) concentration of 1000 μM, adsorbent dose = 3 g/L, initial pH = 5). Additionally, Cu(II) sorption to PEI-silica gel and Cu-PEI-silica gel was performed as a function of initial Cu(II) concentration (initial Cu(II) concentration = 100, 200, 500, 1000, 2000, 5000,

10000 μM, reaction time = 24 h, adsorbent dose = 3 g/L, initial pH = 5). All parameters in the models were obtained using SigmaPlot 10.0 program (Systat Software, Inc. San Jose, CA, USA). The model parameter values were determined by non-linear regression using error functions, such as the determination coefficient (R^2), chi-square coefficient (χ^2), and the sum of the absolute errors (SAE):

$$R^2 = \frac{\sum_{i=1}^{m}(y_c - \bar{y_e})_i^2}{\sum_{i=1}^{m}(y_c - \bar{y_e})_i^2 + \sum_{i=1}^{m}(y_c - y_e)_i^2} \quad (4.2)$$

$$\chi^2 = \sum_{i=1}^{m}\left[\frac{(y_e - y_c)^2}{y_c}\right]_i \quad (4.3)$$

$$SSE = \sum_{i=1}^{m}(y_e - y_c)_i^2 \quad (4.4)$$

Cu(II) selectivity experiments were performed in multinary solutions containing binary metals, including Cu(II), Pb(II), Zn(II), Ni(II), and Co(II). The multinary metal solutions (each metal concentration = 1000 μM) were prepared with $CuCl_2{\cdot}2H_2O$, lead (II) chloride ($PbCl_2$, ≥ 98%), zinc (II) chloride ($ZnCl_2$, ≥ 98%), nickel (II) chloride hexahydrate ($NiCl_2{\cdot}6H_2O$, ≥ 96%), and cobalt (II) chloride hexahydrate ($CoCl_2{\cdot}6H_2O$, ≥ 95%). The solution pH was adjusted to 5 with 0.1 M HCl and 0.1 M NaOH solutions. Cu(II) selectivity experiments were performed under batch conditions (adsorbent dose = 3 g/L).

Firstly, 90 mg of each adsorbent (PEI-silica gel and Cu-PEI-silica gel) was added to 50-mL conical tubes, containing 30 mL of the multinary metal solution. The solutions were shaken in a shaking incubator for 12 h at 120 rpm. After reaction, the samples were collected and filtered through the membrane filter. The metal concentration was analyzed using ICP-OES. Following the same procedures as for the divalent metal ions, Cu(II) selectivity experiments were conducted in multinary solutions containing Cu(II) ions along with trivalent/tetravalent metal ions (Cr(III), Al(III), and Zr(IV)). The multinary metal solutions (each metal concentration = 1 mM) were prepared with $CuCl_2{\cdot}2H_2O$, chromium (III) chloride hexahydrate ($CrCl_3{\cdot}6H_2O$, 96%), aluminum (III) chloride hexahydrate ($AlCl_3{\cdot}6H_2O$, 99%), and zirconium (IV) chloride ($ZrCl_4$, ≥99.5%).

From the selectivity experiments, the distribution coefficients for metal ions (k_d) can be determined using the following equations:

$$k_{d,copper} = \frac{q_{Cu}}{C_f^{Cu}} \tag{4.5}$$

$$k_{d,metals} = \frac{\sum q_{metal}}{\sum C_f^{metal}} \tag{4.6}$$

Based on the distribution coefficients, the Cu(II) selectivity (α) and relative Cu(II) selectivity (α') can be calculated using the following relationships:

$$\alpha = \frac{k_{d,copper}}{k_{d,metals}} \quad (4.7)$$

$$\alpha' = \frac{\alpha_{Cu-PEI-silca\ gel}}{\alpha_{PEI-silca\ gel}} \quad (4.8)$$

4.1.4. Fixed bed column breakthrough experiments

Fixed-bed column experiments were conducted to evaluate the dynamic behavior of Me(II) removal by PEI-silica gel and Cu-PEI-silica gel. Column experiments were conducted using a plexiglas column (column length = 10 cm; inner diameter = 2.5 cm) packed with PEI-silica gel and Cu-PEI-silica gel (porosity = 0.81). For column experiments, column was packed by the tap-fill method and connected to a high performance liquid chromatography pump (HPLC series II, Scientific Systems Inc., PA, USA) operating at a rate of 60 mL/h. Prior to the transport experiments, the packed column was flushed upward with >10 bed volume of deionized water until the column effluent was clear and steady-state flow was established. After stabilization, the injection solutions which have 10 mM of Cu(II), Zn(II), Ni(II), and Co(II) which is pH adjusted into 5 by 0.1 M HCl and 0.1 M NaOH. Injection introduced about 50 BV. Portions of the effluent were collected using an auto collector (Retriever

500, Teledyne, City of Industry, CA, USA) at regular intervals. The metal ion concentrations on collected effluents were measured with ICP-OES.

4.2. Results and Discussion

4.2.1. Characteristics of PEI-silica gel and Cu-PEI-silica gel

FE-SEM and digital images are shown in Fig. 4.4. From the digital images, PEI-silica gel has a light yellow color and Cu-PEI-silica gel has thicker yellow than PEI-silica gel. From the FE-SEM images, PEI-silica gel and Cu-PEI-silica gel had irregular shape. There has no specific difference between PEI-silica gel and Cu-PEI-silica gel.

Figure 4.4. FE-SEM images of PEI-silica gel and Cu-PEI-silica gel (bar = 100 µm, inset = digital image)

FTIR spectra are presented in Fig. 4.5. In the spectra of PEI-silica gel and Cu-PEI-silica gel, the peaks at 1058.9 – 1059.3 cm^{-1} and 799.6 – 800.8 cm^{-1} were attributed to stretching of siloxane (Si-O-Si) (Liu et al., 2011a). The peaks at 1653.5 – 1654.1 cm-1 could be attributed from N-H scissoring band (Wu et al., 2013). It is indicating that PEI was well functionalized on the surface of silica gel with imprinting or without imprinting. Even after glutaraldehyde cross-linking, the spectra of Cu-PEI-silica gel had similar peaks to those of PEI-Silica gel.

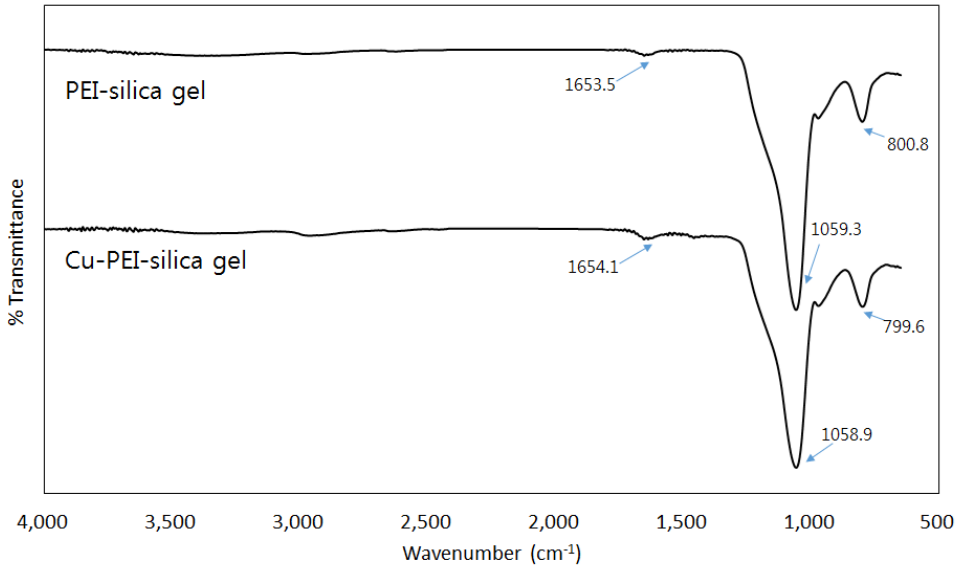

Figure 4.5. Fourier transform infrared spectroscopy measurements of PEI-silica gel and Cu-PEI-silica gel

4.2.2. Cu(II) sorption characteristics of PEI-silica gel and Cu-PEI-silica gel

The data from effect of initial pH on copper removal of PEI-silica gel and Cu-PEI-silica gel experiment are represented in Fig. 4.6. The maximum Cu(II) sorption was achieved at pH 5, with the Cu(II) sorption capacity of 14.64 ± 1.84 and 32.03 ±2.40 μmol/g from PEI-silica gel and Cu-PEI-silica gel. At pH 2 and 4, Cu(II) sorption to PEI-silica gel was negligible because the amine groups on PEI were well protonated into ammonium groups as PEI-SBA-15. However, Cu-PEI-silica gel showed much favorable Cu(II) sorption even initial pH 3. It is considered that the added processes on Cu(II) imprinting is not only Cu(II) selectivity enhance but also PEI coating enhance. By increasing pH into 5, Cu(II) sorption to PEI-silica gel and Cu-PEI-silica gel becomes favorable as PEI-SBA-15. Based on these pH experiments, further Cu(II) sorption experiments were conducted at pH 5.

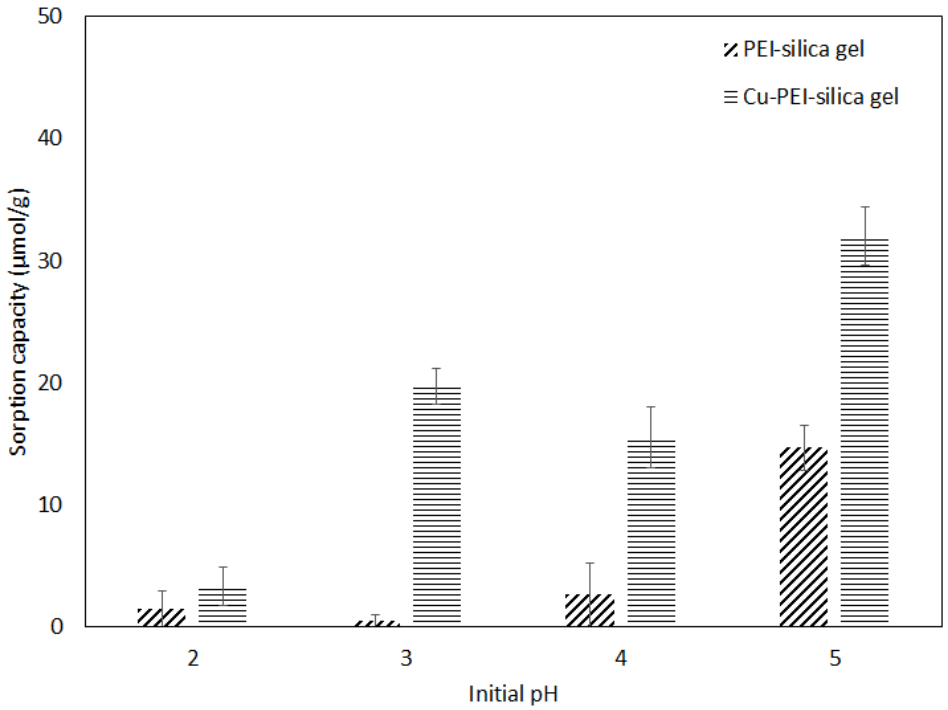

Figure 4.6. The result of effect of initial pH on copper removal by PEI-silica gel and Cu-PEI-silica gel

The data from effect of contact time on copper removal of PEI-silica gel and Cu-PEI-silica gel experiment was fitted (Fig. 4.7) to the following nonlinear equations of pseudo first-order, pseudo second-order, and Elovich kinetic models (Sen Gupta and Bhattacharyya, 2011):

$$q_t = q_e[1 - \exp(-k_1 t)] \qquad (4.9)$$

$$q_t = \frac{k_2 {q_e}^2 t}{1 + k_2 q_e t} \qquad (4.10)$$

$$q_t = \frac{1}{\beta}\ln(\alpha \cdot \beta) + \frac{1}{\beta}\ln(t) \qquad (4.11)$$

where q_t is the amount of adsorbed copper per unit mass of absorbent at time t (μmol/g), and q_e is the amount of adsorbed copper per unit mass of absorbent at equilibrium (μmol/g). k_1 is the pseudo first-order rate constant (1/h), k_2 is the pseudo second-order rate constant (g/μmol·h), α is the initial adsorption rate constant (μmol/g·h), and β is the Elovich adsorption constant (g/μmol).

The kinetic model parameters are provided in Table 4.1. Cu(II) sorption to PEI-silica gel reached an equilibrium at 3 h of reaction time. Cu(II) sorption to Cu-PEI-silica gel reached an equilibrium at 18 h of reaction time with higher sorption capacity. A Elovich model provided the best fit to the kinetic data.

The Cu(II) sorption data as a function of initial Cu(II) concentration in PEI-silica gel and Cu-PEI-silica gel (Fig. 4.8) were analyzed by equilibrium

isotherm models, including the Langmuir, Freundlich, and Redlich–Peterson models (Foo and Hameed, 2010):

$$q_e = \frac{Q_m K_L C_e}{1 + K_L C_e} \qquad (4.12)$$

$$q_e = K_F {C_e}^n \qquad (4.13)$$

$$q_e = \frac{K_R C_e}{1 + a_R C_e^g} \qquad (4.14)$$

where Q_m is the maximum mass of adsorbed copper per unit mass of adsorbent (removal capacity, μmol /g), and C_e is the concentration of copper in the aqueous solution at equilibrium (μmol/L). K_L is the Langmuir constant related to the binding energy (L/g), K_F is the distribution coefficient (L/ μmol), n is the Freundlich constant, K_R is the Redlich-Peterson constant, a_R is the Redlich–Peterson constant related to the affinity of the binding sites, and g is the Redlich–Peterson constant related to the adsorption intensity.

The equilibrium model parameters are provided in Table 4.2. The Redlich–Peterson model gave the best fit to the equilibrium data The maximum Cu(II) sorption capacities of PEI-silica gel and Cu-PEI-silica gel were determined to be 30.727 and 352.540 μmol/g from the Langmuir model.

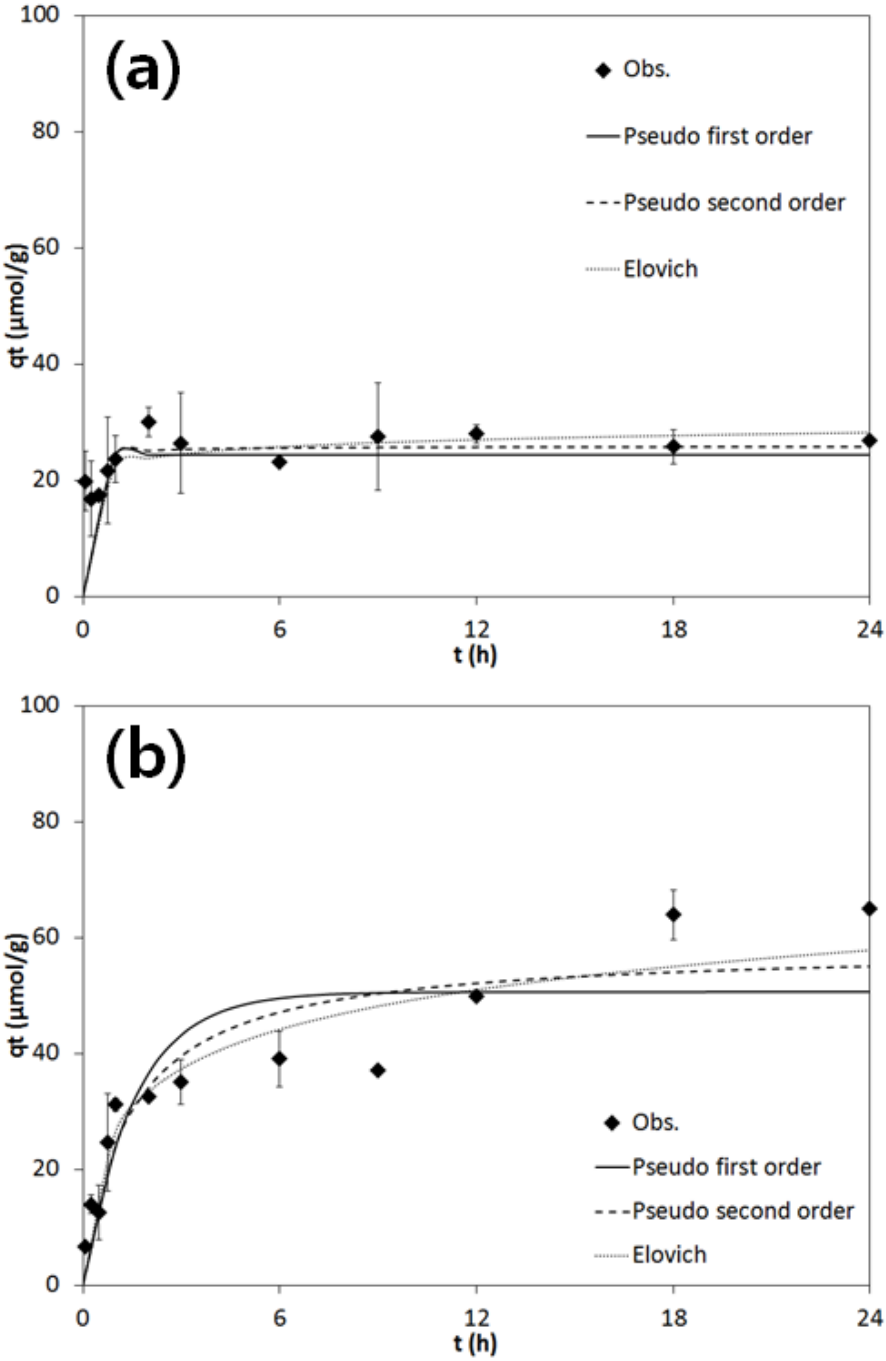

Figure 4.7. The kinetic models analysis results

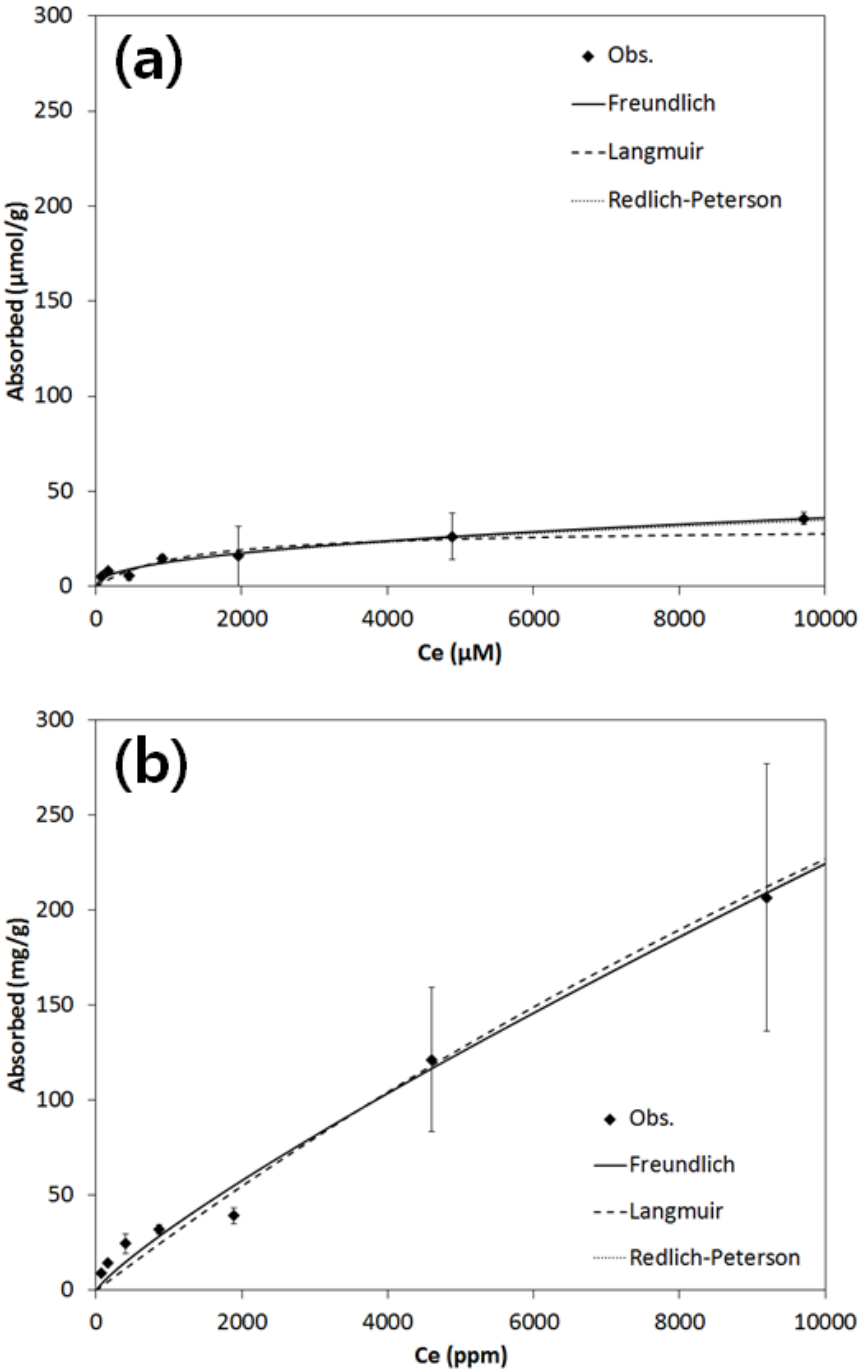

Figure 4.8. The equilibrium models analysis results

Table 4.1. Kinetic model parameters

Adsorbent	Pseudo first order					Pseudo second order						Elovich				
	qe (μmol/g)	k1 (1/h)	R2	χ2	SSE	qe (μmol/g)	k2 (g/μmol/h)	h	R2	χ2	SSE	α (μmol/g/h)	β (g/μmol)	R2	χ2	SSE
PEI-silica gel	24.407	17.030	0.756	1.8.E+02	8.7.E+00	25.893	0.624	1.0.E+01	0.838	1.2.E+02	5.7.E+00	571385.38	0.564	0.880	8.7.E+01	3.7.E+00
Cu-PEI-silica gel	50.611	0.638	0.819	8.9.E+02	2.4.E+01	58.212	0.012	8.5.E-03	0.883	5.8.E+02	1.7.E+01	144.64872	0.101	0.923	3.8.E+02	1.4.E+01

Table 4.2. Equilibrium isotherm model parameters

Adsorbent	Freundlich						Langmuir					Redlich-Peterson						
	K_F (L/g)	n	q_m (μmol/g)	R^2	χ^2	SSE	Q_m (μmol/g)	K_L (L/μmol)	R^2	χ^2	SSE	K_R (L/g)	a_R (1/μmol)	K_R/ a_R (μmol/g)	g	R^2	χ^2	SSE
PEI-silica gel	0.598	0.445	26.165	0.969	3.13	23.82	30.727	8.2.E-4	0.937	6.21	48.90	513.533	783.109	0.656	0.568	0.970	3.12	23.46
Cu-PEI-silica gel	0.096	0.842	119.196	0.986	17.93	458.10	352.540	1.0.E-4	0.981	23.63	625.17	0.264	2.203	0.120	0.172	0.986	18.34	462.35

Selectivity experimental results of PEI-silica gel and Cu-PEI-silica gel in multinary solutions containing divalent metal ions are provided in Table 4.3. Among the divalent ions in multinary solutions, Cu(II) showed the highest sorption capacity, 15.56 ± 1.82 and 51.07 ± 5.55 μmol/g from PEI-silica gel and Cu-PEI-silica gel. This result could be explained by the Irving−Williams series, which refers to the relative stabilities of metal complexes formed by transition metal ions (Kandanapitiye et al., 2015). According to the Irving–Williams series, Cu(II) has higher metal complex stability than other divalent metal ions (Henry et al., 2004). The Cu(II) selectivity values of PEI-silica gel were in the range of 3.42 to 10.68, with the highest value for Cu(II)/Zn(II). The Cu(II) selectivity values of Cu-PEI-silica gel were in the range of 11.55 to ∞, with the highest value for Cu(II)/Pb(II). Overall, the Cu(II) selectivity of PEI-silica gel and Cu-PEI-silica gel for Cu(II)/Me(II) was calculated to be 5.60 and 28.96 (relative selectivity = 5.17). Note that 'Me(II)' indicates all divalent ions in multinary solutions excluding Cu(II) ions.

Selectivity experimental results of PEI-silica gel and Cu-PEI-silica gel in multinary solutions containing trivalent/tetravalent metal ions are presented in Table 4.4. The Cu(II) sorption of PEI-silica gel and Cu-PEI-silica gel capacity were 8.27 ± 2.50 and 57.89 ± 1.73 μmol/g. The Al(III) sorption of PEI-silica gel and Cu-PEI-silica gel capacity were 22.76 ± 4.35 and 72.33 ± 7.73 μmol/g

which was slightly higher than Cu(II) sorption capacity. The Cr(III) sorption of PEI-silica gel and Cu-PEI-silica gel capacity were 13.22 ± 1.42 and 19.22 ± 3.53 μmol/g. Even Cr(III) sorption capacity of Cu-PEI-silica gel was higher than the value of PEI-silica gel, it became lower than Cu(II) sorption capacity. Zr(IV) was not adsorbed to both adsorbents. The Cu(II) selectivity for Cu(II)/Me(III-IV) of PEI-silica gel and Cu-PEI-silica gel were determined to be 0.69 and 2.11 (Me(III-IV) = all trivalent and tetravalent ions in multinary solutions, relative selectivity = 3.06). This results indicate that Cu(II) selectivity were increased by imprinting processes. However, Cu(II) selectivity of Cu-PEI-silica gel was not quite big value for selective removal of Cu(II) in the presence of trivalent or tetravalent ions, especially over Al(III). It is known that the charge to radius ratio (Z/r) is directly related to the sorption capacity of cationic metal ions (Wu and Zhou, 2009; Da'na and Sayari, 2012). The Z/r ratio of Cu(II) is 2.74, which is lower than those of trivalent and tetravalent ions (Cr(III) = 4.84, Al(III) = 5.66, and Zr(IV) = 5.56).

Table 4.3. Comparison of Cu(II) selectivity between PEI-silica gel and Cu-PEI-silica gel in multinary solutions containing divalent ions

Metal ion	PEI-silica gel			Cu-PEI-silica gel			
	q (μmol/g)	kd (L/g)	α	q (μmol/g)	kd (L/g)	α	α'
Cu(II)	15.56±1.82	0.0168±0.0021	-	51.07±5.55	0.0626±0.0081	-	-
Pb(II)	3.76±1.17	0.0038±0.0012	4.39	0±0	0±0	∞	∞
Zn(II)	1.54±1.54	0.0016±0.0016	10.68	1.31±1.31	0.0013±0.0013	46.79	4.38
Ni(II)	4.69±3.46	0.0049±0.0037	3.42	5.1±5.5	0.0054±0.0058	11.55	3.37
Co(II)	1.74±1.74	0.0018±0.0018	9.42	2.1±2.1	0.0022±0.0022	28.85	3.06

Table 4.4. Comparison of Cu(II) selectivity between PEI-silica gel and Cu-PEI-silica gel in multinary solutions containing trivalent/tetravalent ions

Metal ion	PEI-silica gel			Cu-PEI-silica gel			
	q (μmol/g)	kd (L/g)	α	q (μmol/g)	kd (L/g)	α	α'
Cu(II)	8.27±2.5	0.0085±0.0026	-	57.89±1.73	0.0696±0.0025	-	-
Al(III)	22.76±4.35	0.025±0.0051	0.34	72.33±7.73	0.0951±0.013	0.73	2.17
Cr(III)	13.22±1.42	0.0131±0.0015	0.65	19.22±3.53	0.0194±0.0038	3.58	5.56
Zr(IV)	0±0	0±0	∞	0±0	0±0	∞	1

The results of Me(II) dynamic sorption were represented in Fig.4.9. Except Cu(II), all other Me(II) ions were reached quickly to exhaustion (within 1.25 – 5.5 h). After then, Cu(II) was selectively removed until column experiments were stopped. This trends can be explained by Cu(II)/Me(II) selectivity. From the high Cu(II) selectivity over Me(II) of PEI-silica gel, Cu(II) were selectively removed. However, from the higher Cu(II) sorption capacity and Cu(II) selectivity of Cu-PEI-silica gel, Cu(II) were more selectively removed.

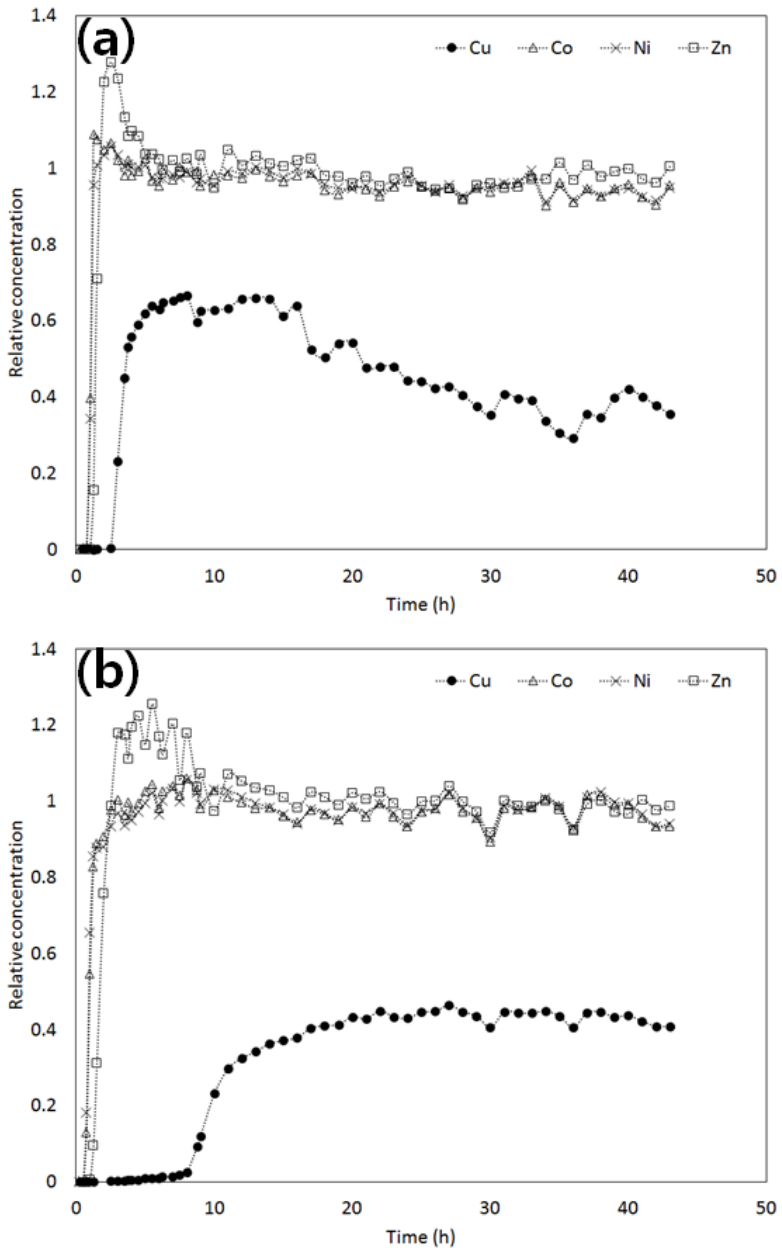

Figure 4.9. Breakthrough curves for Me(II) removal: (a) PEI-silica gel; (b) Cu-PEI-silica gel

Chapter 5 Effect of alkyl chain length of quaternary ammonium functionalized mesoporous silica on the selective nitrate removal in aqueous solution

In this chapter, five different quaternary ammonium functionalized mesoporous silica SBA-15 adsorbents with different alkyl chain lengths (C1Q-, C4Q-, C8Q-, C12Q-, and C18Q-SBA-15) were synthesized for nitrate removal from aqueous solutions. Batch experiments demonstrated that in the presence of competing anions (i.e., chloride, sulfate, phosphate, or bicarbonate), C12Q- and C18Q-SBA-15 with longer alkyl chain lengths were more effective for selective nitrate removal than those with shorter chain lengths. The nitrate-to-sulfate separation factors (NSF) were determined from the nitrate removal experiments in ground water. C1Q- and C4Q-SBA-15 had NSF values of < 0.9, whereas C8Q-, C12Q-, and C18Q-SBA-15 had NSF values of > 2.7.

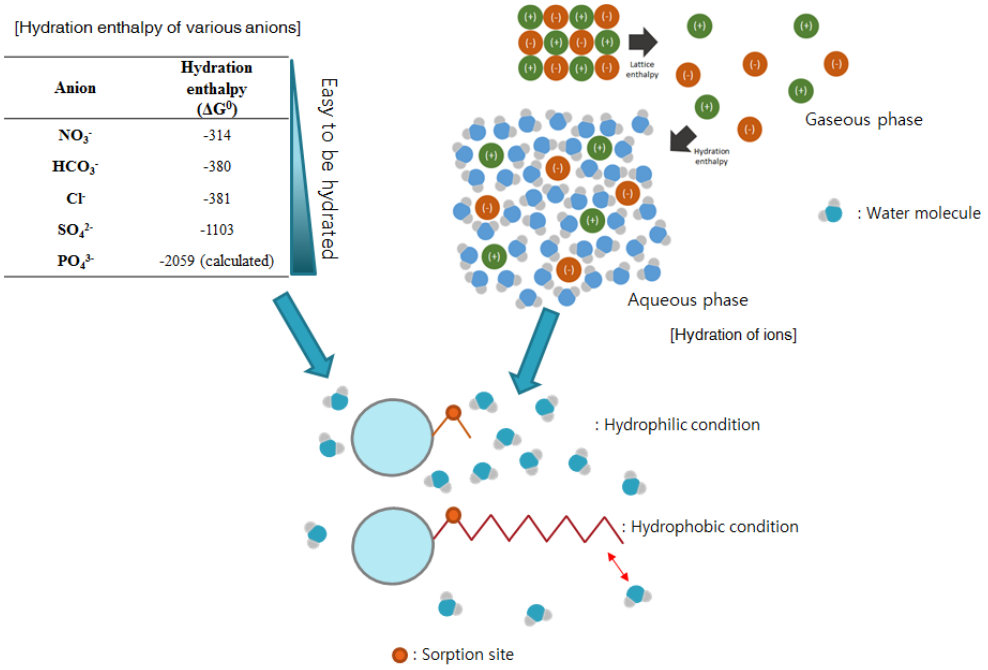

Figure 5.1. Graphical abstract of chapter 5

5.1. Materials and Methods

5.1.1. Synthesis of quaternary ammonium functionalized mesoporous silica SBA-15

All chemicals used in the experiments were purchased from Sigma Aldrich (Saint Louis, MO, USA) unless stated otherwise. A schematic diagram of the synthesis of quaternary ammonium functionalized mesoporous silica is shown in Fig. 5.2 - 6. Prior to the preparation of quaternary ammonium functionalized mesoporous silica, mesoporous silica SBA-15 was synthesized as Liu et al. (2009).

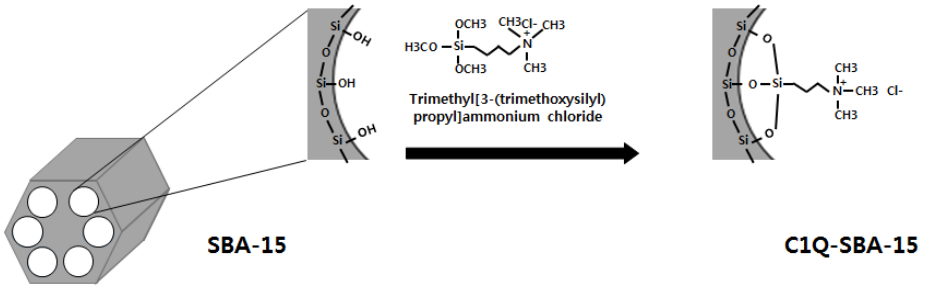

Figure 5.2. Schematic diagram of C1Q-SBA-15 (Trimethylquaternary ammonium functionalized SBA-15) synthesis

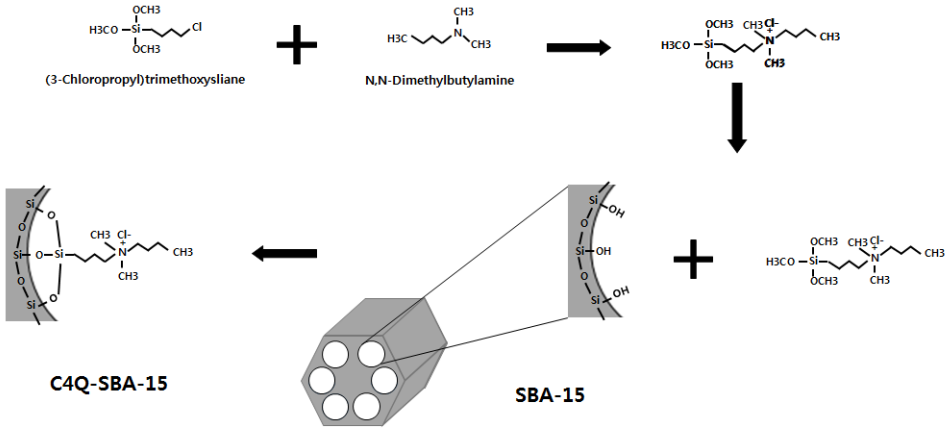

Figure 5.3. Schematic diagram of C4Q-SBA-15

(Dimethylbutylquaternary ammonium functionalized SBA-15) synthesis

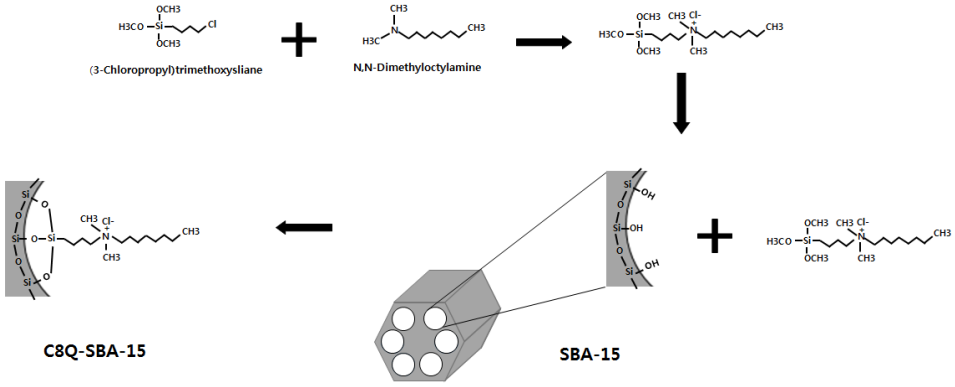

Figure 5.4. Schematic diagram of C8Q-SBA-15

(Dimethyloctylquaternary ammonium functionalized SBA-15) synthesis

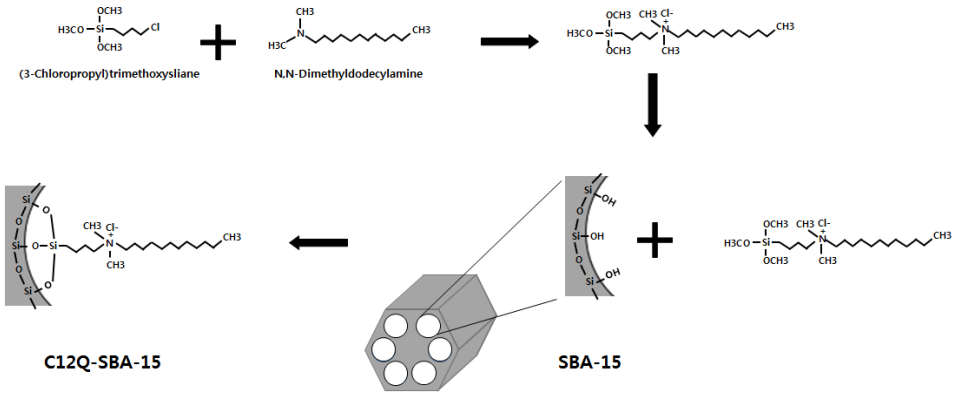

Figure 5.5. Schematic diagram of C12Q-SBA-15 (Dimethyldodecylquaternary ammonium functionalized SBA-15) synthesis

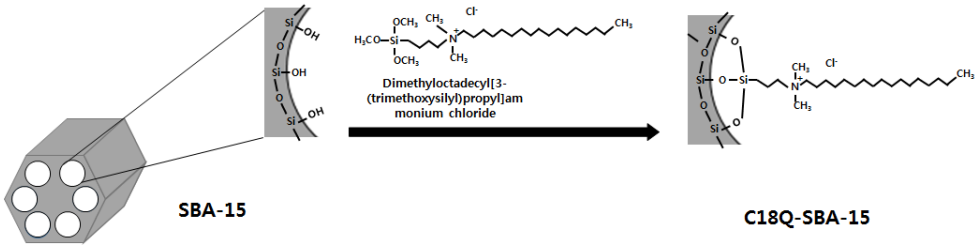

Figure 5.6. Schematic diagram of C18Q-SBA-15

(Dimethyloctadecylquaternary ammonium functionalized SBA-15)

synthesis

Based on the SBA-15 particles, various quaternary ammonium functionalized mesoporous silica, which have different alkyl chain length, were prepared. The preparation of trimethylquaternary ammonium functionalized mesoporous silica were prepared as following procedure. 1 g of mesoporous silica and 7.77 g of Trimethyl [3-(trimethoxysilyl) propyl] ammonium chloride (50% in Methanol, Tokyo Chemical Industry, Japan) was added and stirred into 150 mL of Toluene (99.5 %, Daejung, Siheung, Republic of Korea) for 1 h. 0.5 mL of DI water were added as a hydrolytic deposition reaction initiator and refluxed at 100°C for 48 h. The trimethylquaternary ammonium functionalized mesoporous silica were filtered and washed thoroughly with toluene and DI water until the effluent pH was neutral. The neutralized resultant stirred with 1L of 0.1 M NaCl solution (prepared by using NaCl, > 99.0 %, Daejung) for 6 h. The NaCl reacted resultants were separated and dried in oven (ThermoStable SOF-W 155, Daihan Scientific, Seoul, Korea) at 65 ^{o}C for overnight. After cooling, the trimethylquaternary ammonium functionalized mesoporous silica powder (C1Q-SBA-15) was obtained through fragmentation with mortar and pestle.

The preparation of dimethylbutylquaternary ammonium functionalized mesoporous silica were prepared as following procedure modified procedure from Carpenter et al. (2012).

Firstly, 0.1 M of (3-chloropropyl)trimethoxysliane (≥97%) and 0.1 M of N,N-dimethylbutylamine (99%) were reacted at 85°C for 48 h to synthesis Dimethylbutyl[3-(trimethoxysilyl)propyl]ammonium chloride. After reaction, the resultant was reacted with 6 g of SBA-15 in 300 mL of toluene at 100°C for 1 h. 1 mL of DI water were added as a hydrolytic deposition reaction initiator and refluxed at 100°C for 48 h. The dimethylbutylquaternary ammonium functionalized mesoporous silica was filtered and washed thoroughly with toluene and DI water until the effluent pH was neutral. The neutralized resultant stirred with 2 L of 0.1 M NaCl solution for 6 h. The NaCl reacted resultants were separated and dried at 65 °C for overnight. After cooling, the dimethylbutylquaternary ammonium chloride functionalized mesoporous silica powder (C4Q-SBA-15) was obtained through fragmentation with mortar and pestle.

Base on the C4Q-SBA-15 preparation, the dimethyloctylquaternary ammonium functionalized mesoporous silica powder (C8Q-SBA-15) and the dimethyldodecylquaternary ammonium functionalized mesoporous silica powder (C12Q-SBA-15) were synthesized by substituting N,N-dimethyloctylamine (95%) or N,N-dimethyldodecylamine (97%) for 0.1 M of N,N-dimethylbutylamine.

In addition, the dimethyloctadecylquaternary ammonium functionalized mesoporous silica powder (C18Q-SBA-15) prepared by substituting 20 mL of Dimethyloctadecyl[3-(trimethoxysilyl)propyl]ammonium chloride (42% in Methanol) for 7.77 g of Trimethyl[3-(trimethoxysilyl)propyl]ammonium chloride from C1Q-SBA-15 preparation procedure.

5.1.2. Characterization of Quaternary ammonium functionalized mesoporous silica

Quaternary ammonium functionalized mesoporous silica (C1Q-SBA-15, C4Q-SBA-15, C8Q-SBA-15, C12Q-SBA-15, C18Q-SBA-15) were characterized using several techniques. Field-emission scanning electron microscopy (FE-SEM, Supra 55VP, Carl Zeiss, Oberkochen, Germany) was used to analyze the surface morphology. Fourier-transform infrared (FTIR) spectroscopy (Nicolet 6700, Thermo Fisher Scientific, Waltham, MA, USA) was used to analyze the effect of quaternization on SBA-15. X-ray photoelectron spectroscopy (XPS, Sigma Probe, Kratos Analytical, Shimadzu, Japan) scans with Al Kα radiation ($h\nu$ = 1253.6 eV) was used to analyze the chemical bonding and elements of Quaternary ammonium functionalized mesoporous silica.

The anion exchange capacities were quantified by the method of Neagu and Mikhalovsky (2010). Firstly, 0.3 g of quaternary ammonium functionalized mesoporous silica were loaded on 0.45-μm membrane filter and filtered with 300 mL of DI water and dried at 65°C. The resultants reacted with 5 % Na_2SO_4 solution (adsorbent dose = 1 g/L) for 6 h. After reaction, the samples were collected and filtered through a 0.45-μm membrane filter. The Concentration of chloride were measured by Ion Chromatography (IC, Dionex Aquion Ion Chromatography System, Thermo, USA). The anion exchange capacities (AEC, mmol/g) can be calculated with the following equation:

$$\text{AEC} = \frac{C_{Cl^-}}{C_a} \qquad (5.1)$$

where C_{Cl^-} is the chloride concentration in the aqueous phase after reaction (mmol/L), and C_a is the adsorbent dose (g/L).

5.1.3. Nitrate sorption experiments

Nitrate sorption experiments were performed under batch conditions. The desired concentration of nitrate solution was prepared by diluting a stock solution (1000 mg/L as NO_3^-), which was prepared from the sodium nitrate ($NaNO_3$, 99.0 %, Duksan Pure Chemicals). If there was no additional

description, whole batch experiments were performed at 50 mL polypropylene conical tubes containing 30 mL solutions of Quaternary ammonium functionalized mesoporous silica (adsorbent dose = 1 g/L) and nitrate solution (100 mg/L as NO_3^-). The samples were shaken in a shaking incubator as 120 rpm at 30°C for 180 min in triplicate. After reaction, the samples were collected and filtered through a 0.45-μm membrane filter. Concentration of nitrate were measured with Ion Chromatography (IC, Dionex Aquion Ion Chromatography System, Thermo, USA).

To evaluate the effect of contact time on nitrate removal, the kinetic experiments were performed for 5, 15, 30, 45, 60, 120, 180 min in triplicate. The nitrate sorption capacity at time '*t*'(q_t, mg/g) can be calculated with the following equation:

$$q_t = \frac{C_i - C_t}{C_a} \qquad (5.2)$$

where C_i is the nitrate concentration in the aqueous phase before sorption reaction, C_t is the nitrate concentration in the aqueous phase at time '*t*', and C_a is the adsorbent dose.

The data from effect of contact time on nitrate removal of C1Q-SBA-15, C4Q-SBA-15, C8Q-SBA-15, C12Q-SBA-15, and C18Q-SBA-15 experiment

were fitted to the following equations of pseudo first-order, pseudo second-order, and Elovich kinetic models :

$$q_t = q_e[1 - \exp(-k_1 t)] \quad (5.3)$$

$$q_t = \frac{k_2 {q_e}^2 t}{1 + k_2 q_e t} \quad (5.4)$$

$$q_t = \frac{1}{\beta}\ln(\alpha \cdot \beta) + \frac{1}{\beta}\ln(t) \quad (5.5)$$

where q_t is the amount of adsorbed nitrate per unit mass of absorbent at time t (mg/g), and q_e is the amount of adsorbed nitrate per unit mass of absorbent at equilibrium (mg/g). k_1 is the pseudo first-order rate constant (1/min), k_2 is the pseudo second-order rate constant (g/mg·min), α is the initial adsorption rate constant (mg/g·min), and β is the Elovich adsorption constant (g/mg).

To evaluate the effect of initial concentration on nitrate removal, the isotherm experiments were performed at various nitrate initial concentration (20, 50, 100, 200, 500, 1000 mg/L as NO_3^-). The nitrate sorption capacity (q_e, mg/g) can be calculated with the following equation:

$$q_e = \frac{C_i - C_f}{C_a} \quad (5.6)$$

where C_f is the nitrate concentration in the aqueous phase after reaction, and C_a is the adsorbent dose.

The data from effect of initial concentration on nitrate removal of C1Q-SBA-15, C4Q-SBA-15, C8Q-SBA-15, C12Q-SBA-15, and C18Q-SBA-15 experiment were fitted to the following nonlinear equations of Langmuir, Freundlich, and Redlich-Peterson isotherm models :

$$q_e = \frac{Q_m K_L C_e}{1 + K_L C_e} \qquad (5.7)$$

$$q_e = K_F {C_e}^n \qquad (5.8)$$

$$q_e = \frac{K_R C_e}{1 + a_R C_e^g} \qquad (5.9)$$

where Q_m is the maximum mass of adsorbed nitrate per unit mass of adsorbent (removal capacity, mg/g), and C_e is the concentration of copper in the aqueous solution at equilibrium (mg/L). K_L is the Langmuir constant related to the binding energy (L/g), K_F is the distribution coefficient (L/mg), n is the Freundlich constant, K_R is the Redlich-Peterson constant, a_R is the Redlich–Peterson constant related to the affinity of the binding sites, and g is the Redlich–Peterson constant related to the adsorption intensity.

The effect of pH experiments were also performed by adjusting pH of nitrate solutions (initial pH 2 to 12). pH of nitrate solutions were adjusted using 0.1 M NaOH and 0.1 M HCl solutions (prepared by using NaOH, > 93.0 % and 36 % HCl solution, Duksan Pure Chemicals). The nitrate sorption capacity (q_e, mg/g) was calculated with the Eq. (5.6)

In aqueous condition, bicarbonate, phosphate, sulfate are known as common anions also competing anions for nitrate removal. To simulate the effects of competing anions, specific molar ratio solutions which are include chloride or bicarbonate or phosphate or sulfate over nitrate (molar ratio [Cl^- or HCO_3^- or PO_4^{3-} or SO_4^{2-}]/[NO_3^-] = 0, 0.5, 1, 2, 3, 4 (nitrate = 100 mg/L)) solutions were prepared.

The competing anion experiments were performed with 50 mL polypropylene conical tubes containing 30 mL solutions of Quaternary ammonium functionalized mesoporous silica (adsorbent dose = 1 g/L), which were shaken in a shaking incubator as 120 rpm at 30°C for 180 min in triplicate. The nitrate sorption capacity (q_e, mg/g) was calculated with the Eq. (5.6). The relative nitrate sorption reduction (RNR) was calculated as following the Eq. (5.10).

$$RNR(\%) = \left(1 - \frac{q_e \ {}^{w/} \ competing \ ion}{q_e \ {}^{w}/_{o} \ competing \ ion}\right) * 100 \qquad (5.10)$$

To examine the nitrate removal in ground water, artificial ground water was prepared as following procedure for mimicking the ground water composition reported by Kabay et al. (2007). Firstly, add 1 M HNO_3 1.2 mL and 2 M of HCl 0.41 mL into 1 L flask and add DI water until the volume of solution reached to 1 L. 0.4935 g of $CuSO_4 \cdot 0.5H_2O$, 0.4437 g of $MgSO_4 \cdot 7H_2O$,

0.1190 g of $NaNO_3$, 0.0607 g of KNO_3, 0.0327 g of NaCl, and 0.0269 g of $NaHCO_3$ were added into above solution and stirred. The solution pH was adjusted with 0.1 M NaOH solution into 7.6. After artificial ground water preparation, batch tests were performed with 50 mL polypropylene conical tubes containing 30 mL solutions of quaternary ammonium functionalized mesoporous silica (adsorbent dose = 1 g/L), which were shaken in a shaking incubator as 120 rpm at 30°C for 180 min in triplicate. The nitrate sorption capacity (q_e, mg/g) was calculated with the Eq. (5.6). Nitrate-to-Sulfate separation factor (α_S^N) was calculated by following the Eq. (5.11).

$$\alpha_S^N = \left(\frac{[adsorbed\ \ NO_3^-][SO_4^{2-}]}{[adsorbed\ \ SO_4^{2-}][NO_3^-]}\right) * 100 \qquad (5.11)$$

5.2. Results and Discussion

5.2.1. Characteristics of quaternary ammonium functionalized mesoporous silica SBA-15

FE-SEM images and digital images are presented in Fig. 5.7. From the digital images, C1Q-SBA-15, C12Q-SBA-15, and C18Q-SBA-15 are white

powder. C4Q-SBA-15 and C8Q-SBA-15 are fancy light yellow powder. FE-SEM images showed that SBA-15 were coated and coagulated by quaternization.

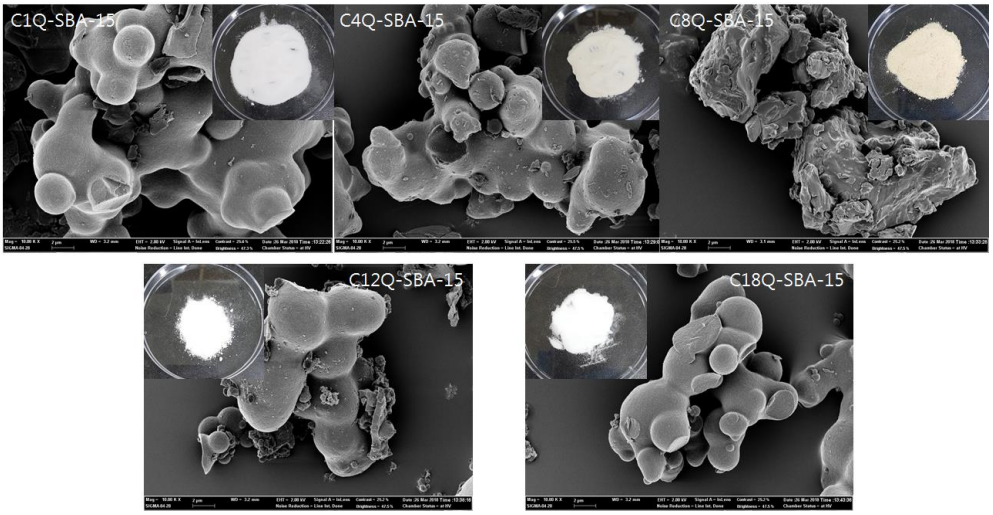

Figure 5.7. FE-SEM images of quaternary ammonium functionalized SBA-15 (bar = 2 μm, inset = digital image)

FTIR spectra are presented in Fig. 5.8. In the spectra, the peaks of SBA-15 at 805.5 and 1049.5 cm^{-1} were attributed to stretching of siloxane (Si-O-Si) (Liu et al., 2011a). C1Q-SBA-15, C4Q-SBA-15, C8Q-SBA-15, C12Q-SBA-15, and C18Q-SBA-15 also has the peaks at 1041 – 1055 cm^{-1} and 797 - 800 cm^{-1} by stretching of siloxane (Si-O-Si). The peak at 797 – 806 cm^{-1} is also considered as comes from Si-C stretching (Simons and Laboratories, 1978). After quaternarization of SBA-15, several new peaks appeared as evidence of successful quaternarization. The peaks of C1Q-SBA-15 and C4Q-SBA-15 at 1481.4 and 1483.4 cm^{-1} is the evidence of C-H_2 asymmetric bending quaternary ammonium functionalization (Simons and Laboratories, 1978; Wan et al., 2010; He et al., 2017). By increasing alkyl chain, the peaks at 1466.5 (C8Q-SBA-15), 1466.7 (C12Q-SBA-15), and 1466.6 cm^{-1} (C18Q-SBA-15) were newly observed which is known as CH_2 or CH_3 asymmetric bending (Simons and Laboratories, 1978) that is regarded as contribution of methylene group in alkyl chain. C-H stretching vibration of alkyl chain was not observed at C1Q-SBA-15. C4Q-SBA-15 shows peak at 2961.8 cm^{-1} contributed from CH_3 asymmetric stretching. By increasing alkyl chain length more (C8Q-SBA-15, C12Q-SBA-15, and C18Q-SBA-15), peaks at 2922 - 2944 cm^{-1} and 2852 – 2856 cm^{-1} known as CH_2 asymmetric stretching and CH_2 symmetric stretching (Simons and Laboratories, 1978) were observe and

getting stronger by increasing of alkyl chain length and methylene group portion.

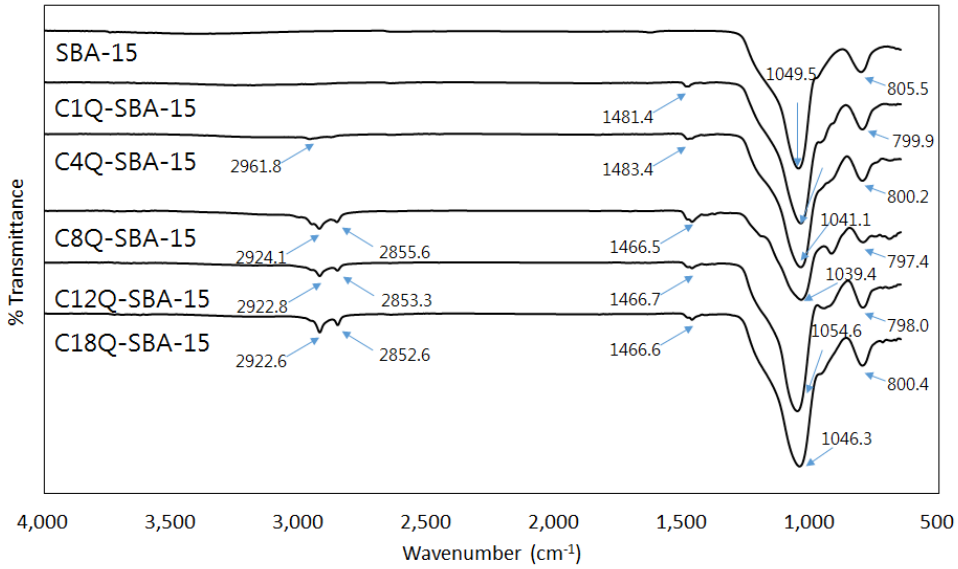

Figure 5.8. FTIR spectra of SBA-15 and quaternary ammonium functionalized SBA-15

XPS spectra are presented in Fig. 5.9 - 10. In the wide scans of C1Q-SBA-15, C4Q-SBA-15, C8Q-SBA-15, C12Q-SBA-15, and C18Q-SBA-15, the photoelectron peaks at the binding energies of 103 and 153 eV were attributed to Si 2p and Si 2s, respectively, whereas those at 198, 284, 400, and 532 eV were attributed to Cl 2p, C 1s, N 1s, and O 1s, respectively. The peaks at 103 eV (Si 2p) and 532 eV (O 1s) were assigned to the characteristic peaks of SBA-15 (He et al., 1992; Moulder et al., 1995). From C1Q-SBA-15 to C18Q-SBA-15, peaks at C 1s are similar in peak binding energy and full width at half maximum (FWHM). Furthermore, C 1s peaks can be deconvoluted into 284.8 and 286.0 eV(C-C and C-N bonds) that is reported as contribution from quaternary ammonium functionalization (Yun et al., 2014; Gao et al., 2018). In the high resolution of Cl 2p, Cl $2p_{3/2}$ from C1Q-SBA-15 to C18Q-SBA-15 are lower than 199 eV which means that chloride in the samples exist as inorganic form than organic form (Araujo et al., 2014). This means that quaternarization between (3-chloropropyl)trimethoxysliane and tertiary amine well reacted and chloride exists as counter ion of quaternary ammonium moieties in the preparation of C4Q-SBA-15, C8Q-SBA-15, and C12Q-SBA-15. In the N 1s spectrum, two deconvoluted peaks could be assigned to N in C-N-C (399 eV), N^+ in quaternary ammonium species (402 eV) which are also the evidence of quaternarization and quaternary ammonium functionalization (Dong et al., 2016; Gao et al., 2018). Deconvoluted C 1s and N 1s peaks shows

no specific correlation with alkyl chain length. After nitrate adsorption, new peak appeared at 405.8 – 406.2 known as NH_4NO_3 (Wagner and Muilenberg, 1979) in the high resolution of N 1s, except C18Q-SBA-15. This new peak is evidence for nitrate sorption on quaternary ammonium. Reason for no new peak detection at C18Q-SBA-15 is considered as low contribution of NH_4NO_3 from C18Q-SBA-15's relatively low nitrate sorption capacity than rest of Quaternary functionalized mesoporous silica.

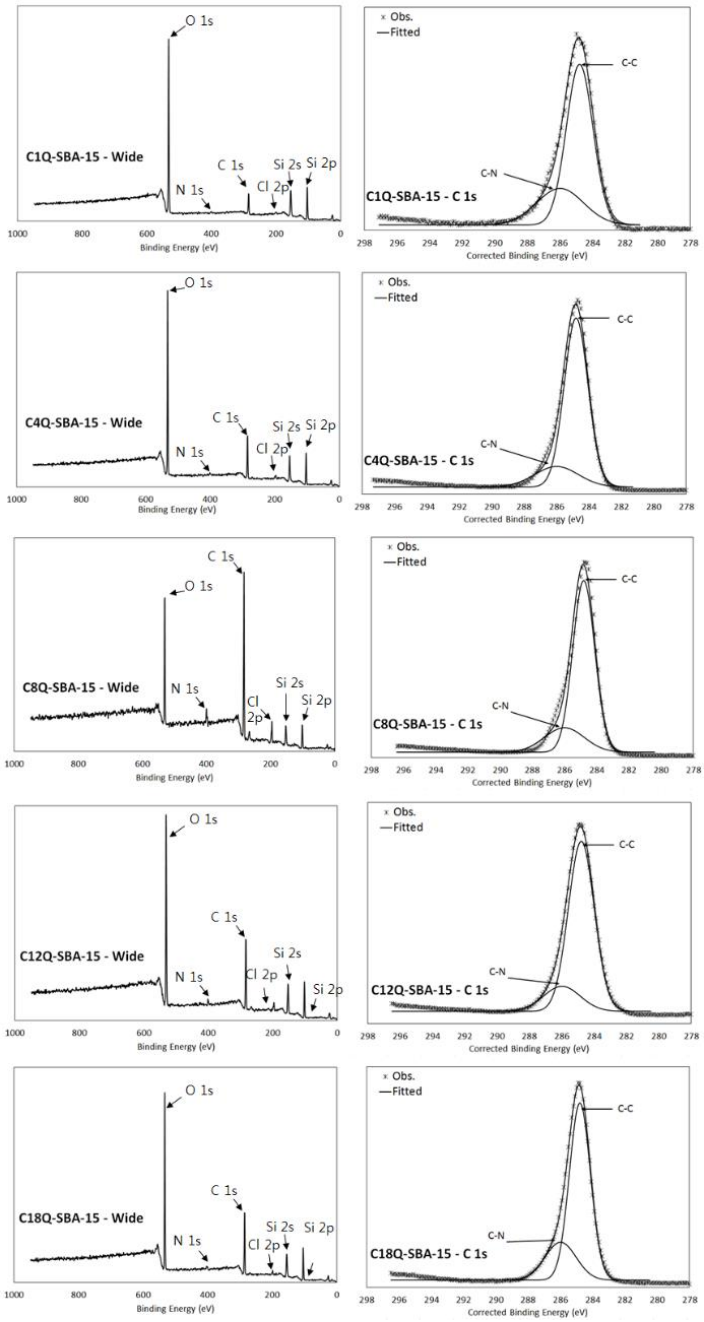

Figure 5.9. XPS spectra of quaternary ammonium functionalized SBA-15 (left = wide, right = C 1s)

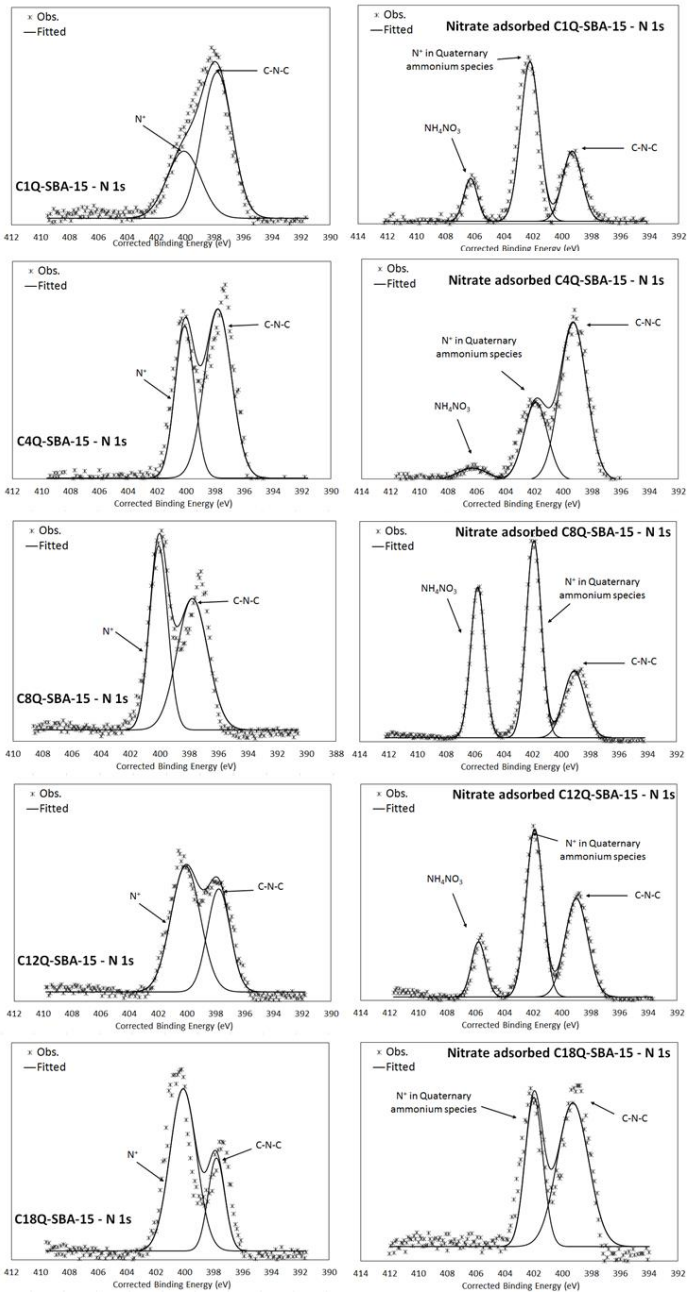

Figure 5.10. XPS spectra of quaternary ammonium functionalized SBA-15 (left = pristine N 1s, right = N 1s after nitrate adsorption)

The anion exchange capacities (AEC, mmol/g) results are represented in Table 5.1. From the results, C18Q-SBA-15 had lowest AEC, 1.759 ± 0.743 mmol/g. The rest of quaternary functionalized mesoporous silica showed similar AEC (C1Q-SBA-15 = 2.453 ± 0.004 mmol/g, C4Q-SBA-15 = 2.883 ± 0.005 mmol/g, C8Q-SBA-15 =2.598 ± 0.025 mmol/g, and C12Q-SBA-15 = 2.474 ± 0.033 mmol/g). The similarity of AEC is considered as preparation of quaternary functionalized mesoporous silica were successfully performed, irrespective of alkyl chain length and preparation method.

Table 5.1. The anion exchange capacities results

Adsorbent	AEC (mmol/g)
C1Q-SBA-15	2.453 ± 0.004
C4Q-SBA-15	2.883 ± 0.005
C8Q-SBA-15	2.598 ± 0.025
C12Q-SBA-15	2.474 ± 0.033
C18Q-SBA-15	1.759 ± 0.743

5.2.2. Nitrate sorption Characteristics of quaternary ammonium functionalized mesoporous silica SBA-15

From the data of effect of contact time on the nitrate removal, the kinetic model analysis results and parameters are presented in Fig. 5.11 and Table 5.2. R^2, χ^2, and SSE indicate that Pseudo first model was most suitable model for describing the kinetic data. k_1 parameters also indicate that nitrate sorption rate of C1Q-SBA-15 (k_1 = 4.551 1/min) and C4Q-SBA-15 (k_1 = 4.551 1/min) was much faster than C8Q-SBA-15 (k_1 = 0.103 1/min), C12Q-SBA-15 (k_1 = 0.149 1/min), and C18Q-SBA-15 (k_1 = 0.102 1/min).

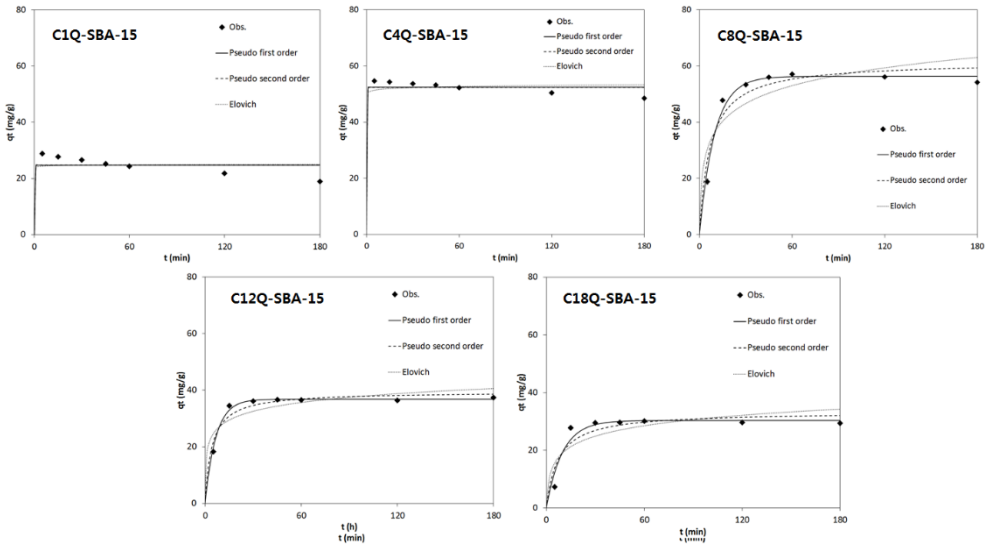

Figure 5.11. The kinetic models analysis results

Table 5.2. Kinetic model parameters obtained from nitrate removal of quaternary ammonium SBA-15

Adsorbents	Kinetic model															
	Pseudo 1st					Pseudo 2nd						Elovich				
	q_e (mg/g)	k_1 (1/min)	R^2	χ^2	SSE	q_e (mg/g)	K_2 (g/mg/min)	h	R^2	χ^2	SSE	α	β	R^2	χ^2	SSE
C1Q-SBA-15	24.77	4.55	0.880	7.3E+01	3.3E+00	24.77	1.4E+05	4.9E+11	0.880	7.3E+01	3.3E+00	2.53E+60	5.846	0.866	8.2E+01	3.7E+00
C4Q-SBA-15	52.44	4.55	0.989	3.0E+01	5.9E-01	52.44	1.4E+05	1.0E+12	0.989	3.0E+01	5.9E-01	6.79E+40	1.875	0.983	4.8E+01	9.5E-01
C8Q-SBA-15	56.28	0.10	0.991	3.3E+01	1.1E+00	61.57	2.4E-03	3.5E-04	0.963	1.3E+02	4.4E+00	5.0E+01	0.109	0.896	3.7E+02	1.1E+01
C12Q-SBA-15	36.87	0.15	0.997	4.3E+00	1.5E-01	39.46	6.0E-03	1.4E-03	0.979	3.0E+01	1.1E+00	2.1E+02	0.223	0.931	9.8E+01	3.7E+00
C18Q-SBA-15	30.25	0.10	0.963	4.1E+01	3.7E+00	33.29	4.2E-03	5.8E-04	0.922	8.6E+01	7.1E+00	2.0E+01	0.191	0.845	1.7E+02	1.3E+01

The effect of initial concentration results are shown in Fig. 5.12. At the initial concentration = 20 mg/L, sorption capacity were calculated as 4.29 ± 0.21, 12.30 ± 0.00, 8.63 ± 0.09, 14.51 ± 0.02, and 11.49 ± 0.13 mg/g (from C1Q-SBA-15, C4Q-SBA-15, C8Q-SBA-15, C12Q-SBA-15, and C18Q-SBA-15). By increasing of initial concentration into 100 mg/L, sorption capacity were increased as 20.11 ± 0.21, 56.51 ± 1.30, 54.23 ± 0.01, 40.65 ± 0.93, and 24.73 ± 0.15 mg/g. Further, when initial concentration is 1000 mg/L, sorption capacity were increased more as 89.43 ± 21.06, 129.89 ± 1.39, 136.37 ± 14.45, 71.88 ± 7.39, 30.68 ± 0.00 mg/g. From the effect of initial concentration results, nitrate sorption capacity were dependent on initial nitrate concentration and AEC, irrespective of alkyl chain length.

The equilibrium model analysis results and parameters are presented in Fig. 5.13 and Table 5.3. R^2, χ^2, and SSE indicate that Redlich-Peterson model was most suitable model for describing the equilibrium data. From the Langmuir model, the maximum nitrate sorption capacities (Q_m) of quaternary ammonium functionalized mesoporous silica were 93.07, 155.46, 155.21, 75.81, and 30.16 mg/g (from C1Q-SBA-15, C4Q-SBA-15, C8Q-SBA-15, C12Q-SBA-15, C18Q-SBA-15).

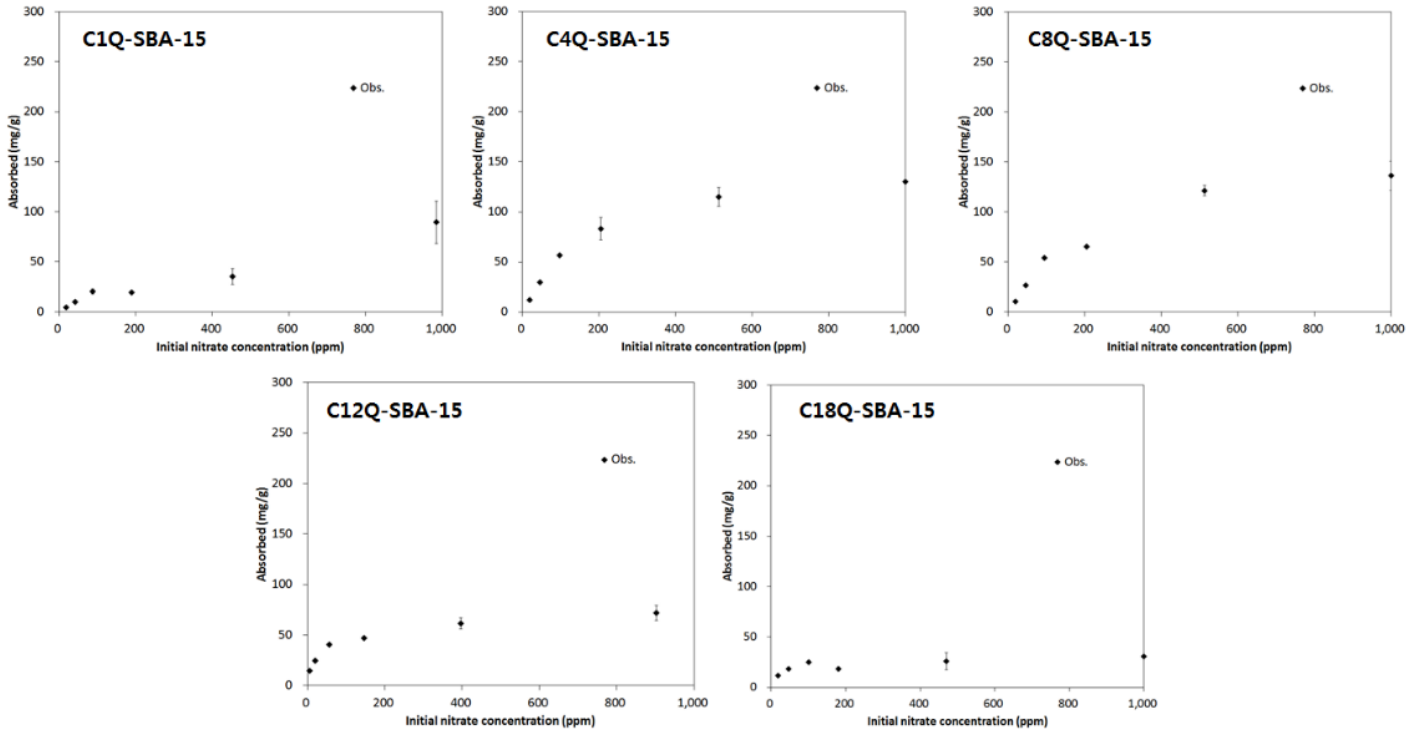

Figure 5.12. The results of initial nitrate concentration effect on the nitrate removal

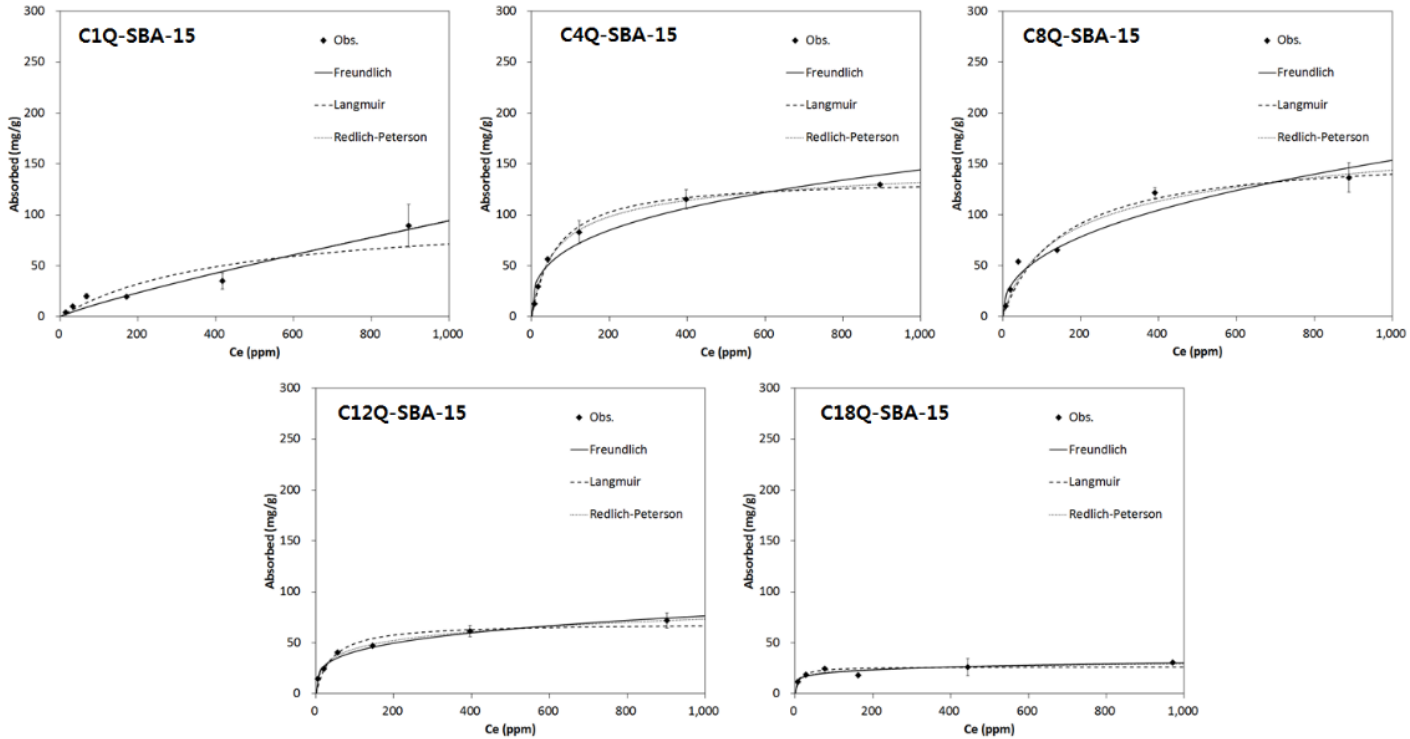

Figure 5.13. The equilibrium models analysis results

Table 5.3. Equilibrium isotherm model parameters

Adsorbents	Freundlich						Langmuir					Redlich-Peterson						
	K_F (L/g)	1/n	q_m (mg/g)	R^2	χ^2	SSE	Qm (mg/)	KL (L/mg)	R^2	χ^2	SSE	K_R (L/g)	a_R (1/mg)	K_R/a_R (mg/g)	g	R^2	χ^2	SSE
C1Q-SBA-15	0.251	0.859	93.070	0.949	11.67	245.60	102.470	0.002	0.839	18.54	779.90	6.401	24.997	0.256	0.142	0.949	11.76	246.05
C4Q-SBA-15	14.857	0.329	145.46	0.944	25.14	613.68	135.613	0.016	0.994	1.02	69.02	2.668	0.035	75.781	0.913	0.998	0.87	23.25
C8Q-SBA-15	8.507	0.419	155.21	0.959	17.90	732.95	161.376	0.007	0.981	13.07	657.75	1.391	0.022	64.684	0.869	0.983	9.12	532.12
C12Q-SBA-15	12.137	0.266	75.810	0.974	2.36	61.32	69.077	0.025	0.942	4.73	134.61	5.166	0.253	20.429	0.813	0.993	0.51	17.09
C18Q-SBA-15	9.964	0.160	30.161	0.924	2.45	48.28	26.408	0.092	0.893	3.29	68.13	7.051	0.546	12.921	0.881	0.931	2.16	43.93

Result of initial pH effect is presented in Fig. 5.14. At the initial pH = 2, sorption capacities were calculated as 8.53 ± 0.03, 25.10 ± 0.14, 30.84 ± 1.23, 19.18 ± 2.19, and 16.85 ± 0.63 mg/g (from C1Q-SBA-15, C4Q-SBA-15, C8Q-SBA-15, C12Q-SBA-15, and C18Q-SBA-15). When initial pH = 4, sorption capacities were increased regardless of alkyl chain length (sorption capacities = 28.28 ± 1.59, 60.47 ± 0.11, 57.59 ± 1.15, 32.45 ± 2.52, and 36.84 ± 0.61 mg/g). This trend is can be explained by restriction in the free movement of nitrate to the sorption site was improved from H^+ ion concentration decreasing (Sowmya and Meenakshi, 2013). By increasing initial pH = 4 to 10, sorption capacities were slightly deceased into 15.38 ± 0.91, 49.54 ± 0.29, 37.93 ± 3.40, 26.30 ± 0.18, and 32.66 ± 1.38 mg/g. Further increasing of initial pH into 12, nitrate sorption capacities were vastly decreased into 3.73 ± 0.25, 2.55 ± 0.27, 2.36 ± 0.27, 3.73 ± 0.25, and 2.55 ± 0.27 mg/g. This trend is related with the exigent OH^- ions as a challenging ion (Sowmya and Meenakshi, 2013, 2014).

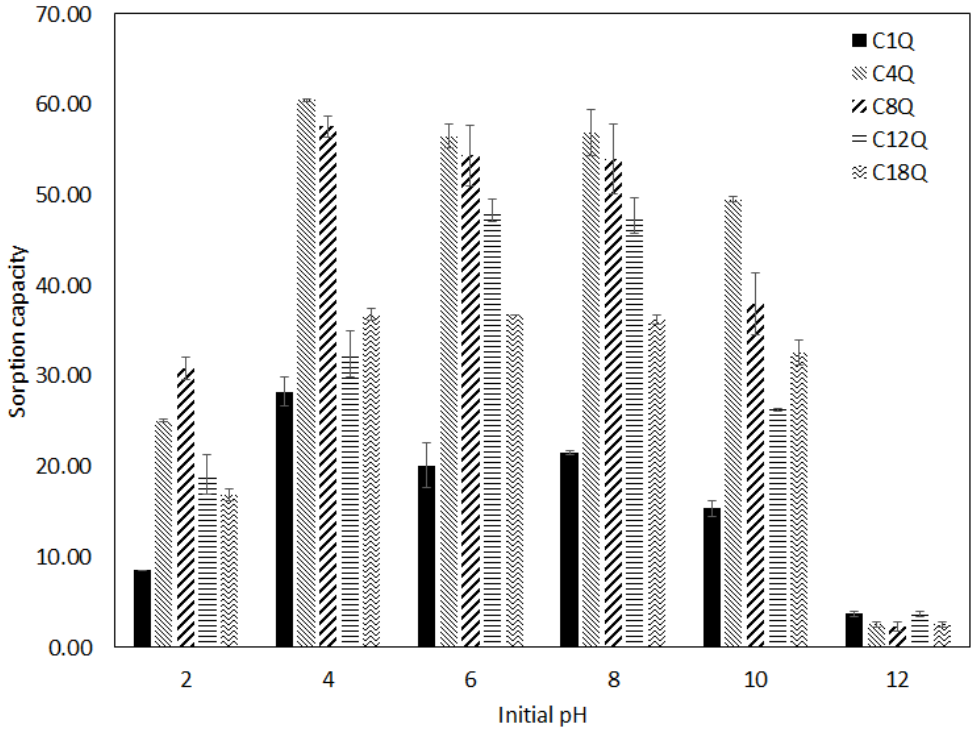

Figure 5.14. Results of initial pH effect on nitrate removal using quaternary ammonium functionalized SBA-15

The effect of competing anion results are shown in Fig. 5.15. From the C1Q-SBA-15 results, nitrate sorption capacity was slightly decreased from 20.11 ± 2.49 mg/g ($[Cl^-]/[NO_3^-] = 0$) to 12.05 ± 1.17 mg/g (RNR = 40.1%, $[Cl^-]/[NO_3^-] = 4$). When HCO_3^- or PO_4^{3-} or SO_4^{2-} exists, nitrate sorption capacity was collapsed even [competing anion]/$[NO_3^-]$ = 0.5 as 1.73 ± 0.34, 0.00 ± 0.00, and 1.07 ± 0.26 mg/g (RNR = 91.4, 100.0, and 94.7%, [competing anion] = HCO_3^-, PO_4^{3-}, and SO_4^{2-}). From this result, nitration sorption on C1Q-SBA-15 was highly affected at competing anions except Cl^-.

The effect of competing anion result of C4Q-SBA-15 is familiar with the result of C1Q-SBA-15. When Cl^- is a competing anion, nitrate sorption capacity was gradually deceased from 56.51 ± 1.30 mg/g ($[Cl^-]/[NO_3^-] = 0$) to 35.78 ± 1.28 mg/g (RNR = 36.7%, $[Cl^-]/[NO_3^-] = 4$). When SO42- is a competing anion, nitrate sorption capacity was suddenly decreased into 24.48 ± 0.40 mg/g (RNR = 56.7%, $[SO_4^{2-}]/[NO_3^-] = 0.5$) and it keeps even $[SO_4^{2-}]/[NO_3^-] = 4$ as 20.94 ± 1.99 mg/g (RNR = 62.9%). When HCO_3^- or PO_4^{3-} exists, nitrate sorption capacity was collapsed when [competing anion]/$[NO_3^-] = 1$ as 6.66 ± 0.74 and 1.44 ± 0.30 mg/g (RNR = 88.2 and 97.5%, [competing anion] = HCO_3^- and PO_4^{3-}) it kept till [HCO_3^- or PO_4^{3-}]/$[NO_3^-]$ = 4. From this result, nitrate sorption on C4Q-SBA-15 was also highly affected at HCO_3^- and PO_4^{3-}. However, effect of SO_4^{2-} reduced than C1Q-SBA-15.

From the C8Q-SBA-15 results, nitrate sorption capacity was increased from 45.06 ± 0.01 mg/g ($[Cl^-]/[NO_3^-] = 0$) to 53.50 ± 1.24 mg/g (RNR = -18.7%, $[Cl^-]/[NO_3^-] = 0.5$) and it slightly decreased to 42.60 ± 3.91 mg/g (RNR = 5.5%, $[Cl^-]/[NO_3^-] = 1$) and kept till $[Cl^-]/[NO_3^-] = 4$ as 40.63 ± 3.47 mg/g (RNR = 9.8%) when Cl^- is a competing anion. When SO_4^{2-} is a competing anion, nitrate sorption capacity was decreased into 17.43 ± 1.99 mg/g (RNR = 61.3%, $[SO_4^{2-}]/[NO_3^-] = 0.5$) and slightly increased to 28.50 ± 1.49 mg/g (RNR = 36.8%, $[SO_4^{2-}]/[NO_3^-] = 1$) and kept till $[SO_4^{2-}]/[NO_3^-] = 4$ as 23.09 ± 0.50 mg/g (RNR = 48.8%). When HCO_3^- or PO_4^{3-} exists, nitrate sorption capacity was collapsed when [competing anion]/$[NO_3^-] = 0.5$ as 13.28 ± 1.95 and 17.77 ± 0.89 mg/g (RNR = 70.5 and 60.6%, [competing anion] = HCO_3^- and PO_4^{3-}) it continuously decreased till $[HCO_3^-$ or $PO_4^{3-}]/[NO_3^-] = 4$ as 4.51 ± 1.07 and 2.54 ± 0.29 mg/g (RNR = 90.0 and 94.4%). From this result, effect of competing ion at nitrate sorption on C8Q-SBA-15 was familiar with C4Q-SBA-15.

From the C12Q-SBA-15 results, nitrate sorption capacity was increased from 40.65 ± 1.50 mg/g ($[Cl^-]/[NO_3^-] = 0$) to 43.88 ± 0.84 mg/g (RNR = -7.9%, $[Cl^-]/[NO_3^-] = 0.5$) and it slightly decreased to 40.93 ± 1.03 mg/g (RNR = -0.7%, $[Cl^-]/[NO_3^-] = 1$) and continuously decreased till $[Cl^-]/[NO_3^-] = 4$ as 25.78 ± 0.40 mg/g (RNR = 36.6%) when Cl^- is a competing anion. Except Cl^-,

effect of competing HCO_3^- or PO_4^{3-} or SO_4^{2-} was similar but weakened than C1Q-SBA-15, C4Q-SBA-15, and C8Q-SBA-15. Nitrate sorption capacities were reduced about half as 26.49 ± 3.54 mg/g (RNR = 34.8%), 17.77 ± 0.89 mg/g (RNR = 56.3%), and 24.25 ± 1.32 mg/g (RNR = 40.3%) when [HCO_3^- or PO_4^{3-} or SO_4^{2-}]/[NO_3^-] = 0.5. Even [HCO_3^- or PO_4^{3-} or SO_4^{2-}]/[NO_3^-] = 4, nitrate sorption capacity were 12.34 ± 0.74, 10.22 ± 0.56, and 15.76 ± 0.47 mg/g (RNR = 69.6, 74.9, and 61.2%) that is smaller decreasing than C1Q-SBA-15, C4Q-SBA-15, and C8Q-SBA-15 except SO_4^{2-} competing. Effect of SO_4^{2-} is lower than C1Q-SBA-15 but similar with results from C4Q-SBA-15, and C8Q-SBA-15.

The effect of competing anion result of C18Q-SBA-15 is familiar with the result of C12Q-SBA-15. However, its RNR is lower than C12Q-SBA-15. Nitrate sorption capacity was 24.73 ± 0.15 mg/g ([competing anion]/[NO_3^-] = 0) was changed as 34.82 ± 2.71, 28.03 ± 0.03, 18.20 ± 0.39, and 18.75 ± 0.32 mg/g (RNR = -40.8, -13.3, 26.4, and 24.2%) when [competing anion]/[NO_3^-] = 0.5 (competing anion = Cl^-, HCO_3^-, PO_4^{3-}, and SO_4^{2-}). Even [competing anion]/[NO_3^-] = 4, nitrate sorption capacities were 25.15 ± 0.55, 17.70 ± 0.49, 11.63 ± 1.07, and 14.96 ± 1.75 mg/g (RNR = -1.7, 28.4, 53.0, and 39.5%, competing anion = Cl^-, HCO_3^-, PO_4^{3-}, and SO_4^{2-}). From the effect of competing anion results, the longer alkyl chain length, the lower effect on nitrate sorption

reduction, except Cl^-. It is known that hydration enthalphy (ΔG^o) of Cl^-, NO_3^-, HCO_3^-, and SO_4^{2-} is -381, -314, -380, and -1,103 kJ/mol (Smith, 1977; Gu et al., 2004). Hydration energy of PO_4^{3-} can be calculated as -2059 kJ/mol (Smith, 1977; Marcus, 1988).

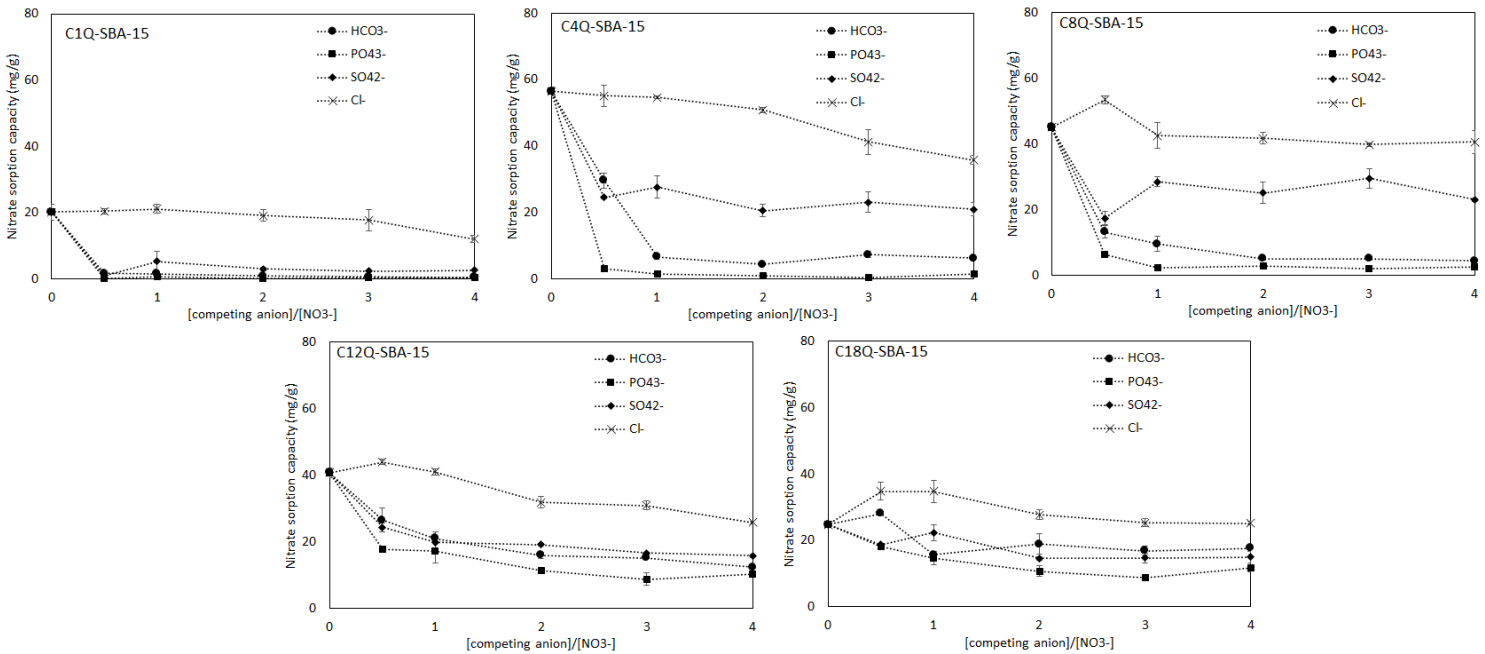

Figure 5.15. Results of competing anion on nitrate removal by using quaternaized SBA-15

Results of nitrate removal in artificial ground water are presented in Table X. From the results, initial concentration of Cl^-, NO_3^-, SO_4^{2-} were measured as 47.71, 153.84, 445.41 mg/L. As can be predicted through competing anion test results, α_S^N is related with alkyl chain length. α_S^N of C1Q-SBA-15 was 0.05. Compare with this value, α_S^N of C4Q-SBA-15, C8Q-SBA-15, and C12Q-SBA-15 were 0.81, 3.75, and 4.43. However, α_S^N of C18Q-SBA-15 was 2.72. low value from C18Q-SBA-15 is considered as contribution of C18Q-SBA-15's relatively low Q_m and low AEC. Therefore, proper length of alkyl chain and high value of AEC is required for quaternary ammonium functionalized mesoporous silica for its application to remove nitrate in aqueous solution. Longer alkyl chain quaternary ammonium has more hydrophobicity (Sharma et al., 2016). Therefore, longer alkyl chain quaternary ammonium functionalized silica gel has less hydrated environment. As a result, nitrate, which have highest hydrate energy, can be selectively removable among other anions (SenGupta, 1995).

Chapter 6 Synthesis and characterization of Quaternary ammonium functionalized silica gel

In this chapter, two different quaternary ammonium functionalized silica gel adsorbents with different alkyl chain lengths (C8Q-, and C18Q-silica gel) were synthesized from the modified chapter 5 method. From the characterization and batch experiments, quaternary ammonium functionalization well performed on silica gel. From the results of coexisting ions effects, C12Q-silica gel was selected as a proper adsorbent for selective nitrate removal. From the column experiments, breakthrough curves from various initial nitrate concentration, flow rate were well fitted with Bohart-Adams and Modified dose-resoponse model. Breakthrough curves from various column depth were well fitted with Bed-Depth-Service-Time model. Sorption capacity of packed column varied from 17.2 to 34.6 mg/g. From the regeneration experiments, nitrate sorption capacity maintained even after 2 times of regeneration. From the column experiments & model data, it is considered that C12Q-silica gel applicable for pilot-scale.

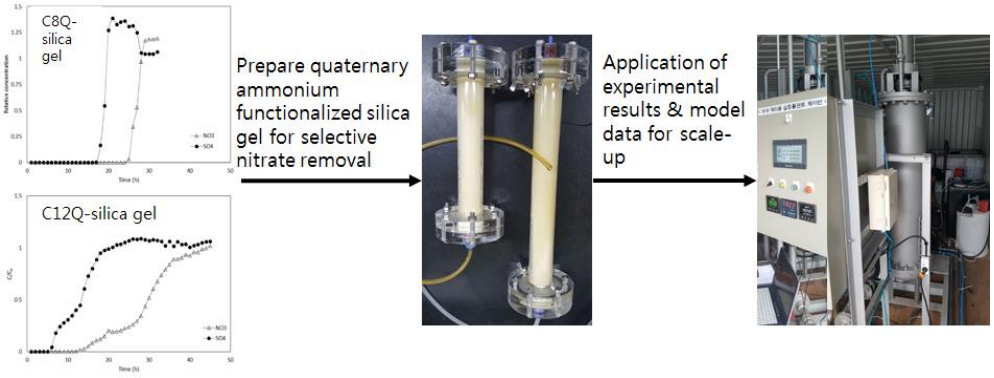

Figure 6.1. Graphical abstract of chapter 6

6.1. Materials and Methods

6.1.1. Synthesis of quaternary ammonium functionalized silica gel

All chemicals used in the experiments were purchased from Sigma Aldrich (Saint Louis, MO, USA) unless stated otherwise. A schematic diagram of the synthesis of quaternary ammonium functionalized silica gel is shown in Fig. 1. Firstly, silica gel (35-60 mesh) activation performed as following modified method from Li et al. (2011a). 300 g of silica gel was added into reaction flask contained 800 mL of 6 M HCl and refluxed for 8 h. After activation, separated activated silica gel washed with DI water to neutral, and dried at 65 °C for overnight. Based on the activated silica gel, two kinds of quaternary ammonium were functionalized which have different alkyl chain length (dimethyloctylquaternary ammonium and dimethyldodecylquaternary ammonium) on activated silica gel. The preparation of dimethylbutyl quaternary ammonium functionalized mesoporous silica were prepared as following procedure modified procedure from Carpenter et al. (2012). Firstly, 0.2 M of (3-chloropropyl)trimethoxysliane (≥97%) and 0.2 M of N,N-dimethyloctylamine (95%) were reacted at 85 °C for 48 h to synthesis Dimethyloctyl[3-(trimethoxysilyl)propyl]ammonium chloride. After reaction,

the resultant was reacted with 60 g of activated silica gel in 300 mL of toluene at 100 °C for 1 h. 1 mL of DI water were added as a hydrolytic deposition reaction initiator and refluxed at 100 °C for 48 h. The dimethyloctylquaternary ammonium functionalized silica gel was filtered and washed thoroughly with toluene and DI water until the effluent pH was neutral. The neutralized resultant stirred with 2 L of 0.1 M NaCl solution for 6 h. The NaCl reacted resultants were separated and dried at 65°C for overnight. After cooling, the dimethyloctylquaternary ammonium chloride functionalized silica gel (C8Q-silica gel) was obtained through fragmentation with mortar and pestle.

Base on the C8Q-silica gel preparation, the dimethyldodecylquaternary ammonium functionalized silica gel (C12Q-silica gel) were synthesized by substituting 0.2 M of N,N-dimethyldodecylamine (97%) for 0.2 M of N,N-dimethylbutylamine.

6.1.2. Characterization of Quaternary ammonium functionalized silica gel

Quaternary ammonium functionalized silica gel (C8Q-silica gel and C12Q-silica gel) were characterized using several techniques. Field-emission scanning electron microscopy (FE-SEM, Supra 55VP, Carl Zeiss, Oberkochen,

Germany) was used to analyze the surface morphology. Fourier-transform infrared (FTIR) spectroscopy (Nicolet 6700, Thermo Fisher Scientific, Waltham, MA, USA) was used to analyze the effect of quaternization on silica gel.

The anion exchange capacities were quantified by the method of Neagu and Mikhalovsky (2010). Firstly, 0.3 g of quaternary ammonium functionalized silica gel were loaded on 0.45-μm membrane filter and filtered with 300 mL of DI water and dried at 65°C. The resultants reacted with 5 % Na_2SO_4 solution (adsorbent dose = 1 g/L) for 6 h. After reaction, the samples were collected and filtered through a 0.45-μm membrane filter. The Concentration of chloride were measured by Ion Chromatography (IC, Dionex Aquion Ion Chromatography System, Thermo, USA). The anion exchange capacities (AEC, mmol/g) can be calculated with the following equation:

$$\mathrm{AEC} = \frac{C_{Cl^-}}{C_a} \tag{6.1}$$

where C_{Cl^-} is the chloride concentration in the aqueous phase after reaction (mmol/L), and C_a is the adsorbent dose (g/L).

6.1.3. Nitrate sorption batch experiments

Nitrate sorption experiments were performed under batch conditions. The desired concentration of nitrate solution was prepared by diluting a stock solution (1000 mg/L as NO_3^-), which was prepared from the sodium nitrate ($NaNO_3$, 99.0 %, Duksan Pure Chemicals). If there was no additional description, whole batch experiments were performed at 50 mL polypropylene conical tubes containing 30 mL solutions of Quaternary ammonium functionalized mesoporous silica (adsorbent dose = 1 g/L) and nitrate solution (100 mg/L as NO_3^-). The samples were shaken in a shaking incubator as 120 rpm at 30°C for 180 min in triplicate. After reaction, the samples were collected and filtered through a 0.45-μm membrane filter. Concentration of nitrate were measured with Ion Chromatography (IC, Dionex Aquion Ion Chromatography System, Thermo, USA).

To evaluate the effect of contact time on nitrate removal, the kinetic experiments were performed for 5, 15, 45, 60, 120, 180 min in triplicate. The nitrate sorption capacity at time '*t*'(q_t, mg/g) can be calculated with the following equation:

$$q_t = \frac{C_i - C_t}{C_a} \tag{6.2}$$

where C_i is the nitrate concentration in the aqueous phase before sorption reaction, C_t is the nitrate concentration in the aqueous phase at time 't', and C_a is the adsorbent dose.

The data from effect of contact time on nitrate removal of C8Q-silica gel and C12Q-silica gel experiment were fitted to the following nonlinear equations of pseudo first-order, pseudo second-order, and Elovich kinetic models :

$$q_t = q_e[1 - \exp(-k_1 t)] \tag{6.3}$$

$$q_t = \frac{k_2 {q_e}^2 t}{1 + k_2 q_e t} \tag{6.4}$$

$$q_t = \frac{1}{\beta}\ln(\alpha \cdot \beta) + \frac{1}{\beta}\ln(t) \tag{6.5}$$

where *qt* is the amount of adsorbed nitrate per unit mass of absorbent at time t (mg/g), and *qe* is the amount of adsorbed nitrate per unit mass of absorbent at equilibrium (mg/g). k_1 is the pseudo first-order rate constant (1/min), k_2 is the pseudo second-order rate constant (g/mg·min), α is the initial adsorption rate constant (mg/g·min), and β is the Elovich adsorption constant (g/mg).

To evaluate the effect of initial concentration on nitrate removal, the isotherm experiments were performed at various nitrate initial concentration (20, 50, 100, 200, 500, 1000 mg/L as NO_3^-). The nitrate sorption capacity (q_e, mg/g) can be calculated with the following equation:

$$q_e = \frac{C_i - C_f}{C_a} \tag{6.6}$$

where C_f is the nitrate concentration in the aqueous phase after reaction, and C_a is the adsorbent dose.

The data from effect of initial concentration on nitrate removal of C8Q-silica gel and C12Q-silica gel experiment were fitted to the following nonlinear equations of Langmuir, Freundlich, and Redlich-Peterson isotherm models :

$$q_e = \frac{Q_m K_L C_e}{1 + K_L C_e} \tag{6.7}$$

$$q_e = K_F {C_e}^n \tag{6.8}$$

$$q_e = \frac{K_R C_e}{1 + a_R C_e^g} \tag{6.9}$$

where Q_m is the maximum mass of adsorbed nitrate per unit mass of adsorbent (removal capacity, mg/g), and C_e is the concentration of copper in the aqueous solution at equilibrium (mg/L). K_L is the Langmuir constant related to the binding energy (L/g), K_F is the distribution coefficient (L/mg), n is the Freundlich constant, K_R is the Redlich-Peterson constant, a_R is the Redlich–Peterson constant related to the affinity of the binding sites, and g is the Redlich–Peterson constant related to the adsorption intensity.

The effect of pH experiments were also performed by adjusting pH of nitrate solutions (initial pH 2 to 12). pH of nitrate solutions were adjusted using 0.1 M NaOH and 0.1 M HCl solutions (prepared by using NaOH, > 93.0 % and 36 % HCl solution, Duksan Pure Chemicals). The nitrate sorption capacity (q_e, mg/g) was calculated with the Eq. (6.6)

To simulate the effects of competing anions, specific molar ratio solutions which are include chloride or bicarbonate or phosphate or sulfate over nitrate (molar ratio [Cl^- or HCO_3^- or PO_4^{3-} or SO_4^{2-}]/[NO_3^-] = 0, 0.5, 1, 2, 3, 4 (nitrate = 100 mg/L)) solutions were prepared. The competing anion experiments were performed with 50 mL polypropylene conical tubes containing 30 mL solutions of quaternary ammonium functionalized silica gel (adsorbent dose = 1 g/L), which were shaken in a shaking incubator as 120 rpm at 30°C for 180 min in triplicate. The nitrate sorption capacity (q_e, mg/g) was calculated with the Eq. (6.6). The relative nitrate sorption reduction (*RNR*) was calculated as following the Eq. (6.10).

$$RNR(\%) = \left(1 - \frac{q_e \ \ w/ \ \ competing \ \ ion}{q_e \ ^{w}/_{o} \ competing \ \ ion}\right) * 100 \qquad (6.10)$$

6.1.4. Fixed bed column breakthrough experiments

Fixed-bed column experiments were conducted to evaluate the dynamic behavior of nitrate removal by C8Q-silica gel and C12Q-silica gel. Column experiments were conducted using a plexiglas column (column length = 10 cm; inner diameter = 2.5 cm) packed with C8Q-silica gel and C12Q-silica gel (porosity = 0.66) if there has no other description. For column experiments, column was packed by the tap-fill method and connected to a high performance liquid chromatography pump (HPLC series II, Scientific Systems Inc., PA, USA) operating at a rate of 60 mL/h. Prior to the transport experiments, the packed column was flushed upward with >10 bed volume of deionized water until the column effluent was clear and steady-state flow was established. After stabilization, the injection solutions which have specific condition were introduced until nitrate concentration of effluent was same as influent. Portions of the effluent were collected using an auto collector (Retriever 500, Teledyne, City of Industry, CA, USA) at regular intervals (about 1 times of bed volume). The anion concentrations on collected effluents were measured with IC.

Firstly, to examine the dynamic nitrate removal of C8Q-silica gel and C12Q-silica gel, 100 mg/L as NO_3^- solution was injected continuously at flow rate = 60 ml/h.

Secondly, to examine the effect of competing anion on the dynamic nitrate removal of C8Q-silica gel and C12Q-silica gel, the ground water composition reported by Kabay et al. (2007) was injected. The mimicked ground water prepared as following. Firstly, add 1 M HNO_3 1.2 mL and 2 M of HCl 0.41 mL into 1 L flask and add DI water until the volume of solution reached to 1 L. 0.4935 g of $CuSO_4 \cdot 0.5H_2O$, 0.4437 g of $MgSO_4 \cdot 7H_2O$, 0.1190 g of $NaNO_3$, 0.0607 g of KNO_3, 0.0327 g of NaCl, and 0.0269 g of $NaHCO_3$ were added into above solution and stirred. The solution pH was adjusted with 0.1 M NaOH solution into 7.6.

From the results batch tests and first and second column experiments, C12Q-silica gel chosen as a proper quaternary ammonium functionalized silica gel for selective nitrate removal than C8Q-silica gel. To examine the effect of flow rate on the dynamic nitrate removal of C12Q-silica gel, 100 mg/L as NO_3^- solution was injected continuously at flow rate = 120 and 180 mL/h. In addition, 300 and 500 mg/L as NO_3^- solution was injected continuously at flow rate = 180 mL/h to examine the effect of influent concentration on the dynamic nitrate removal of C12Q-silica gel.

Furthermore, to identify the effect of bed depth, column were packed with Plexiglas column which are length = 20, 30 cm (inner diameter = 2.5 cm) with

same porosity of 10 cm column. 500 mg/L as NO_3^- solution was injected continuously at flow rate = 180 mL/h.

To examine the effect of competing anion on the dynamic nitrate removal of C12Q-silica gel more, HCO_3^- were added into the ground water composition reported by Kabay et al. (2007) as 1 times and 2 times molar concentration of nitrate. Prepared solutions were injected continuously at flow rate = 60 mL/h.

Additionally, to examine the effect of regeneration on the dynamic nitrate removal of C12Q-silica gel, nitrate adsorbed C12Q-silica gel at 500 mg/L as NO_3^- and flow rate = 180 mL/h was regenerated. Regeneration process was conducted with injection of 3 BV of 10% NaCl solution and 2 BV of DI water. After regeneration, 500 mg/L as NO_3^- solution was injected continuously at flow rate = 180 mL/h. Regeneration and nitrate dynamic removal tests were performed twice.

Summary of column experimental conditions are represented in Table 6.1.

Table 6.1. The experimental conditions for column experiments

Ex.	Adsorbent	Influent condition	C_0 (mg/L)	u (cm/h)	Q (mL/h)	Z (cm)	Bed volume (cm^3)	EBCT (h)	Porosity	Mass of adsorbent (g)
1	C8Q-gel	100 mg/L as NO_3^-	100 (NO_3^-)	12.22	60	10	49.09	0.818	0.664	28.7
2	C12Q-gel	100 mg/L as NO_3^-	100 (NO_3^-)	12.22	60	10	49.09	0.818	0.664	28.8
3	C8Q-gel	AGW	140 (NO_3^-), 440 (SO_4^{2-}), 20 (HCO_3^-)	12.22	60	10	49.09	0.818	0.664	28.7
4	C12Q-gel	AGW	140 (NO_3^-), 440 (SO_4^{2-}), 20 (HCO_3^-)	12.22	60	10	49.09	0.818	0.664	28.8
5	C12Q-gel	100 mg/L as NO_3^-	100 (NO_3^-)	24.44	120	10	49.09	0.409	0.664	28.8
6	C12Q-gel	100 mg/L as NO_3^-	100 (NO_3^-)	36.66	180	10	49.09	0.273	0.664	28.8
7	C12Q-gel	300 mg/L as NO_3^-	300 (NO_3^-)	36.66	180	10	49.09	0.273	0.664	28.8
8	C12Q-gel	500 mg/L as NO_3^-	500 (NO_3^-)	36.66	180	10	49.09	0.273	0.664	28.8
9	C12Q-gel	500 mg/L as NO_3^-	500 (NO_3^-)	36.66	180	20	98.18	0.546	0.664	57.6
10	C12Q-gel	500 mg/L as NO_3^-	500 (NO_3^-)	36.66	180	30	147.27	0.819	0.664	86.4
11	C12Q-gel	AGW + HCO_3 140 mg/L	140 (NO_3^-), 440 (SO_4^{2-}), 160 (HCO_3^-)	12.22	60	10	49.09	0.818	0.664	28.8
12	C12Q-gel	AGW + HCO3 280 mg/L	140 (NO_3^-), 440 (SO_4^{2-}), 300 (HCO_3^-)	12.22	60	10	49.09	0.818	0.664	28.8
13	C12Q-gel (regenerated w/ 10% NaCl)	500 mg/L as NO_3^-	500 (NO_3^-)	36.66	180	10	49.09	0.273	0.664	28.8

The nitrate adsorption capacity at breakthrough (when C_t = 0.01 – 0.05) and exhaustion (when C_t = 1) from column experiments (q_i^{col}, q_e^{col}, mg/g) can be calculated as following Equation (Golie and Upadhyayula, 2016) :

$$q_i^{col} = \frac{Q}{M} C_0 \int_0^{t_i} \left(1 - \frac{C_t}{C_0}\right) \mathrm{dt} \qquad (6.11)$$

$$q_e^{col} = \frac{Q}{M} C_0 \int_0^{t_e} \left(1 - \frac{C_t}{C_0}\right) \mathrm{dt} \qquad (6.12)$$

where Q is the volumetric flow rate (mL/h), M is the amount of the adsorbent packed in the column (g), C_0 is the nitrate concentration of influent (mg/L), t_i is the time when breakthrough (h), t_e is the time when exhaustion (exhaustion time, h), C_t is the nitrate concentration at time t (mg/L). The total solute removal percent (Mr, %) also can be calculated as following:

$$Mr = \frac{q_e \times M}{Q \times C_0 \times t_e} \times 100 \ \ (\%) \qquad (6.13)$$

The data from effect of flow rate and effect of initial nitrate concentration were fitted to the following equations of Bohart-Adams, Clark, and modified dose-response models (Lee et al., 2015):

$$\frac{C_\mathrm{t}}{C_0} = \frac{1}{e^{\frac{k_{BA} \times N_0 \times Z}{u} - k_{BA} \times C_0 \times t} + 1} \qquad (6.14)$$

$$\frac{C_t}{C_0} = \left(\frac{1}{Ae^{-rt}+1}\right)^{\frac{1}{n-1}} \quad (6.15)$$

$$\frac{C_t}{C_0} = 1 - \frac{1}{\left(\frac{C_0 Qt}{q_0 X}\right)^{a} + 1} \quad (6.16)$$

where k_{BA} is the Bohart-Adams rate constant (L/h/mg), N_0 is the sorption capacity per unit volume of fixed-bed (mg/L), *Z* is the the total bed depth (cm), *u* is the linear flow velocity (cm/h), *A* is the Clark model constant (-), *r* is the Clark model constant (L/h), q_0 is the sorption capacity per unit mass of adsorbent (mg/g), *X* is the mass of the adsorbent packed in the column (g), *a* is the modified dose-response model constant (-). Thomas model was not used in this study from the reason that the actual Thomas model is able to be reduced into Bohart-Adams model (Chu, 2010; Lee et al., 2015).

The data from effect of bed depth were fitted to the following bed depth service time (BDST) model.

$$t_b = \left(\frac{N_0 Z}{C_0 u}\right) - \left(\frac{1}{k_{BA} C_0}\right) \times \ln\left(\frac{C_0}{C_b} - 1\right) \quad (6.17)$$

where k_α is the kinetic BDST constant (L/h/mg).

6.2. Results and Discussion

6.2.1. Characteristics of quaternary ammonium functionalized silica gel

FE-SEM images and digital images are presented in Fig. 6.2. From the digital images, C8Q-silica gel has a fancy light yellow color and C12Q-silica gel has lighter yellow than C8Q-silica gel. From the FE-SEM images, C8Q-silica gel and C12Q-silica gel had irregular shape bigger than 100 μm. Unlike C8Q-SBA-15 and C12Q-SBA-15, C8Q-silica gel and C12Q-silica gel was not coagulated.

Figure 6.2. FE-SEM images of C8Q-silica gel and C12Q-silica gel (bar = 150 μm, inset = digital image)

FTIR spectra are presented in Fig. 6.3. In the spectra, the peaks of at 798.8 – 799.6 cm^{-1} and 1057.1 – 1059.3 cm^{-1} were attributed to stretching of siloxane (Si-O-Si) (Liu et al., 2011a). The peak at 797 – 806 cm^{-1} is also considered as comes from Si-C stretching (Simons and Laboratories, 1978). Like quaternarized SBA-15, several new peaks also appeared at C8Q-silica gel and C12Q-silica gel. The peaks at 1468.1 (C8Q-silica gel) and 1467.7 cm^{-1} (C12Q-silica gel) were newly observed which is known as CH_2 or CH_3 asymmetric bending (Simons and Laboratories, 1978) that is considered as contribution of methylene group in alkyl chain. The peaks at 2928.1 – 2923.2 cm^{-1} and 2853.3 cm^{-1} known as CH_2 asymmetric stretching and CH_2 symmetric stretching (Simons and Laboratories, 1978) were also observe like C8Q-SBA-15 and C12Q-SBA-15. Those FTIR spectra showed that quaternization on silica gel was well performed as quaternization on SBA-15.

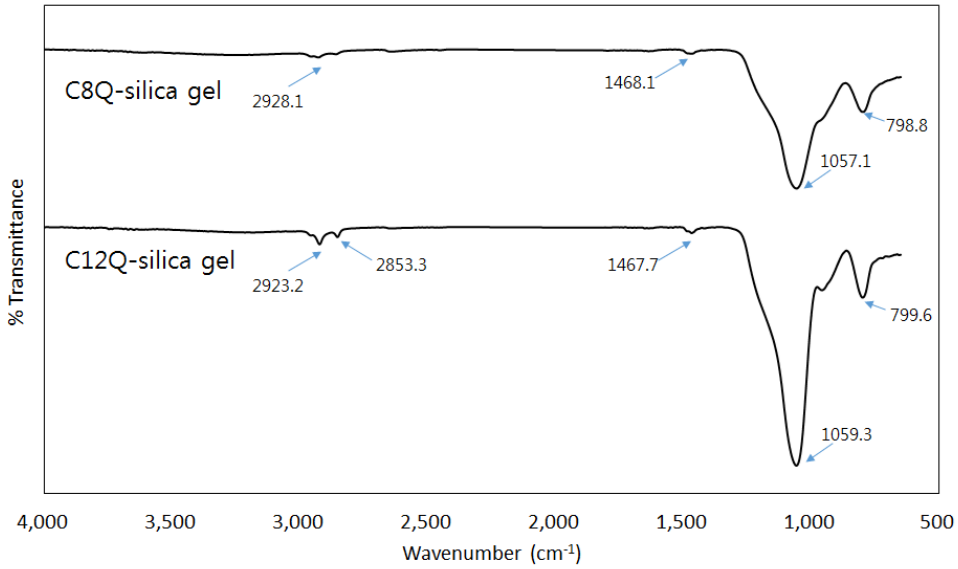

Figure 6.3. FTIR spectra of C8Q-silica gel and C12Q-silica gel

The anion exchange capacities (AEC, mmol/g) results are represented in Table 6.2. From the results, C8Q-silica gel and C12Q-slica gel's AEC were 0.646 ± 0.0044 and 0.761±0.2621 mmol/g. The similarity of AEC is considered as preparation of quaternary functionalized silica gel were successfully performed, irrespective of alkyl chain length.

Table 6.2. The anion exchange capacities results

Adsorbent	AEC (mmol/g)
C8Q-silica gel	0.646±0.0044
C12Q-silica gel	0.761±0.2621

6.2.2. Nitrate sorption Characteristics of quaternary ammonium functionalized silica gel

From the data of effect of contact time on the nitrate removal, the kinetic model analysis results and parameters are presented in Fig. 6.4 and Table 6.3. R^2, χ^2, and SSE indicate that Pseudo first model was most suitable model for describing the kinetic data of C8Q-silica gel and Pseudo second model for C12Q-silica gel. k_1 parameters also indicate that nitrate sorption rate of C8Q-silica gel (k_1 = 0.344 1/min) was faster than C12Q-silica gel (k_1 = 0.067 1/min). However, adsorbed nitrate sorption capacity at equilibrium (q_e from Pseudo first model) of C8Q-silica gel (35.98 mg/g) was similar with C12Q-silica gel (33.77 mg/g).

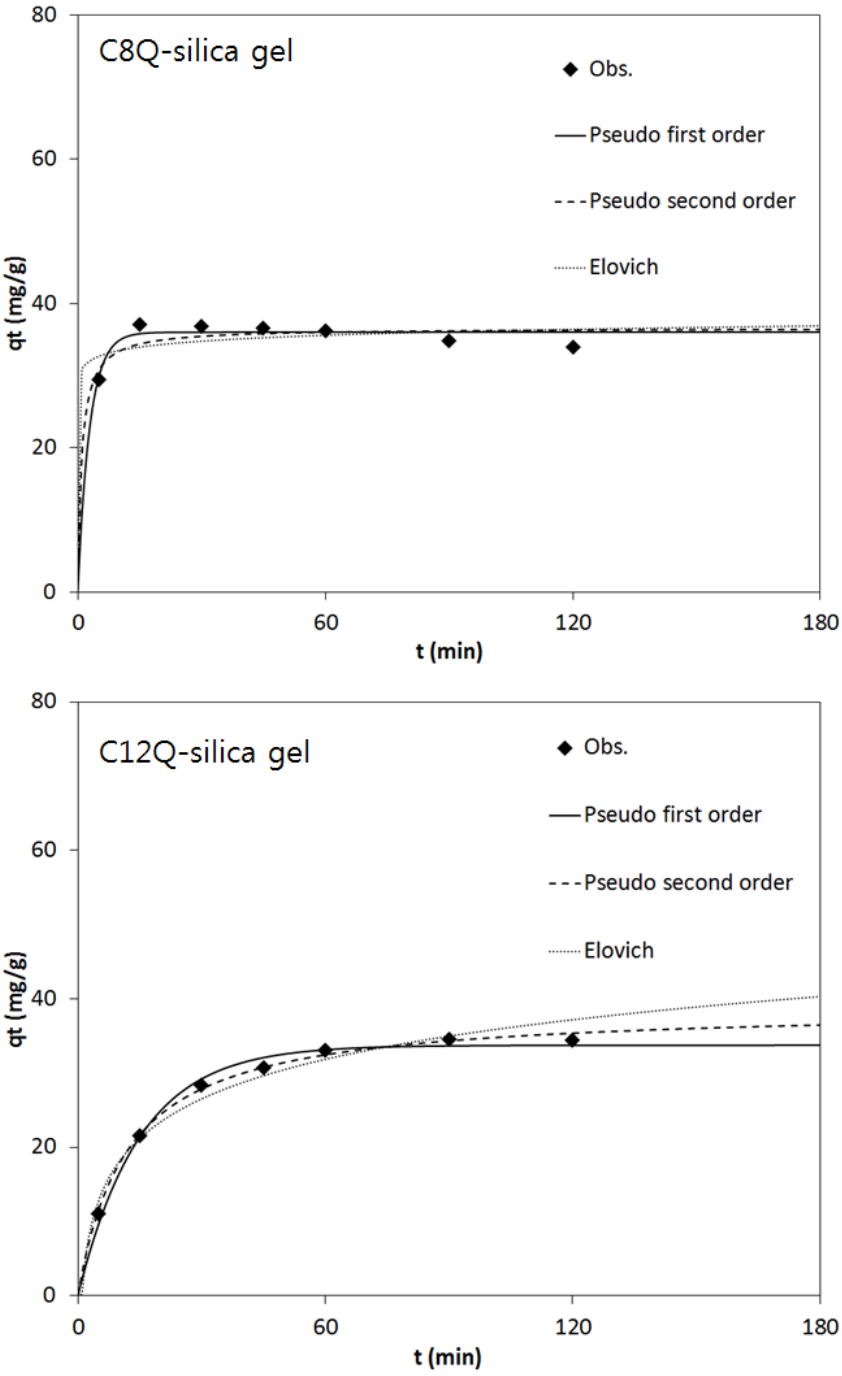

Figure 6.4. The kinetic models analysis results

Table 6.3. Kinetic model parameters obtained from nitrate removal of C8Q-silica gel and C12Q-silica gel

Adsorbents	Kinetic model															
	Pseudo 1st					Pseudo 2nd						Elovich				
	q_e (mg/g)	k_1 (1/min)	R^2	χ^2	SSE	q_e (mg/g)	K_2 (g/mg/min)	h	R^2	χ^2	SSE	α (mg/g/min)	β ((g/mg)	R^2	χ^2	SSE
C8Q-silica gel	35.98	0.344	0.849	2.6E+1	7.8E-1	36.640	0.028	2.9E-2	0.655	4.0E+1	1.2E+0	2.285E+11	0.844	0.369	6.1E+1	1.9E+0
C12Q-silica gel	33.77	0.067	0.989	9.3E+0	4.0E-1	38.879	0.002	1.8E-4	0.996	2.6E+0	9.2E-2	8.06	0.130	0.967	3.8E+1	1.3E+0

The effect of initial concentration results are shown in Fig. 6.5. At the initial concentration = 20 mg/L, sorption capacity were calculated as 10.61 ± 0.03, 12.43 ± 0.05 mg/g (from C8Q-silica gel and C12Q-silica gel). By increasing of initial concentration into 100 mg/L, sorption capacity were increased as, 31.34 ± 0.61, 38.84 ± 0.02 mg/g. Further, when initial concentration is 1000 mg/L, sorption capacity were increased more as 60.16 ± 5.80, 56.44 ± 10.21 mg/g. From the effect of initial concentration results, nitrate sorption capacity were dependent on initial nitrate concentration and ~~AEC, irrespective of alkyl chain length.~~

The equilibrium model analysis results and parameters are presented in Fig. 6.6 and Table 6.4. R^2, χ^2, and SSE indicate that Redlich-Peterson model was most suitable model for describing the equilibrium data. From the Langmuir model, the maximum nitrate sorption capacities (Q_m) of C8Q-silica gel and C12Q-silica gel were 51.88, 46.367 mg/g.

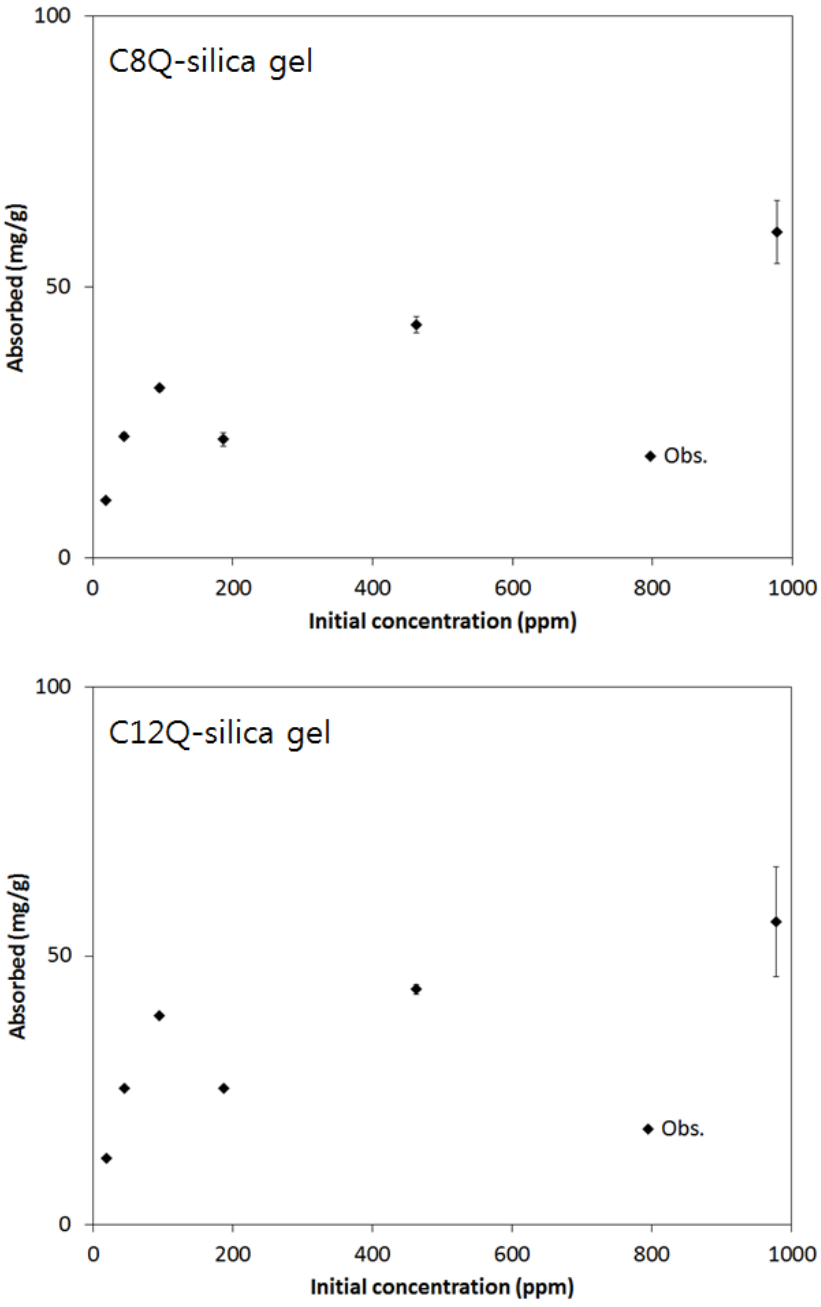

Figure 6.5. The results of initial nitrate concentration effect on the nitrate removal

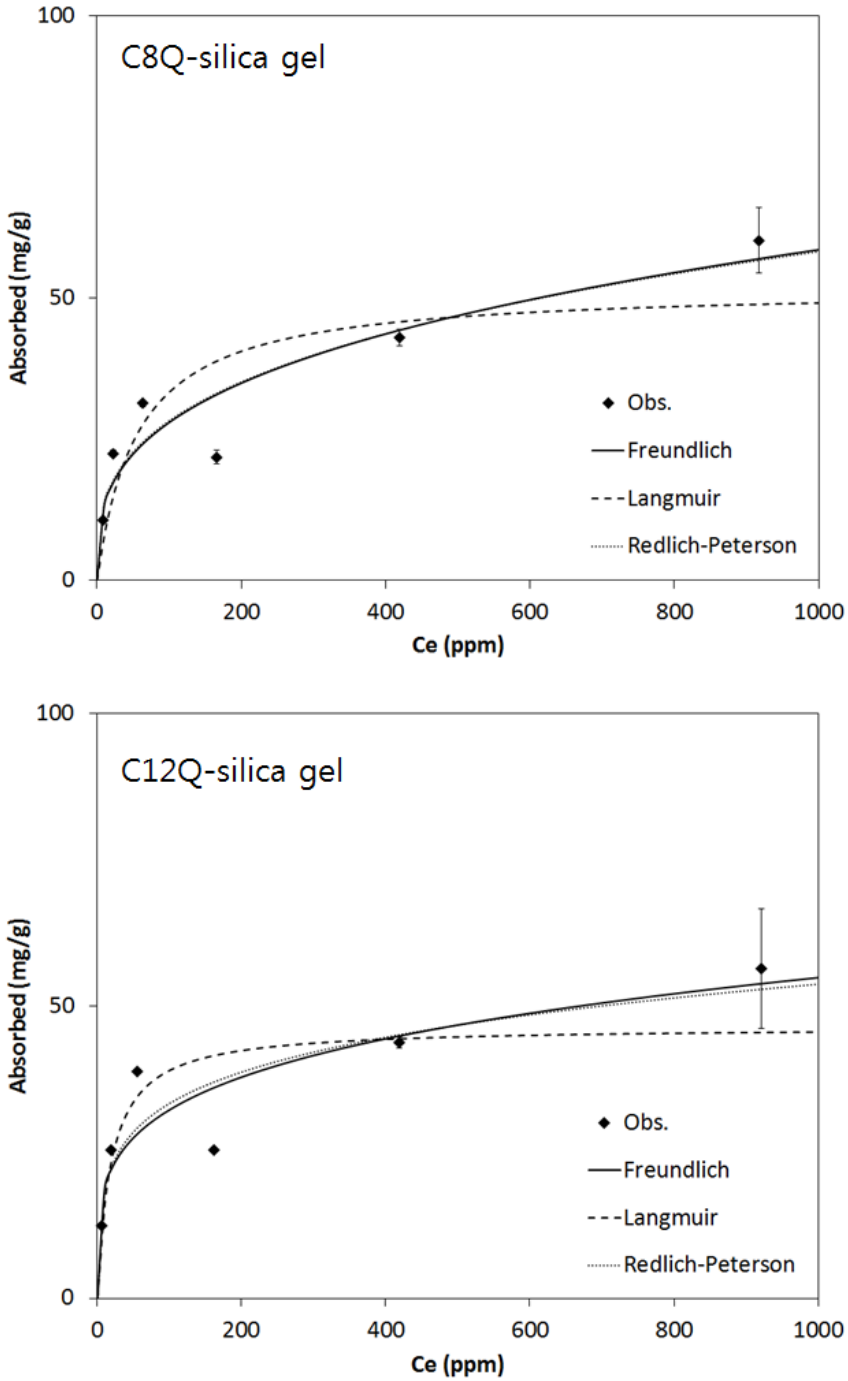

Figure 6.6. The equilibrium models analysis results

Table 6.4. Equilibrium isotherm model parameters

Adsorbents	Freundlich						Langmuir					Redlich-Peterson						
	K_F (L/g)	1/n	q_m (mg/g)	R^2	χ^2	SSE	Q_m (mg/)	K_L (L/mg)	R^2	χ^2	SSE	K_R (L/g)	a_R (1/mg)	K_R/a_R (mg/g)	g	R^2	χ^2	SSE
C8Q-silica gel	6.389	0.321	58.091	0.863	8.95	214.51	51.881	0.018	0.677	19.71	505.34	2861.4	428.5	6.68	0.687	0.863	9.07	215.02
C12Q-silica gel	11.138	0.231	54.538	0.784	9.74	266.52	46.367	0.053	0.675	12.91	400.71	11.055	0.794	13.93	0.804	0.789	9.18	260.55

Result of initial pH effect is presented in Fig. 6.7. Trend of nitrate sorption on C8Q-silica gel and C12Q-silica gel was familiar with the results from quaternary ammonium functionalized SBA-15. Briefly, nitrate sorption was decreased when initial pH was decreased from 4 into 2. This trend is can be explained by nitrate movement restriction to the sorption site was enhanced from H^+ ion concentration increasing (Sowmya and Meenakshi, 2013). By increasing initial pH = 4 to 10, sorption capacities were gradually deceased from 37.10 ± 2.17, 39.26 ± 0.35 mg/g (from C8Q-silica gel and C12Q-silica gel) to 21.74 ± 0.88, 29.81 ± 0.30, mg/g. Further increasing of initial pH into 12, nitrate sorption capacities were vastly decreased into 5.51 ± 0.45, 5.50 ± 0.04 mg/g. This trend can be explained as effect of OH^- ions as a challenging ion increase (Sowmya and Meenakshi, 2013, 2014).

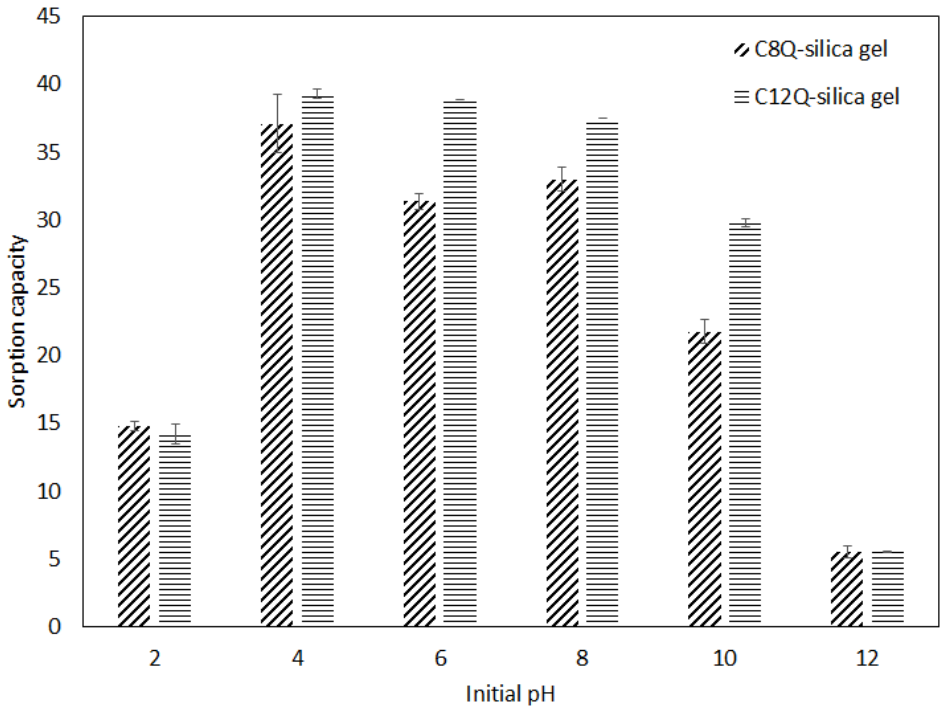

Figure 6.7. Results of initial pH effect on nitrate removal using C8Q-silica gel and C12Q-silica gel

The effect of competing anion results are shown in Fig. 6.8. From the C8Q-silica gel results, nitrate sorption capacity was increased from 31.34 ± 0.61 mg/g ($[Cl^-]/[NO_3^-] = 0$) to 26.91 ± 0.04 mg/g (RNR = 14.1%, $[Cl^-]/[NO_3^-] = 0.5$) and it slightly further decreased to 25.80 ± 0.15 mg/g (RNR = 17.7%, $[Cl^-]/[NO_3^-] = 1$) and continuously decreased till $[Cl^-]/[NO_3^-] = 4$ as 19.45 ± 1.41 mg/g (RNR = 37.9%) when Cl^- is a competing anion. Effect of competing HCO_3^- or PO_4^{3-} or SO_4^{2-} was similar as Cl^- coexisting effect. Nitrate sorption capacities were reduced more than half as 14.95 ± 0.07 mg/g (RNR = 52.3%), 6.04 ± 0.15 mg/g (RNR = 80.7%), and 14.39 ± 0.77 mg/g (RNR = 54.1%) when $[HCO_3^-$ or PO_4^{3-} or $SO_4^{2-}]/[NO_3^-] = 0.5$. Even $[HCO_3^-$ or PO_4^{3-} or $SO_4^{2-}]/[NO_3^-] = 4$, nitrate sorption capacity were 4.22 ± 0.41, 3.18 ± 0.10, and 9.36 ± 0.26 mg/g (RNR = 86.5, 89.8, and 70.1%). From the results, Cl^- coexisting effect was lowest and PO_4^{3-} coexisting effect was highest in C8Q-silica gel nitrate removal.

The effect of competing anion result of C12Q-silica gel was familiar with the result of C8Q-silica gel. However, its RNR is lower than C8Q-silica gel. Nitrate sorption capacity was 38.34 ± 0.02 mg/g ($[\text{competing anion}]/[NO_3^-] = 0$) was changed as 31.23 ± 0.15, 22.03 ± 0.53, 12.45 ± 0.16, and 20.33 ± 1.04 mg/g (RNR = 19.6, 42.3, 67.9, and 47.7%) when $[\text{competing anion}]/[NO_3^-] = 0.5$ (competing anion = Cl^-, HCO_3^-, PO_4^{3-}, and SO_4^{2-}). Even [competing

anion]/[NO_3^-] = 4, nitrate sorption capacities were 20.53 ± 0.19, 9.21 ± 0.10, 7.12 ± 0.01, and 12.43 ± 0.02 mg/g (RNR = 47.2, 76.3, 81.7, and 68.0%, competing anion = Cl^-, HCO_3^-, PO_4^{3-}, and SO_4^{2-}). From the effect of competing anion results, the C12Q-silica gel showed higher nitrate sorption capacity and lower RNR values, except Cl^- was competing anion.

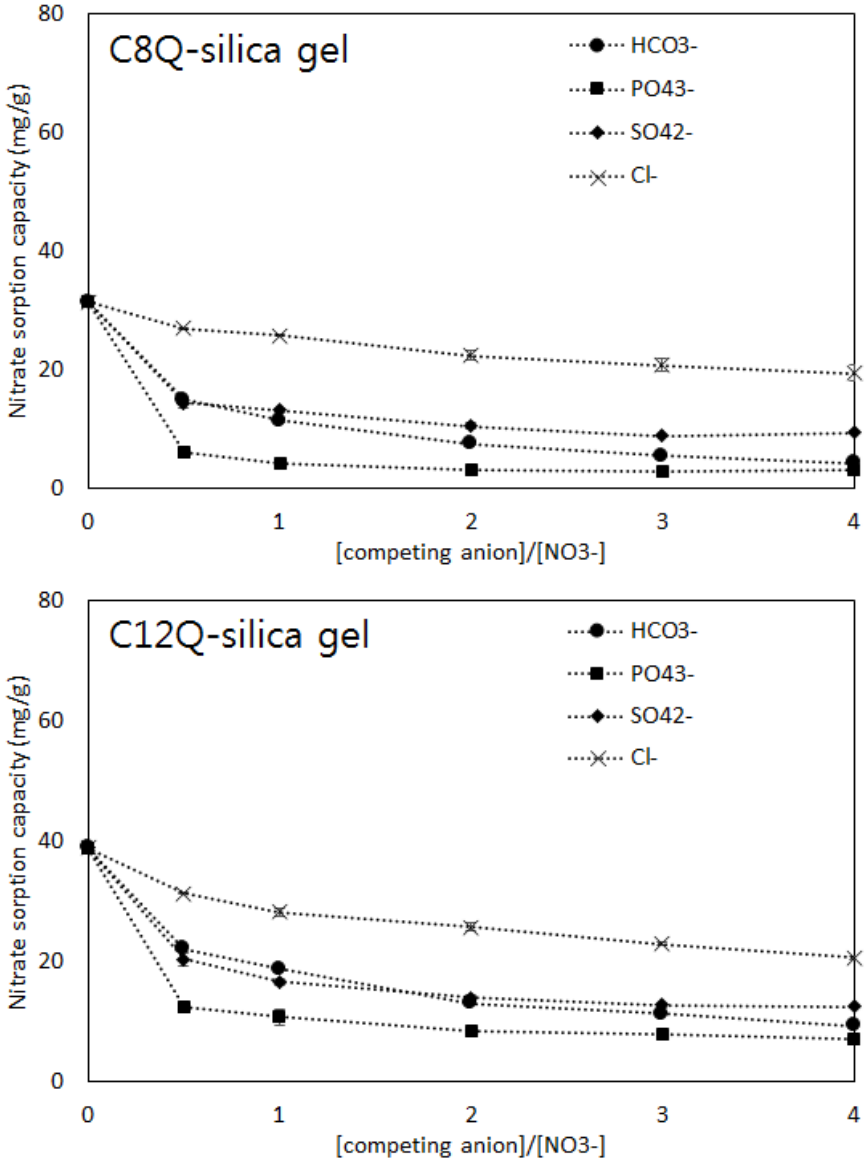

Figure 6.8. Results of competing anion on nitrate removal by using C8Q-silica gel and C12Q-silica gel

The model fitting results and q_e^{col} for column experiments are presented in Table 6.5. Converted q_e^{col} into mg/L dimension are also represented for the comparison with N_0. The breakthrough curves from the column experiment and its model fitting results when influent = 100 mg/L as NO_3^-, flow rate = 60 mL/h (Ex.1, 2) are represented in Fig.6.9. Model analysis results are represented in Table 6.5. From the breakthrough curves, C8Q-silica gel's breakthrough occurred at 85 h and C12Q-silica gel's breakthrough was faster (at 70 h). On the contrary to breakthrough, exhaustion of C8Q-silica gel was 111 h which is faster than C12Q-silica gel (145 h). q_e^{col} of C8Q-silica gel and C12Q-silica gel were 19.87, 16.67 mg/g. It is considered that difference between breakthrough curve shapes of C8Q-silica gel and C12Q-silica gel is contributed from nitrate sorption rate. From the Bohart-Adams model fitting results, k_{BA} of C8Q-silica gel was 0.0022 L/mg/h bigger than 0.0013 L/mg/h from C12Q-silica gel. k_{BA} is the rate constant on quasi-chemical rate expression as following equation (Chu, 2010);

$$\frac{\partial \mathrm{q}}{\partial \mathrm{t}} = k_{BA} C (q_0 - q) \qquad (6.18)$$

Therefore, higher value of k_{BA} means faster sorption characteristics without reference to sorption capacity. From C8Q-silica gel's faster nitrate sorption characteristics than C12Q-silica gel, nitrate was not discharged until C8Q-silica gel's nitrate sorption mostly maximized. Until breakthrough occurred,

q_i^{col} of C8Q-silica gel nitrate sorption capacity was 16.57 mg/g which was bigger than 13.23 mg/g from C12Q-silica gel. Those similar sorption capacity and difference on kinetics are corresponded to characteristics from batch experiments.

Table 6.5. Model parameters and q_e^{col} for fixed bed column experiments

	q_e^{col}		Bohart-Adams					Clark					Modified dose-response				
Ex.	mg/g	mg/L	kBA (L/mg/h)	N_0 (mg/L)	R^2	χ^2	SSE	A (-)	r (L/h)	R^2	χ^2	SSE	q_0 (mg/g)	a (-)	R^2	χ^2	SSE
1	19.87	11658	0.0022	11838	0.9906	0.63	0.04	3.23E+14	0.3124	0.9948	0.01	0.02	20.228	21.0268	0.9887	0.66	0.05
2	16.67	12990	0.0013	10170	0.9980	2.59	0.06	1.55E+10	0.2301	0.9914	9.28	0.26	17.236	10.7249	0.9992	1.26	0.02
5	18.7	10971	0.0018	10979	0.9909	7.57	0.14	2.40E+08	0.3576	0.9758	18.62	0.37	18.522	7.6910	0.9959	3.15	0.06
6	21.8	12790	0.0022	12733	0.9898	7.25	0.15	1.18E+07	0.3771	0.9749	29.96	0.37	21.451	7.3773	0.9928	2.27	0.11
7	22.5	13201	0.0028	12244	0.9743	9.49	0.16	4.23E+09	1.5784	0.9602	27.24	0.25	20.79	8.4802	0.9807	4.90	0.12
8	22.7	13318	0.0025	12793	0.9915	305.41	0.06	1.63E+08	2.0638	0.9820	572.58	0.12	21.648	8.5657	0.9948	198.78	0.04
9	35.4	20769	0.00056	20669	0.9865	25.68	0.08	1.91E+06	0.4668	0.9689	94.35	0.18	34.624	6.0921	0.9901	5.64	0.06
10	30.4	17836	0.00025	17265	0.9695	1.97	0.18	4.10E+03	0.1794	0.9479	4.25	0.30	28.177	3.6384	0.9756	0.53	0.14

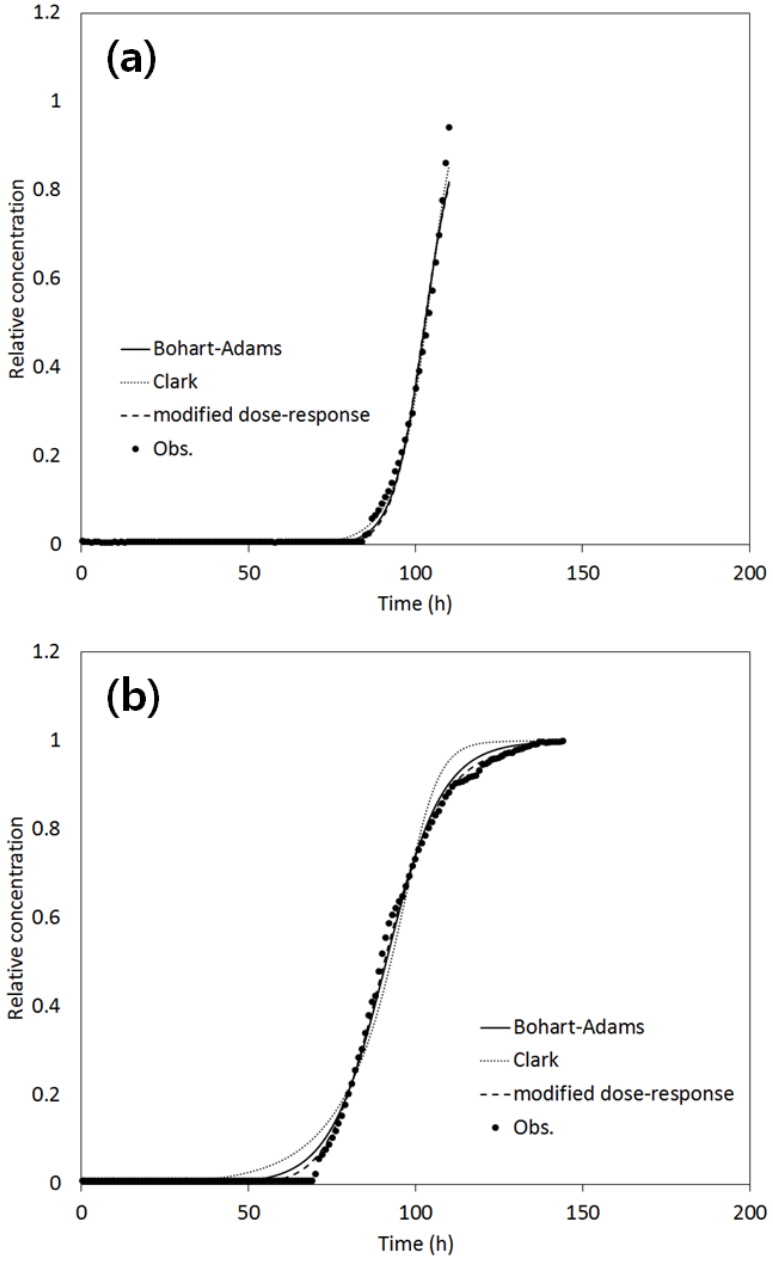

Figure 6.9. Breakthrough curves for nitrate removal using quaternized silica gel (C_0 = 100 mg/L as NO_3^-); (a) C8Q-silica gel, (b) C12Q-silica gel

The breakthrough curves from the column experiment when influent = artificial groundwater, flow rate = 60 mL/h (Ex.3, 4) are represented in Fig.6.10. From the results, time for breakthrough of SO_4^{2-} were 17 h and 5h from C8Q-silica gel and C12Q-silica gel. Time for breakthrough of NO_3^- were 25 h and 13 h from C8Q-silica gel and C12Q-silica gel. Gap between time for breakthrough of SO_4^{2-} and NO_3^- were 8 h, irrespective of alkyl chain length. Even its similar gap, shape of breakthrough curves and q_e^{col} are quite different. The breakthrough curve from C8Q-silica gel was steeper than the curve from C12Q-silica gel like Fig. 6.10. q_e^{col} for NO_3^- were 8.22, 8.27 mg/g from C8Q-silica gel and C12Q-silica gel, while SO_4^{2-} were 16.19, 10.41 mg/g from C8Q-silica gel and C12Q-silica gel. From those results, C12Q-silica gel is considered more proper quaternized silica gel than C8Q-silica gel for selective nitrate removal, though slower sorption kinetics.

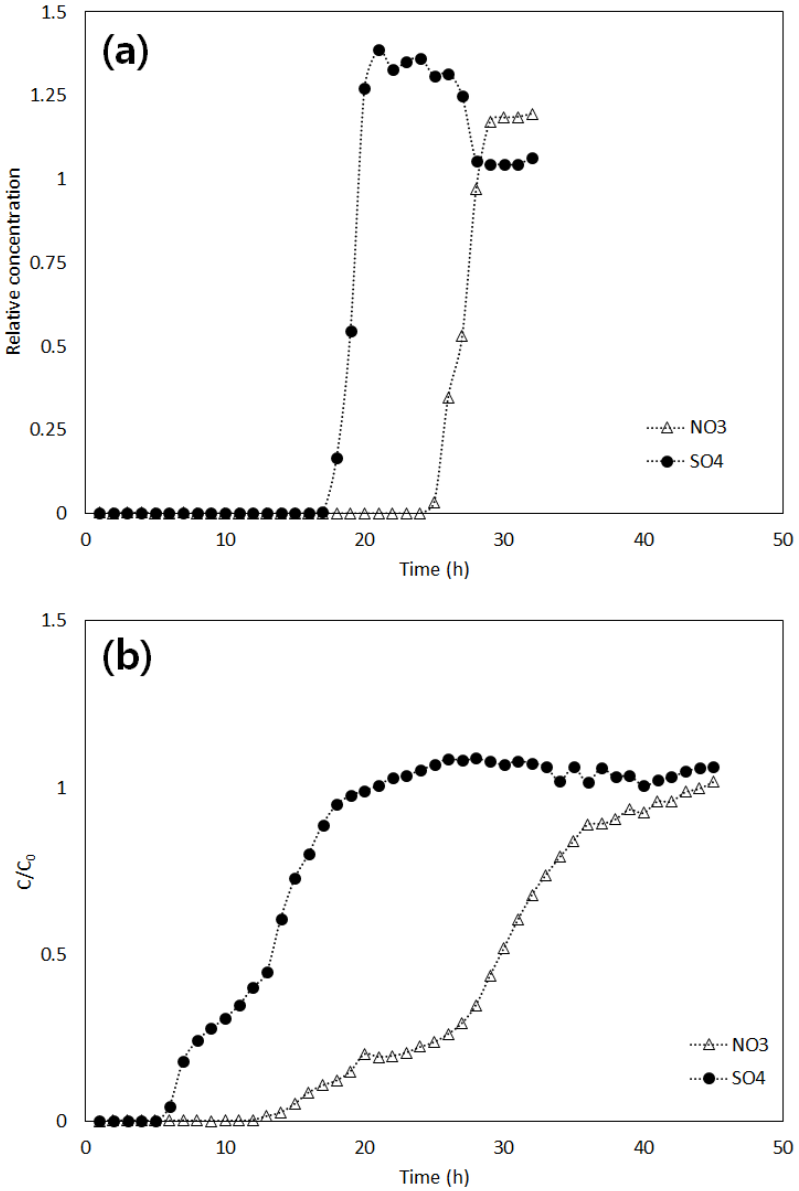

Figure 6.10. Breakthrough curves for nitrate and sulfate removal on C8Q-gel and C12Q-gel in artificial groundwater; (a) C8Q-silica gel, (b) C12Q-silica gel

The breakthrough curves and model fitted data from the column experiment when influent = 100 mg/L as NO_3^-, flow rate = 60, 120, and 180 mL/h (Ex.2, 5, and 6) are represented in Fig.6.12. From the results, time for breakthrough were 71, 33.5, and 24.3 h when flow rate 60, 120, and 180 mL/h. Even those time for breakthrough difference, q_i^{col} was not related into flow rate (13.2, 13.1, and 13.4 mg/g when flow rate 60, 120, and 180 mL/h). Time for exhaustion were also getting faster by flow rate increasing (145, 76, and 56.7 h when flow rate 60, 120, and 180 mL/h). q_e^{col} were also not related into flow rate (22.1, 18.7, and 21.8 mg/g when flow rate 60, 120, and 180 mL/h). If nitrate removal kinetics too fast to be affected to flow rate, breakthrough curves will be overlapped when X-axis is bed volume (Concentrations of effluent are only affected passed quantity of solution). Breakthrough curves when X-axis is bed volume is presented in Fig.6.11(a). From the Fig.6.11(a), Bed volume for breakthrough from various flow rates are mostly overlapped (86.78, 81.89, and 89.23 BV when flow rate = 60, 120, and 180 mL/h). However, bed volume for exhaustion is getting later by flow rate increasing (177.24, 185.24, and 207.79 BV when flow rate = 60, 120, and 180 mL/h). Therefore, it is expected that k_{BA} will be lower with higher flow rate. However, k_{BA} was higher with higher flow rate (0.00130, 0.00179, and 0.00216 L/mg/h, when flow rate = 60, 120, and 180 mL/h). In conclusion, k_{BA} from various flow

rate cannot be directly comparable. To compare k_{BA} even various flow rate, Bohart-Adams model was modified as following;

$$\frac{C_t}{C_0} = \frac{1}{e^{\frac{k_{BA,BV} \times N_0 \times Z}{u_{BV}} - k_{BA,BV} \times C_0 \times \mathrm{BV}} + 1} \quad (6.19)$$

where $k_{BA,BV}$ is the modified Bohart-Adams rate constant (L/BV/mg), N_0 is the sorption capacity per unit volume of fixed-bed (mg/L), Z is the the total bed depth (cm), u_{BV} is the modified linear flow velocity (cm/BV). Model fitted results using modified Bohart-Adams model is represented in Fig.6.12(b). From the modified Bohart-Adams fitting, $k_{BA,BV}$ were calculated as 0.001063, 0.000732, and 0.000589 L/BV/mg when flow rate 60, 120, and 180 mL/h. $k_{BA,BV}$ are getting lower by increasing flow rate as expected.

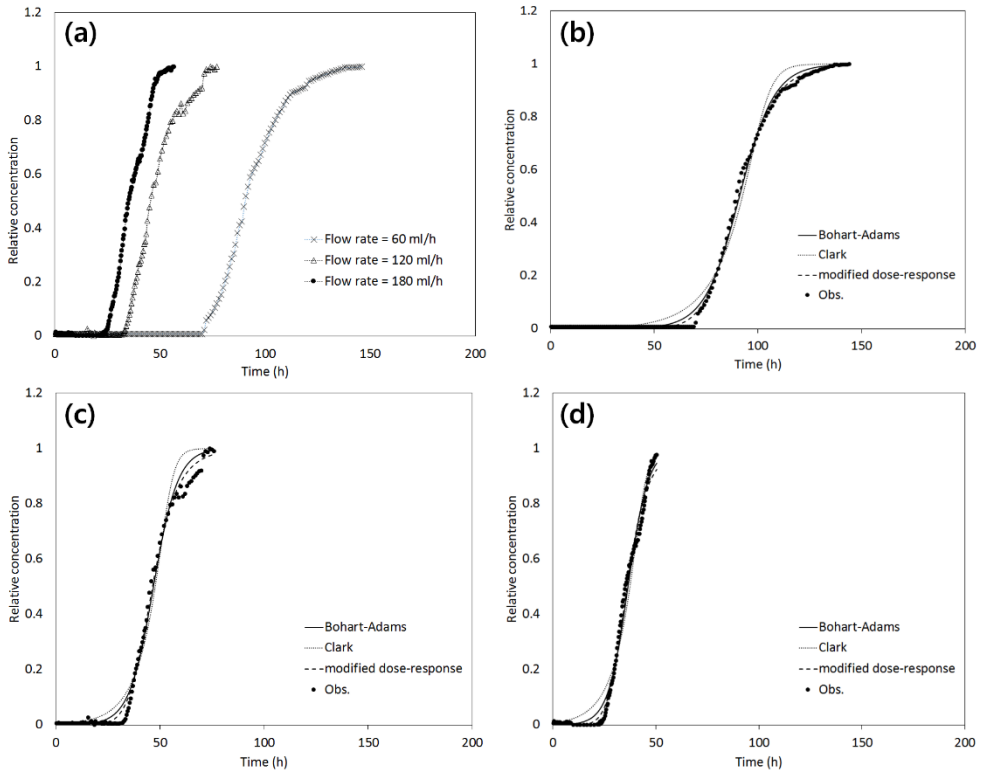

Figure 6.11. Effect of flow rate on breakthrough curves for nitrate removal on C12Q-gel in nitrate solution (C_0= 100 mg/L as NO_3^-): (a) Breakthrough curves from various flow rate; (b) model fitted results from flow rate = 60 mL/h; (c) model fitted results from flow rate = 120 mL/h; (d) model fitted results from flow rate = 180 mL/h

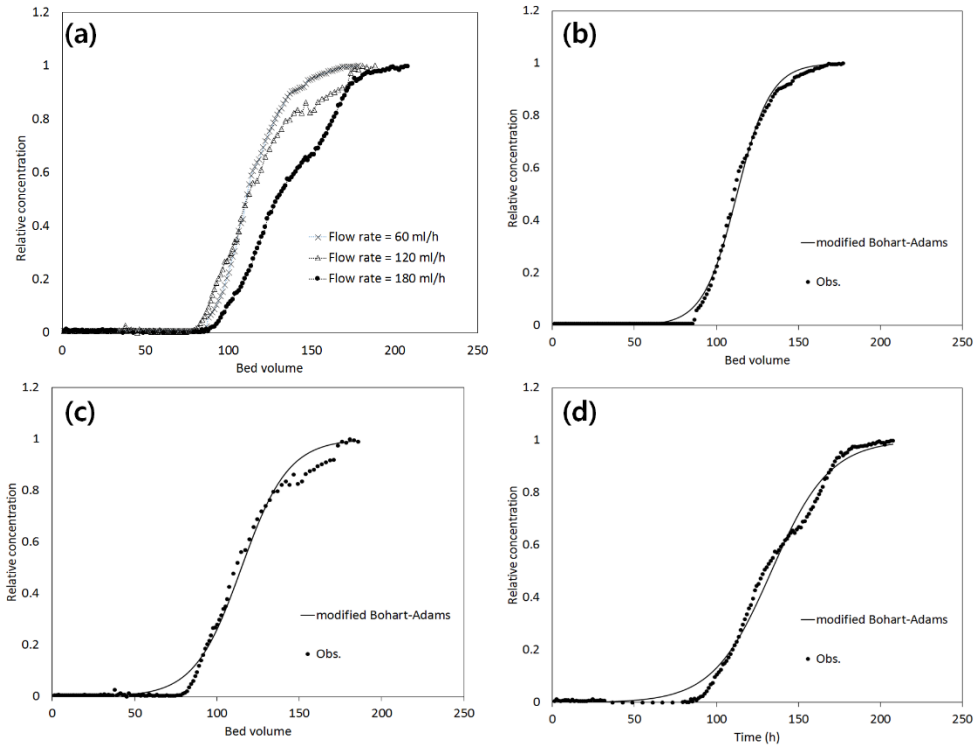

Figure 6.12. Effect of flow rate on breakthrough curves for nitrate removal on C12Q-gel in nitrate solution (C_0= 100 mg/L as NO_3^-) when X-axis is bed volume: (a) Breakthrough curves from various flow rate; (b) modified Bohart-Adams model fitted from flow rate = 60 mL/h; (c) modified Bohart-Adams model fitted from flow rate = 120 mL/h; (d) modified Bohart-Adams model fitted from flow rate = 180 mL/h

The breakthrough curves and model fitted data from the column experiment when influent = 100, 300, and 500 mg/L as NO_3^-, flow rate = 180 mL/h (Ex.6, 7, and 8) are represented in Fig.6.13. From the results, time for breakthrough were shortened as 24.3, 9.3, and 6.7 h when initial concentration = 100, 300, and 500 mg/L. Even the gap of the time for breakthrough, q_i^{col} were slightly increased as 13.4, 15.4, and 18.0 mg/g when initial concentration = 100, 300, and 500 mL/h. Time for exhaustion were also shortened as 56.7, 28.7, and 18 h when initial concentration = 100, 300, and 500 mL/h. However, q_e^{col} were not related into initial concentration (21.8, 22.5, and 22.7 mg/g when initial concentration = 100, 300, and 500 mg/L). From the fitted model parameters, it is considered that Bohart-Adams model and modified dose-response model parameter were not affected at initial concentration. On the other hand, '*A*' parameter of Clark model seems not related to initial concentration. However, '*A*' is related to '*r*' as following (Clark, 1987):

$$\mathrm{A} = \left(\frac{C_i^{n-1}}{C_b^{n-1}} - 1\right) e^{rt_b} \qquad (6.20)$$

where, C_b is the breakthrough concentration (mg/L) and t_b is the breakthrough time (h). '*r*' parameter of Clark model is originated as following equation (Clark, 1987):

$$\mathrm{r} = (n-1)\frac{K_T}{u}V \qquad (6.21)$$

where, K_T is the mass transfer coefficient (1/h) and V is the velocity of the adsorption zone (cm/h). From this equation, 'r' is a constant at initial concentration. However, 'r' values were increased as 0.3771, 1.5784, and 2.0638 L/h when initial concentration = 100, 300, and 500 mL/h.

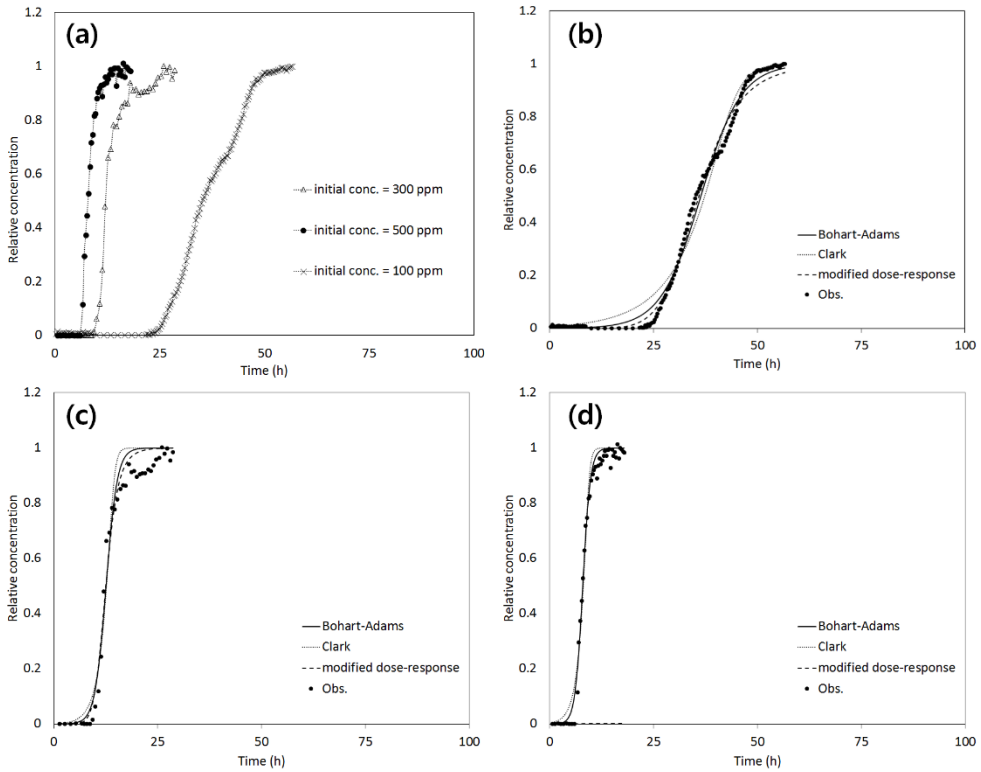

Figure 6.13. Effect of initial concentration on breakthrough curves for nitrate removal on C12Q-gel in nitrate solution (flow rate = 60 mL/h): (a) Breakthrough curves from various initial concentration; (b) Model fitted from C_0= 100 mg/L as NO_3^-; (c) Model fitted from C_0= 300 mg/L as NO_3^-; (d) Model fitted from C_0= 500 mg/L as NO_3^-

The breakthrough curves and model fitted data from the column experiment when bed depth = 10, 20, and 30 mg/L, initial concentration 500 mg/L as NO_3^-, flow rate = 180 mL/h (Ex.8, 9, and 10) and BDST fitting result are represented in Fig.6.14. In this study, C_b was chosen as 250 mg/L bigger than other articles from high concentration of influent. From the slope and y-intercept from BDST fitting, k_{BA} and N_0 were calculated as 0.00031 L/mg/h and 19829 mg/L.

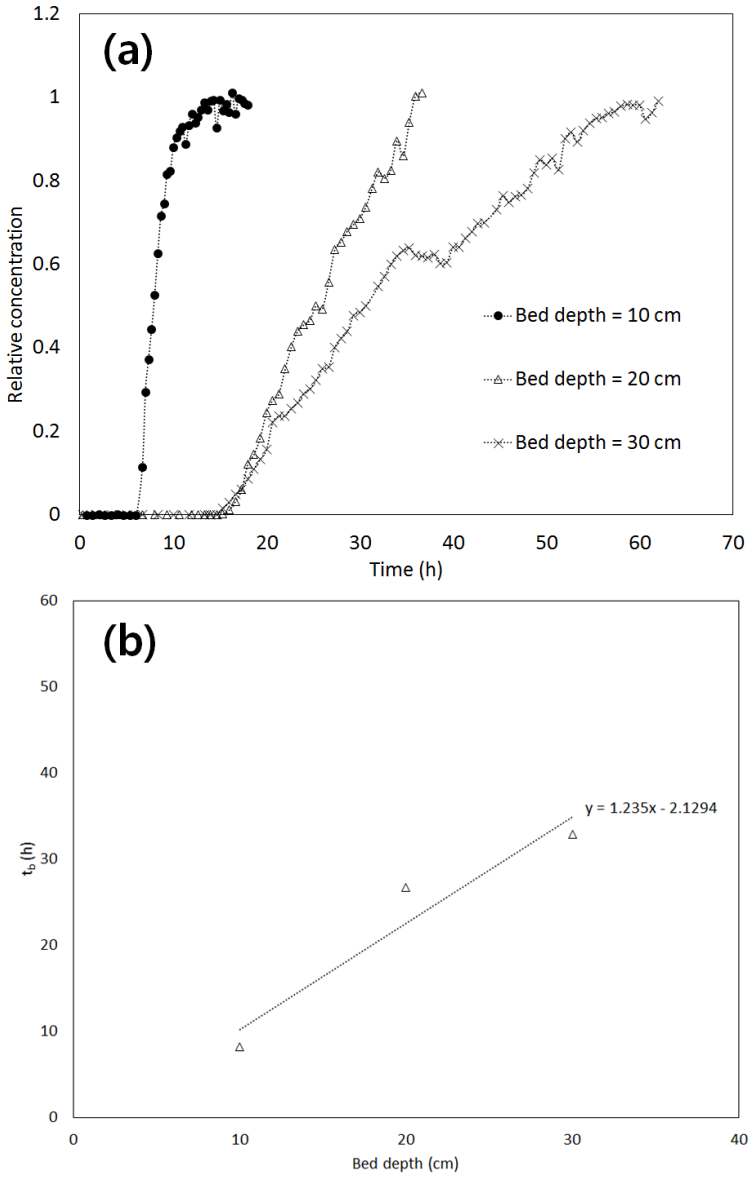

Figure 6.14. Effect of Bed depth on breakthrough curves for nitrate removal on C12Q-gel in nitrate solution (Flow rate = 3.0 mL/min, C_0= 500 mg/L as NO_3^-): (a) Breakthrough curves from bed depth; (b) Model fitted using Bed Depth Service Time

The breakthrough curves from the column experiment when influent were artificial groundwater, 140 mg/L HCO_3^- added artificial groundwater, and 280 mg/L HCO_3^- added artificial groundwater when flow rate = 60 mL/h (Ex.4, 11, and 12) are represented Fig.6.15. From the results, q_e^{col} for NO_3^- were 8.3, 9.5, and 7.7 mg/g experiment when influent were artificial groundwater, 140 mg/L HCO_3^- added artificial groundwater, and 280 mg/L HCO_3^- added artificial groundwater. While q_e^{col} for SO_4^2 were 10.4, 14.0, and 12.5 mg/g. From the q_e^{col} data, there has no specific effect of HCO_3^-. However, adsorbed SO_4^{2-} were eluted more by increasing HCO_3^- concentration. It is considered that SO_4^{2-} and HCO_3^- are in the dynamic competitive sorption and desorption processes while NO_3^- is in quite stable adsorbed state.

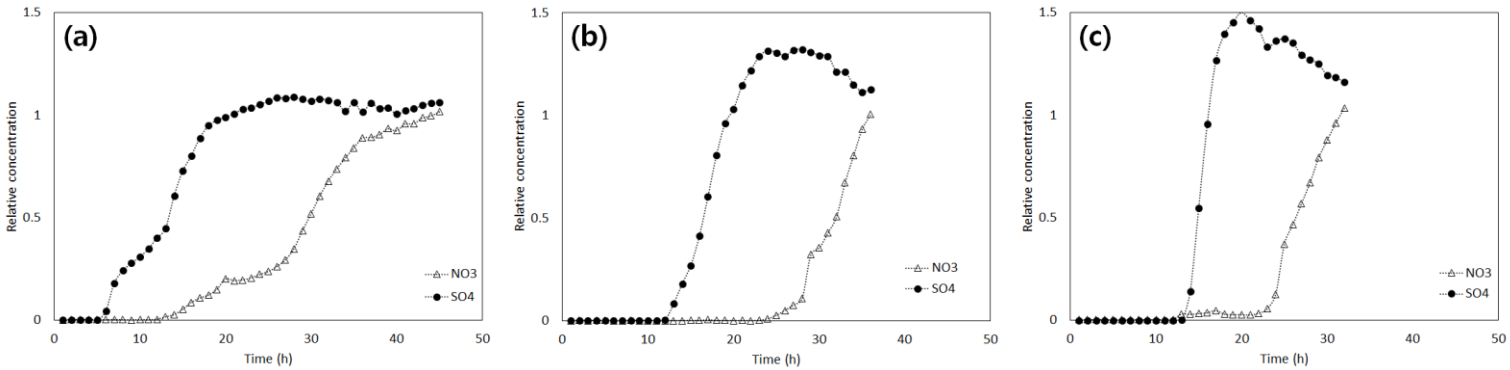

Figure 6.15. Effect of bicarbonate on breakthrough curves for nitrate removal on C12Q-gel in artificial groundwater (Flow rate = 60 mL/h): (a) Breakthrough curves from artificial groundwater ; (b) Breakthrough curves from 140 mg/L HCO_3^- added artificial groundwater; (c) Breakthrough curves from 280 mg/L HCO_3^- added artificial groundwater

The breakthrough curves from the regeneration were presented in Fig.6.16. From the results, regenerated C12Q-silica gel showed mostly overlapped breakthrough curve even 2 times of regeneration. q_e^{col} were calculated as 22.7, 23.2, and 24.6 mg/g when pristine C12Q-silica gel, 1 times regenerated, and 2 times regenerated.

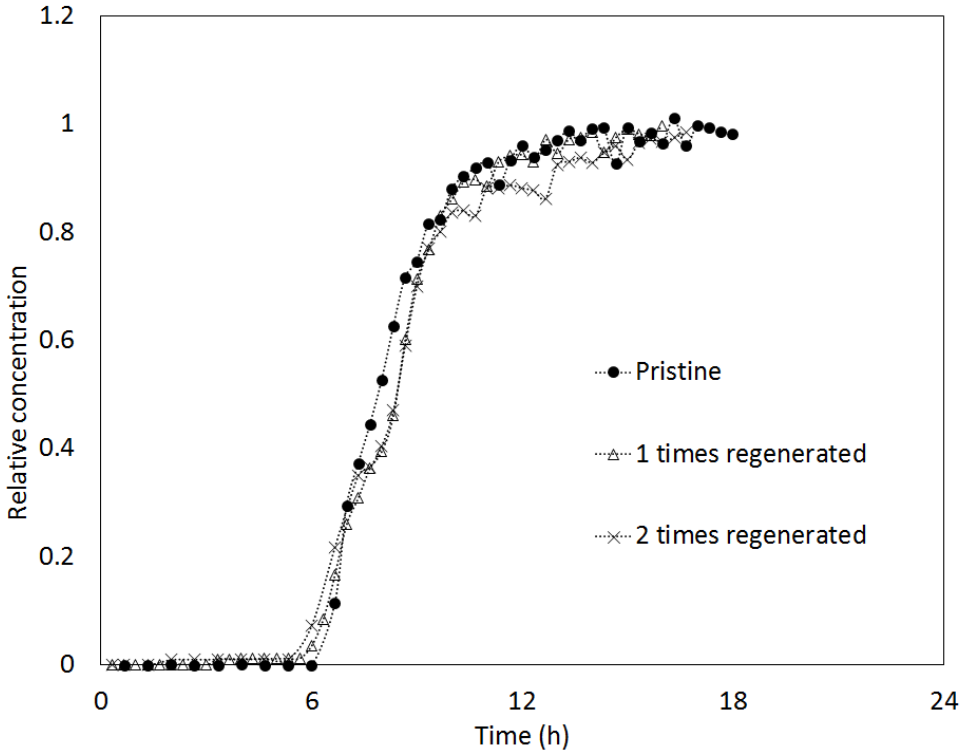

Figure 6.16. Effect of regeneration on breakthrough curves for nitrate removal on C12Q-gel in nitrate solution (Flow rate = 3.0 mL/min, C_0= 500 mg/L as NO_3^-)

Chapter 7 General Conclusion and Recommendations

7.1. General conclusion

In this dissertation, two types of functionalization method were used - ion imprinting, alkyl chain length intended quaternization - for selective removal of Cu(II) and nitrate in aqueous solution.

1. In Chapter 3, Cu-imprinted PEI-SBA-15 was synthesized for selective sorption of Cu(II) from aqueous solutions. The Cu(II) selectivity of Cu-imprinted PEI SBA-15 was enhanced through Cu(II) loading on PEI-SBA-15 under high $[Cl^-]/[Cu(II)]$ ratios, followed by imprinting processes (crosslinking and elution) on the Cu-loaded PEI-SBA-15. Selectivity experiments in multinary solutions containing divalent or trivalent/tetravalent ions revealed that Cu-imprinted PEI-SBA-15 prepared at a high $[Cl^-]/[Cu(II)]$ ratio had higher Cu(II) selectivity than PEI-SBA-15. Cu-imprinted PEI-SBA-15 prepared at a ratio of 500 showed the highest Cu(II) selectivity, 79.62, and a relative selectivity of 29.24 in divalent ion solutions, with a selectivity of 3.40 and a relative selectivity of 3.96 in trivalent/tetravalent ion solutions. This study demonstrated that the Cu(II) selectivity of surface-imprinted SBA-15 could be enhanced through its preparation under high $[Cl^-]/[Cu(II)]$ ratios.

2. In Chapter 4, Cu imprinted PEI coated silica gel was synthesized and characterized for selective Cu(II) sorption from aqueous solutions. To imprint Cu(II) on coated PEI, Cu(II) loading process was added into PEI-coated silica gel preparation processes. From the Cu(II) batch test, Cu-PEI-silica gel showed much higher Cu(II) sorption capacity (352.540 mg/g) than PEI-silica gel (30.727 mg/g). In multinary solutions containing divalent ions or trivalent and tetravalent ions, the relative Cu(II) selectivity for Cu-PEI-silica gel over PEI-silica gel was 5.17 or 3.06. In this study, it is demonstrated that the Cu(II) selectivity and Cu(II) sorption capacity were enhanced via Cu(II) surface imprinting process.

3. In Chapter 5, quaternary ammonium functionalized mesoporous silica SBA-15 with various length of alkyl chain were synthesized and characterized for selective nitrate sorption from aqueous solutions. The results of nitrate batch test indicate that the quaternary ammonium functionalized SBA-15 which contain the longer alkyl chain length have the slower sorption kinetics. On the other hand, nitrate sorption capacity was not related to alkyl chain length. From the result of competing anion effect tests, it was observed that the adsorbents with longer alkyl chain removed nitrate more selectively

against other competing anions than the adsorbents with shorter alkyl chain. Nitrate has highest hydration energy among all other competing anions. In addition, longer alkyl chain quaternary ammonium functionalized silica gel has less hydrated environment Among various competing anions. Therefore, nitrate can be removed more selectively by adsorbents with longer alkyl chain. In this study, various quaternary ammonium functionalized mesoporous silica were prepared well and the effect of alkyl chain length on nitrate selectivity via competing anion tests was demonstrated.

4. In Chapter 6, C8Q-silica gel and C12Q-slica gel were synthesized and characterized for selective nitrate sorption from aqueous solutions. From the nitrate batch test and column tests, C12Q-slica gel was chosen as a more proper adsorbent for selective nitrate removal. From the column experiments, Bohart-Adams and bed depth service time models are considered proper models to explain and estimate the nitrate removal in flow through conditions. From the artificial groundwater flow through tests, C12Q-silica gel removed nitrate selectively even in bicarbonate-added conditions. After the 2 times of regeneration of C12Q silica gel, the breakthrough curves from the column experiments was mostly

overlapped with previous curves. In this study, quaternary ammonium functionalized silica gel were prepared well and its characteristics in flow through conditions were examined.

7.2. Recommandations

The following recommendations are proposed for the future researches on the application and expansion of the resultants for practical water treatment

1. Cu-imprinted PEI-SBA-15 was synthesized through Cu(II) loading enhanced conditions. From the result, It was possible to make Cu(II) selectivity enhanced imprinted material through Cu(II) ion loading enhancement. However, only [Cl^-]/[Cu(II)] ratio was considered for loading enhancement. Further studies should consider effect of other counter ions, kind of solvent, temperature, etc. Moreover, trial of other metal ion imprinting through the method from chapter 3 is required.

2. Cu imprinted PEI coated silica gel was synthesized. From the result, it was possible to make Cu(II) imprinted material through relatively easy method than previous studies. However, application of the resultant on Cu(II) separation & recovery from wastewater. Further studies should contain the above mentioned substance as a point of view in expansion of the application and expansion of the resultants for practical water treatment.

3. Alkyl chain length intended quaternary ammonium functionalized mesoporous silica or silica gels were prepared. However, only one

alkyl chain length intended, left two alkyl chain lengths were not regulated. Further studies should regulate all of alkyl chain length to prepare more nitrate selective adsorbents.

4. Alkyl chain length intended quaternary ammonium functionalized silica gels were synthesized. From the result, it was possible to scale-up for pilot scale studies. Therefore, further studies should contain the pilot scale experiments for the application and expansion of the resultants for practical water treatment.

Reference

Agrawal, A., Kumari, S., Sahu, K.K., 2009. Iron and Copper Recovery/Removal from Industrial Wastes: A Review. Industrial & Engineering Chemistry Research 48, 6145-6161.

An, F., Gao, B., 2007. Chelating adsorption properties of PEI/SiO2 for plumbum ion. Journal of Hazardous Materials 145, 495-500.

An, F., Gao, B., 2009. Adsorption characteristics of Cr(III) ionic imprinting polyamine on silica gel surface. Desalination 249, 1390-1396.

Araujo, J.R., Archanjo, B.S., de Souza, K.R., Kwapinski, W., Falcão, N.P.S., Novotny, E.H., Achete, C.A., 2014. Selective extraction of humic acids from an anthropogenic Amazonian dark earth and from a chemically oxidized charcoal. Biology and Fertility of Soils 50, 1223-1232.

Aroua, M.K., Zuki, F.M., Sulaiman, N.M., 2007. Removal of chromium ions from aqueous solutions by polymer-enhanced ultrafiltration. Journal of Hazardous Materials 147, 752-758.

Banerjee, S.S., Chen, D.-H., 2007. Fast removal of copper ions by gum arabic modified magnetic nano-adsorbent. Journal of Hazardous Materials 147, 792-799.

Banu, H.T., Meenakshi, S., 2017. Synthesis of a novel quaternized form of melamine–formaldehyde resin for the removal of nitrate from water. Journal of Water Process Engineering 16, 81-89.

Bayramoğlu, G., Yakup Arica, M., 2008. Adsorption of Cr(VI) onto PEI immobilized acrylate-based magnetic beads: Isotherms, kinetics and thermodynamics study. Chemical Engineering Journal 139, 20-28.

Bhatnagar, A., Kumar, E., Sillanpää, M., 2010. Nitrate removal from water by nano-alumina: Characterization and sorption studies. Chemical Engineering Journal 163, 317-323.

Bi, X., Lau, R.J., Yang, K.-L., 2007. Preparation of Ion-Imprinted Silica Gels Functionalized with Glycine, Diglycine, and Triglycine and Their Adsorption Properties for Copper Ions. Langmuir 23, 8079-8086.

Blum, F.D., 2016. Silane Coupling Agents. Encyclopedia of Polymer Science and Technology.

Branger, C., Meouche, W., Margaillan, A., 2013. Recent advances on ion-imprinted polymers. Reactive and Functional Polymers 73, 859-875.

Carpenter, A.W., Worley, B.V., Slomberg, D.L., Schoenfisch, M.H., 2012. Dual Action Antimicrobials: Nitric Oxide Release from Quaternary Ammonium-Functionalized Silica Nanoparticles. Biomacromolecules 13, 3334-3342.

Chabani, M., Amrane, A., Bensmaili, A., 2006. Kinetic modelling of the adsorption of nitrates by ion exchange resin. Chemical Engineering Journal 125, 111-117.

Chanda, M., Rempel, G.L., 1995. Polyethyleneimine gel-coat on silica. High uranium capacity and fast kinetics of gel-coated resin. Reactive Polymers 25, 25-36.

Chanda, M., Rempel, G.L., 1997. Chromium(III) Removal by Epoxy-Cross-Linked Poly(ethylenimine) Used as Gel-Coat on Silica. 1. Sorption Characteristics. Industrial & Engineering Chemistry Research 36, 2184-2189.

Chang, X., Jiang, N., Zheng, H., He, Q., Hu, Z., Zhai, Y., Cui, Y., 2007. Solid-phase extraction of iron(III) with an ion-imprinted functionalized silica gel sorbent prepared by a surface imprinting technique. Talanta 71, 38-43.

Chang, X., Wang, X., Jiang, N., He, Q., Zhai, Y., Zhu, X., Hu, Z., 2008. Silica gel surface-imprinted solid-phase extraction of Zr(IV) from aqueous solutions. Microchimica Acta 162, 113-119.

Chatterjee, S., Woo, S.H., 2009. The removal of nitrate from aqueous solutions by chitosan hydrogel beads. Journal of Hazardous Materials 164, 1012-1018.

Chiu, H.-F., Tsai, S.-S., Yang, C.-Y., 2007. Nitrate in Drinking Water and Risk of Death from Bladder Cancer: An Ecological Case-Control Study in Taiwan. Journal of Toxicology and Environmental Health, Part A 70, 1000-1004.

Chu, K.H., 2010. Fixed bed sorption: Setting the record straight on the Bohart–Adams and Thomas models. Journal of Hazardous Materials 177, 1006-1012.

Clark, R.M., 1987. Evaluating the cost and performance of field-scale granular activated carbon systems. Environmental Science & Technology 21, 573-580.

Cui, H.-Z., Li, Y.-L., Liu, S., Zhang, J.-F., Zhou, Q., Zhong, R., Yang, M.-L., Hou, X.-F., 2017. Novel Pb(II) ion-imprinted materials based on bis-pyrazolyl functionalized mesoporous silica for the selective removal of Pb(II) in water samples. Microporous and Mesoporous Materials 241, 165-177.

Dahaghin, Z., Mousavi, H.Z., Sajjadi, S.M., 2017. A novel magnetic ion imprinted polymer as a selective magnetic solid phase for separation of trace lead(II) ions from agricultural products, and optimization using a Box–Behnken design. Food Chemistry 237, 275-281.

Dana, E., Sayari, A., 2012. Adsorption of heavy metals on amine-functionalized SBA-15 prepared by co-condensation: Applications to real water samples. Desalination 285, 62-67.

Dai, S., Burleigh, M.C., Ju, Y.H., Gao, H.J., Lin, J.S., Pennycook, S.J., Barnes, C.E., Xue, Z.L., 2000. Hierarchically Imprinted Sorbents for the Separation of Metal Ions. Journal of the American Chemical Society 122, 992-993.

De Lima, A.C.A., Nascimento, R.F., de Sousa, F.F., Filho, J.M., Oliveira, A.C., 2012. Modified coconut shell fibers: A green and economical sorbent for the removal of anions from aqueous solutions. Chemical Engineering Journal 185-186, 274-284.

Demiral, H., Gündüzoğlu, G., 2010. Removal of nitrate from aqueous solutions by activated carbon prepared from sugar beet bagasse. Bioresource Technology 101, 1675-1680.

Deng, S., Ting, Y.P., 2005. Polyethylenimine-Modified Fungal Biomass as a High-Capacity Biosorbent for Cr(VI) Anions: Sorption Capacity and Uptake Mechanisms. Environmental Science & Technology 39, 8490-8496.

Dey, R.K., Jha, U., Patnaik, T., Singh, A.C., Singh, V.K., 2009. Removal of Toxic/Heavy Metal Ions Using Ion-Imprinted Aminofunctionalized Silica Gel. Sep. Sci. Technol. 44, 1829-1850.

Ding, L.-l., Long, S.-q., Zhou, Y.-h., Deng, Y., 2012. Synthesis and Characteristics of Cu (II)-Imprinted Silica Gel Sorbent. Asian Journal of Chemistry 24, 4733.

Dioum, A., Hamoudi, S., 2014. Mono- and quaternary-ammonium functionalized mesoporous silica materials for nitrate adsorptive removal from water and wastewaters. Journal of Porous Materials 21, 685-690.

Divband Hafshejani, L., Hooshmand, A., Naseri, A.A., Mohammadi, A.S., Abbasi, F., Bhatnagar, A., 2016. Removal of nitrate from aqueous solution by modified sugarcane bagasse biochar. Ecological Engineering 95, 101-111.

Dong, X., Hou, S., Mao, H., Zheng, J., Zhang, S., 2016. Novel hydrophilic-hydrophobic block copolymer based on cardo poly(arylene ether sulfone)s with bis-quaternary ammonium moieties for anion exchange membranes. Journal of Membrane Science 518, 31-39.

Faghihian, H., Asghari, K., 2013. Selective Solid-phase Extraction of Cu2+ by a Novel Cu(II)-imprinted Silica Gel. Journal of the Chinese Chemical Society 60, 1491-1499.

Fan, H.T., Tang, Q., Sun, Y., Zhang, Z.-G., Li, W.-X., 2014a. Selective removal of antimony(III) from aqueous solution using antimony(III)-imprinted organic–inorganic hybrid sorbents by combination of surface imprinting technique with sol–gel process. Chemical Engineering Journal 258, 146-156.

Fan, H.T., Fan, X., Li, J., Guo, M., Zhang, D., Yan, F., Sun, T., 2012a. Selective removal of arsenic(V) from aqueous solution using a surface-ion-imprinted amine-functionalized silica gel sorbent. Industrial and Engineering Chemistry Research 51, 5216-5223.

Fan, H.T., Li, J., Li, Z.C., Sun, T., 2012b. An ion-imprinted amino-functionalized silica gel sorbent prepared by hydrothermal assisted surface imprinting technique for selective removal of cadmium (II) from aqueous solution. Applied Surface Science 258, 3815-3822.

Fan, H.T., Sun, T., 2012. Selective removal of iron from aqueous solution using ion imprinted cyanato-functionalized silica gel sorbents. Sep. Sci. Technol. 47, 507-512.

Fan, Z., Li, S., Li, R., Shen, J., 2014. Adsorption of Cu(II) on Surface Ion-Imprinted Poly(Allylamine)-Silica Material from Aqueous Solution. Polymer-Plastics Technology and Engineering 53, 30-37.

Fang, G.-Z., Tan, J., Yan, X.-P., 2005. An ion-imprinted functionalized silica gel sorbent prepared by a surface imprinting technique combined with a sol-gel process for selective solid-phase extraction of cadmium(II). Analytical Chemistry 77, 1734-1739.

Foo, K.Y., Hameed, B.H., 2010. Insights into the modeling of adsorption isotherm systems. Chemical Engineering Journal 156, 2-10.

Fu, J., Chen, L., Li, J., Zhang, Z., 2015. Current status and challenges of ion imprinting. Journal of Materials Chemistry A 3, 13598-13627.

Ganesan, P., Kamaraj, R., Vasudevan, S., 2013. Application of isotherm, kinetic and thermodynamic models for the adsorption of nitrate ions on graphene from aqueous solution. Journal of the Taiwan Institute of Chemical Engineers 44, 808-814.

Gao, B., An, F., Liu, K., 2006. Studies on chelating adsorption properties of novel composite material polyethyleneimine/silica gel for heavy-metal ions. Applied Surface Science 253, 1946-1952.

Gao, B., An, F., Zhu, Y., 2007. Novel surface ionic imprinting materials prepared via couple grafting of polymer and ionic imprinting on surfaces of silica gel particles. Polymer 48, 2288-2297.

Gao, B., Meng, J., Xu, Y., Zhang, Y., 2015. Preparation of Fe(III) ion surface-imprinted material for removing Fe(III) impurity from lanthanide ion solutions. Journal of Industrial and Engineering Chemistry 24, 351-358.

Gao, B., Wang, X., Zhang, Y., 2013. Preparation of chromate anion surface-imprinted material IIP-PVI/SiO2 based on polyvinylimidazole-grafted particles PVI/SiO2 and its ionic recognition characteristic. Materials Chemistry and Physics 140, 478-486.

Gao, K., Guo, Y., Niu, Q., Han, L., Zhou, L., Wang, L., 2018. Quaternary ammonium-functionalized carbon dots for sensitive and selective detection of 2,4,6-trinitrophenol in aqueous medium. Sensors and Actuators B: Chemical 262, 298-305.

Golie, W.M., Upadhyayula, S., 2016. Continuous fixed-bed column study for the removal of nitrate from water using chitosan/alumina composite. Journal of Water Process Engineering 12, 58-65.

Goon, I.Y., Zhang, C., Lim, M., Gooding, J.J., Amal, R., 2010. Controlled Fabrication of Polyethylenimine-Functionalized Magnetic Nanoparticles for the Sequestration and Quantification of Free Cu2+. Langmuir 26, 12247-12252.

Gu, B., Ku, Y.-K., Jardine, P.M., 2004. Sorption and Binary Exchange of Nitrate, Sulfate, and Uranium on an Anion-Exchange Resin. Environmental Science & Technology 38, 3184-3188.

Guo, B., Deng, F., Zhao, Y., Luo, X., Luo, S., Au, C., 2014. Magnetic ion-imprinted and –SH functionalized polymer for selective removal of Pb(II) from aqueous samples. Applied Surface Science 292, 438-446.

Guo, J.-J., Su, Q.-D., Gan, W.-E., 2009. On-Line Selective Solid-Phase Extraction of Copper with a Surface Ion Imprinted Silica Gel Sorbent. Journal of the Chinese Chemical Society 56, 763-770.

Guo, W., Chen, R., Liu, Y., Meng, M., Meng, X., Hu, Z., Song, Z., 2013. Preparation of ion-imprinted mesoporous silica SBA-15 functionalized with triglycine for selective adsorption of Co(II). Colloids and Surfaces A: Physicochemical and Engineering Aspects 436, 693-703.

Hamoudi, S., Belkacemi, K., 2013. Adsorption of nitrate and phosphate ions from aqueous solutions using organically-functionalized silica materials: Kinetic modeling. Fuel 110, 107-113.

Hanafi-Bojd, M.Y., Jaafari, M.R., Ramezanian, N., Xue, M., Amin, M., Shahtahmassebi, N., Malaekeh-Nikouei, B., 2015. Surface functionalized mesoporous silica nanoparticles as an effective carrier for epirubicin delivery to cancer cells. European Journal of Pharmaceutics and Biopharmaceutics 89, 248-258.

He, G., Ke, W., Chen, X., Kong, Y., Zheng, H., Yin, Y., Cai, W., 2017. Preparation and properties of quaternary ammonium chitosan-g-poly(acrylic acid-co-acrylamide) superabsorbent hydrogels. Reactive and Functional Polymers 111, 14-21.

He, J.W., Xu, X., Corneille, J.S., Goodman, D.W., 1992. X-ray photoelectron spectroscopic characterization of ultra-thin silicon oxide films on a Mo(100) surface. Surface Science 279, 119-126.

He, Q., Chang, X., Wu, Q., Huang, X., Hu, Z., Zhai, Y., 2007. Synthesis and applications of surface-grafted Th(IV)-imprinted polymers for selective solid-phase extraction of thorium(IV). Analytica Chimica Acta 605, 192-197.

He, Q., Chang, X., Zheng, H., Jiang, N., Wang, X., 2008. Determination of chromium(III) and total chromium in natural waters using a surface ion-imprinted silica gel as selective adsorbent. International Journal of Environmental Analytical Chemistry 88, 373-384.

He, R., Wang, Z., Tan, L., Zhong, Y., Li, W., Xing, D., Wei, C., Tang, Y., 2018. Design and fabrication of highly ordered ion imprinted SBA-15 and MCM-41 mesoporous organosilicas for efficient removal of Ni2+ from different properties of wastewaters. Microporous and Mesoporous Materials 257, 212-221.

Henry, W.D., Zhao, D., SenGupta, A.K., Lange, C., 2004. Preparation and characterization of a new class of polymeric ligand exchangers for

selective removal of trace contaminants from water. Reactive and Functional Polymers 60, 109-120.

Islam, M., Chandra Mishra, P., Patel, R., 2010. Physicochemical characterization of hydroxyapatite and its application towards removal of nitrate from water. Journal of Environmental Management 91, 1883-1891.

Islam, M., Patel, R., 2009. Nitrate sorption by thermally activated Mg/Al chloride hydrotalcite-like compound. Journal of Hazardous Materials 169, 524-531.

Islam, M., Patel, R., 2010. Synthesis and physicochemical characterization of Zn/Al chloride layered double hydroxide and evaluation of its nitrate removal efficiency. Desalination 256, 120-128.

Islam, M., Patel, R., 2011. Physicochemical characterization and adsorption behavior of Ca/Al chloride hydrotalcite-like compound towards removal of nitrate. Journal of Hazardous Materials 190, 659-668.

Ivánová, D., Albert, P., Kavuličová, J., 2018. Nitrate removal from model aqueous solutions and real water by calcined Mg/Al layered double hydroxides. Applied Clay Science 152, 65-72.

Jóźwiak, T., Filipkowska, U., Szymczyk, P., Kuczajowska-Zadrożna, M., Mielcarek, A., 2017. The use of cross-linked chitosan beads for nutrients (nitrate and orthophosphate) removal from a mixture of P-PO4, N-NO2 and N-NO3. International Journal of Biological Macromolecules 104, 1280-1293.

Jiang, N., Chang, X., Zheng, H., He, Q., Hu, Z., 2006. Selective solid-phase extraction of nickel(II) using a surface-imprinted silica gel sorbent. Analytica Chimica Acta 577, 225-231.

Kabay, N., Yüksel, M., Samatya, S., Arar, Ö., Yüksel, Ü., 2007. Removal of Nitrate from Ground Water by a Hybrid Process Combining Electrodialysis and Ion Exchange Processes. Sep. Sci. Technol. 42, 2615-2627.

Kamaraj, R., Pandiarajan, A., Jayakiruba, S., Naushad, M., Vasudevan, S., 2016. Kinetics, thermodynamics and isotherm modeling for removal of nitrate from liquids by facile one-pot electrosynthesized nano zinc hydroxide. Journal of Molecular Liquids 215, 204-211.

Kandanapitiye, M.S., Wang, F.J., Valley, B., Gunathilake, C., Jaroniec, M., Huang, S.D., 2015. Selective Ion Exchange Governed by the Irving–

Williams Series in K2Zn3[Fe(CN)6]2 Nanoparticles: Toward a Designer Prodrug for Wilson's Disease. Inorganic Chemistry 54, 1212-1214.

Kang, R., Qiu, L., Fang, L., Yu, R., Chen, Y., Lu, X., Luo, X., 2016. A novel magnetic and hydrophilic ion-imprinted polymer as a selective sorbent for the removal of cobalt ions from industrial wastewater. Journal of Environmental Chemical Engineering 4, 2268-2277.

Katal, R., Baei, M.S., Rahmati, H.T., Esfandian, H., 2012. Kinetic, isotherm and thermodynamic study of nitrate adsorption from aqueous solution using modified rice husk. Journal of Industrial and Engineering Chemistry 18, 295-302.

Kilpimaa, S., Runtti, H., Kangas, T., Lassi, U., Kuokkanen, T., 2015. Physical activation of carbon residue from biomass gasification: Novel sorbent for the removal of phosphates and nitrates from aqueous solution. Journal of Industrial and Engineering Chemistry 21, 1354-1364.

Lau, Y.L., Yeong, Y.F., 2016. Optimization of Nitrate Removal from Aqueous Solution by Amine-functionalized MCM-41 Using Response Surface Methodology. Procedia Engineering 148, 1239-1246.

Lee, C.-G., Kim, J.-H., Kang, J.-K., Kim, S.-B., Park, S.-J., Lee, S.-H., Choi, J.-W., 2015. Comparative analysis of fixed-bed sorption models using phosphate breakthrough curves in slag filter media. Desalination and Water Treatment 55, 1795-1805.

Li, C.X., Pan, J.M., Gao, J., Yan, Y.S., Zhao, G.Q., 2009. An ion-imprinted polymer supported by attapulgite with a chitosan incorporated sol–gel process for selective separation of Ce(III). Chinese Chemical Letters 20, 985-989.

Li, M., Feng, C., Li, M., Zeng, Q., Gan, Q., 2015a. Synthesis and application of a surface-grafted In (III) ion-imprinted polymer for selective separation and pre-concentration of indium (III) ion from aqueous solution. Hydrometallurgy 154, 63-71.

Li, M., Feng, C., Li, M., Zeng, Q., Gan, Q., Yang, H., 2015b. Synthesis and characterization of a surface-grafted Cd(II) ion-imprinted polymer for selective separation of Cd(II) ion from aqueous solution. Applied Surface Science 332, 463-472.

Li, M., Meng, X., Liang, X., Yuan, J., Hu, X., Wu, Z., Yuan, X., 2018. A novel In(III) ion-imprinted polymer (IIP) for selective extraction of In(III) ions from aqueous solutions. Hydrometallurgy 176, 243-252.

Li, Z.C., Fan, H.T., Sun, T., 2011. Application of imprinted functionalized silica gel sorbent for selective removal of cadmium (II) from industial wastewaters. Advanced Materials Research 213, 441-444.

Li, Z.C., Fan, H.T., Zhang, Y., Chen, M.X., Yu, Z.Y., Cao, X.Q., Sun, T., 2011b. Cd(II)-imprinted polymer sorbents prepared by combination of surface imprinting technique with hydrothermal assisted sol-gel process for selective removal of cadmium(II) from aqueous solution. Chemical Engineering Journal 171, 703-710.

Liang, Q., Geng, J., Luo, H., Fang, W., Yin, Y., 2017. Fast and selective removal of Cr(VI) from aqueous solutions by a novel magnetic Cr(VI) ion-imprinted polymer. Journal of Molecular Liquids 248, 767-774.

Lin, C., Wang, H., Wang, Y., Cheng, Z., 2010. Selective solid-phase extraction of trace thorium(IV) using surface-grafted Th(IV)-imprinted polymers with pyrazole derivative. Talanta 81, 30-36.

Liu, F., Zou, H., Peng, J., Hu, J., Liu, H., Chen, Y., Lu, F., 2016. Removal of copper(II) using deacetylated konjac glucomannan conjugated soy protein isolate. International Journal of Biological Macromolecules 86, 338-344.

Liu, X., Li, L., Du, Y., Guo, Z., Ong, T.T., Chen, Y., Ng, S.C., Yang, Y., 2009. Synthesis of large pore-diameter SBA-15 mesostructured spherical silica and its application in ultra-high-performance liquid chromatography. Journal of Chromatography A 1216, 7767-7773.

Liu, Y., Liu, Z., Dai, J., Gao, J., Xie, J., Yan, Y., 2011. Selective adsorption of Co(II) by mesoporous silica SBA-15-supported surface ion imprinted polymer: Kinetics, isotherms, and thermodynamics studies. Chinese Journal of Chemistry 29, 387-398.

Liu, Y., Liu, Z., Gao, J., Dai, J., Han, J., Wang, Y., Xie, J., Yan, Y., 2011b. Selective adsorption behavior of Pb(II) by mesoporous silica SBA-15-supported Pb(II)-imprinted polymer based on surface molecularly imprinting technique. Journal of Hazardous Materials 186, 197-205.

Loganathan, P., Vigneswaran, S., Kandasamy, J., Bolan, N.S., 2014. Removal and Recovery of Phosphate From Water Using Sorption. Critical Reviews in Environmental Science and Technology 44, 847-907.

Luo, X., Luo, S., Zhan, Y., Shu, H., Huang, Y., Tu, X., 2011. Novel Cu (II) magnetic ion imprinted materials prepared by surface imprinted technique combined with a sol–gel process. Journal of Hazardous Materials 192, 949-955.

Makote, R.D., Dai, S., 2001. Matrix-induced modification of imprinting effect for Cu2+ adsorption in hybrid silica matrices. Analytica Chimica Acta 435, 169-175.

Marcus, Y., 1988. Ionic radii in aqueous solutions. Chemical Reviews 88, 1475-1498.

Markowitz, M.A., Kust, P.R., Klaehn, J., Deng, G., Gaber, B.P., 2001. Surface-imprinted silica particles: the effects of added organosilanes on catalytic activity. Analytica Chimica Acta 435, 177-185.

Mazarji, M., Aminzadeh, B., Baghdadi, M., Bhatnagar, A., 2017. Removal of nitrate from aqueous solution using modified granular activated carbon. Journal of Molecular Liquids 233, 139-148.

Meng, M., Meng, X., Liu, Y., Liu, Z., Han, J., Wang, Y., Luo, M., Chen, R., Ni, L., Yan, Y., 2014. An ion-imprinted functionalized SBA-15 adsorbent synthesized by surface imprinting technique via reversible addition–fragmentation chain transfer polymerization for selective removal of Ce(III) from aqueous solution. Journal of Hazardous Materials 278, 134-143.

Milja, T.E., Prathish, K.P., Prasada Rao, T., 2011. Synthesis of surface imprinted nanospheres for selective removal of uranium from simulants of Sambhar salt lake and ground water. Journal of Hazardous Materials 188, 384-390.

Milmile, S.N., Pande, J.V., Karmakar, S., Bansiwal, A., Chakrabarti, T., Biniwale, R.B., 2011. Equilibrium isotherm and kinetic modeling of the adsorption of nitrates by anion exchange Indion NSSR resin. Desalination 276, 38-44.

Monier, M., Abdel-Latif, D.A., 2013a. Synthesis and characterization of ion-imprinted chelating fibers based on PET for selective removal of Hg2+. Chemical Engineering Journal 221, 452-460.

Monier, M., Abdel-Latif, D.A., 2013b. Synthesis and characterization of ion-imprinted resin based on carboxymethyl cellulose for selective removal of UO22+. Carbohydrate Polymers 97, 743-752.

Monier, M., Abdel-Latif, D.A., Abou El-Reash, Y.G., 2016. Ion-imprinted modified chitosan resin for selective removal of Pd(II) ions. Journal of Colloid and Interface Science 469, 344-354.

Monier, M., Abdel-Latif, D.A., Youssef, I., 2018. Preparation of ruthenium (III) ion-imprinted beads based on 2-pyridylthiourea modified chitosan. Journal of Colloid and Interface Science 513, 266-278.

Monier, M., Ibrahim, A.A., Metwally, M.M., Badawy, D.S., 2015. Surface ion-imprinted amino-functionalized cellulosic cotton fibers for selective extraction of Cu(II) ions. International Journal of Biological Macromolecules 81, 736-746.

Moulder, J.F., Chastain, J., King, R.C., 1995. Handbook of X-ray Photoelectron Spectroscopy: A Reference Book of Standard Spectra for Identification and Interpretation of XPS Data. Physical Electronics.

Navarro, R.R., Sumi, K., Fujii, N., Matsumura, M., 1996. Mercury removal from wastewater using porous cellulose carrier modified with polyethyleneimine. Water Research 30, 2488-2494.

Neagu, V., Mikhalovsky, S., 2010. Removal of hexavalent chromium by new quaternized crosslinked poly(4-vinylpyridines). Journal of Hazardous Materials 183, 533-540.

Nie, Y., Deng, S., Wang, B., Huang, J., Yu, G., 2014. Removal of clofibric acid from aqueous solution by polyethylenimine-modified chitosan beads. Frontiers of Environmental Science & Engineering 8, 675-682.

Olgun, A., Atar, N., Wang, S., 2013. Batch and column studies of phosphate and nitrate adsorption on waste solids containing boron impurity. Chemical Engineering Journal 222, 108-119.

Öztürk, N., Bektaş, T.E.l., 2004. Nitrate removal from aqueous solution by adsorption onto various materials. Journal of Hazardous Materials 112, 155-162.

Pang, Y., Zeng, G., Tang, L., Zhang, Y., Liu, Y., Lei, X., Li, Z., Zhang, J., Xie, G., 2011. PEI-grafted magnetic porous powder for highly effective adsorption of heavy metal ions. Desalination 281, 278-284.

Peng, Y.-S., Lai, P.-L., Peng, S., Wu, H.-C., Yu, S., Tseng, T.-Y., Wang, L.-F., Chu, I.M., 2014. Glial cell line-derived neurotrophic factor gene delivery via a polyethylene imine grafted chitosan carrier. International Journal of Nanomedicine 9, 3163-3174.

Rao, T.P., Kala, R., Daniel, S., 2006. Metal ion-imprinted polymers—Novel materials for selective recognition of inorganics. Analytica Chimica Acta 578, 105-116.

Rashidi Nodeh, H., Sereshti, H., Zamiri Afsharian, E., Nouri, N., 2017. Enhanced removal of phosphate and nitrate ions from aqueous media using nanosized lanthanum hydrous doped on magnetic graphene nanocomposite. Journal of Environmental Management 197, 265-274.

Raval, N.P., Shah, P.U., Shah, N.K., 2016. Adsorptive removal of nickel() ions from aqueous environment: A review. Journal of Environmental Management 179, 1-20.

Ren, Y., Liu, P., Feng, J., Ma, J., Wen, Q., Zhang, M., 2013. Selective recognition of molybdenum(VI) from water by Mo(VI) oxy ion-imprinted particle as an adsorbent. Chemical Engineering Journal 219, 286-294.

Ren, Y., Liu, P., Liu, X., Feng, J., Fan, Z., Luan, T., 2014. Preparation of zirconium oxy ion-imprinted particle for the selective separation of trace zirconium ion from water. Journal of Colloid and Interface Science 431, 209-215.

Schoeman, J.J., Steyn, A., 2003. Nitrate removal with reverse osmosis in a rural area in South Africa. Desalination 155, 15-26.

Sen Gupta, S., Bhattacharyya, K.G., 2011. Kinetics of adsorption of metal ions on inorganic materials: A review. Advances in Colloid and Interface Science 162, 39-58.

SenGupta, A.K., 1995. Ion Exchange Technology: Advances in Pollution Control. Taylor & Francis.

Sengupta, A.K., Zhu, Y., 1992. Metals sorption by chelating polymers: a unique role of ionic strength. AIChE journal 38, 153-157.

Shabanian, M., Khoobi, M., Hemati, F., Khonakdar, H.A., Faghihi, K., Wagenknecht, U., ebrahimi, S.e.S., Shafiee, A., 2015. Effects of polyethyleneimine-functionalized MCM-41 on flame retardancy and thermal stability of polyvinyl alcohol. Particuology 19, 14-21.

Shakerian, F., Kim, K.-H., Kwon, E., Szulejko, J.E., Kumar, P., Dadfarnia, S., Haji Shabani, A.M., 2016. Advanced polymeric materials: Synthesis and analytical application of ion imprinted polymers as selective sorbents for solid phase extraction of metal ions. TrAC Trends in Analytical Chemistry 83, Part B, 55-69.

Sharma, N.K., Singh, M., Bhattarai, A., 2016. Hydrophobic study of increasing alkyl chain length of platinum surfactant complexes: synthesis, characterization, micellization, thermodynamics, thermogravimetrics and surface morphology. RSC Advances 6, 90607-90623.

Shubair, T., Eljamal, O., Khalil, A.M.E., Matsunaga, N., 2018. Multilayer system of nanoscale zero valent iron and Nano-Fe/Cu particles for nitrate removal in porous media. Separation and Purification Technology 193, 242-254.

Simons, W.W., Laboratories, S.R., 1978. The Sadtler Handbook of Infrared Spectra. Sadtler.

Singh, N.B., Nagpal, G., Agrawal, S., Rachna, 2018. Water purification by using Adsorbents: A Review. Environmental Technology & Innovation 11, 187-240.

Smith, D.W., 1977. Ionic hydration enthalpies. Journal of Chemical Education 54, 540.

Song, X., Li, L., Geng, Z., Zhou, L., Ji, L., 2017. Effective and selective adsorption of As(III) via imprinted magnetic Fe3O4/HTCC composite nanoparticles. Journal of Environmental Chemical Engineering 5, 16-25.

Sowmya, A., Meenakshi, S., 2013. An efficient and regenerable quaternary amine modified chitosan beads for the removal of nitrate and phosphate anions. Journal of Environmental Chemical Engineering 1, 906-915.

Sowmya, A., Meenakshi, S., 2014. A novel quaternized chitosan–melamine–glutaraldehyde resin for the removal of nitrate and phosphate anions. International Journal of Biological Macromolecules 64, 224-232.

Taghizadeh, M., Hassanpour, S., 2017. Selective adsorption of Cr(VI) ions from aqueous solutions using a Cr(VI)-imprinted polymer supported by magnetic multiwall carbon nanotubes. Polymer 132, 1-11.

Vasapollo, G., Sole, R.D., Mergola, L., Lazzoi, M.R., Scardino, A., Scorrano, S., Mele, G., 2011. Molecularly Imprinted Polymers: Present and Future Prospective. International Journal of Molecular Sciences 12, 5908-5945.

Vatanpour, V., Madaeni, S.S., Zinadini, S., Rajabi, H.R., 2011. Development of ion imprinted technique for designing nickel ion selective membrane. Journal of Membrane Science 373, 36-42.

Wagner, C.D., Muilenberg, G.E., 1979. Handbook of X-ray Photoelectron Spectroscopy: A Reference Book of Standard Data for Use in X-ray Photoelectron Spectroscopy. Perkin-Elmer.

Wan, Y., Peppley, B., Creber, K.A.M., Bui, V.T., 2010. Anion-exchange membranes composed of quaternized-chitosan derivatives for alkaline fuel cells. Journal of Power Sources 195, 3785-3793.

Wang, F., Liu, P., Nie, T., Wei, H., Cui, Z., 2013a. Characterization of a Polyamine Microsphere and Its Adsorption for Protein. International Journal of Molecular Sciences 14, 17.

Wang, J., Li, Z., 2015. Enhanced selective removal of Cu(II) from aqueous solution by novel polyethylenimine-functionalized ion imprinted hydrogel: Behaviors and mechanisms. Journal of Hazardous Materials 300, 18-28.

Wang, W.-S., Li, Y.-B., Gao, B.-J., Huang, X.-W., Zhang, Y.-Q., Xu, Y., An, F.-Q., 2013b. Effective removal of Fe(II) impurity from rare earth solution using surface imprinted polymer. Chemical Engineering Research and Design 91, 2759-2764.

Wang, Z., Wu, G., He, C., 2009. Ion-imprinted thiol-functionalized silica gel sorbent for selective separation of mercury ions. Microchimica Acta 165, 151-157.

Wu, G., Song, G., Wu, D., Shen, Y., Wang, Z., He, C., 2010. Synthesis of ion-imprinted mesoporous silica gel sorbent for selective adsorption of copper ions in aqueous media. Microchimica Acta 171, 203-209.

Wu, L., Wang, H., Lan, H., Liu, H., Qu, J., 2013. Adsorption of Cu(II)–EDTA chelates on tri-ammonium-functionalized mesoporous silica from aqueous solution. Separation and Purification Technology 117, 118-123.

Wu, P., Zhou, Y.-s., 2009. Simultaneous removal of coexistent heavy metals from simulated urban stormwater using four sorbents: A porous iron sorbent and its mixtures with zeolite and crystal gravel. Journal of Hazardous Materials 168, 674-680.

Wu, Y., Wang, Y., Wang, J., Xu, S., Yu, L., Philippe, C., Wintgens, T., 2016. Nitrate removal from water by new polymeric adsorbent modified with amino and quaternary ammonium groups: Batch and column adsorption study. Journal of the Taiwan Institute of Chemical Engineers 66, 191-199.

Xu, X., Gao, B., Yue, Q., Li, Q., Wang, Y., 2013. Nitrate adsorption by multiple biomaterial based resins: Application of pilot-scale and lab-scale products. Chemical Engineering Journal 234, 397-405.

Xu, Z., Deng, P., Li, J., Tang, S., 2018. Fluorescent ion-imprinted sensor for selective and sensitive detection of copper (II) ions. Sensors and Actuators B: Chemical 255, 2095-2104.

Yun, H.-J., Hong, H., Lee, J., Choi, C.-J., 2014. Chemical and Structural Properties of Polyethyleneimine Film Coated on a SiO2 Substrate in Different Concentrations. MATERIALS TRANSACTIONS 55, 801-805.

Zhang, N., Hu, B., 2012. Cadmium (II) imprinted 3-mercaptopropyltrimethoxysilane coated stir bar for selective extraction of trace cadmium from environmental water samples followed by inductively

coupled plasma mass spectrometry detection. Analytica Chimica Acta 723, 54-60.

Zhang, N., Hu, B., Huang, C., 2007. A new ion-imprinted silica gel sorbent for on-line selective solid-phase extraction of dysprosium(III) with detection by inductively coupled plasma-atomic emission spectrometry. Analytica Chimica Acta 597, 12-18.

Zheng, H., De, Z., Wang, W.Y., Fan, Y.Q., Li, J., Han, H.P., 2007. Highly selective determination of palladium(II) after preconcentration using Pd(II)-imprinted functionalized silica gel sorbent prepared by a surface imprinting technique. Microchimica Acta 157, 7-11.

Zheng, H., Yang, S., Wang, J., Sun, W., 2011. Highly selective determination of rhodium(III) using silica gel surface-imprinted solid-phase extraction. International Journal of Environmental Analytical Chemistry 91, 1013-1023.

Zhu, X., Cui, Y., Chang, X., Zou, X., Li, Z., 2009. Selective solid-phase extraction of lead(II) from biological and natural water samples using surface-grafted lead(II)-imprinted polymers. Microchimica Acta 164, 125-132.

국문초록

본 논문에서는 구리 각인된 메조포러스 실리카 SBA-15 와 실리카 겔을 합성하고 특성을 분석하는 한편, 구리에 대한 선택적인 흡착특성을 살펴보았다. 또한 질산이온에 대한 선택성이 증진된 사급암모늄으로 기능화된 메조포러스 실리카 SBA-15 와 실리카 겔을 합성하고 특성을 분석하는 한편, 질산이온에 대한 선택적인 흡착특성을 살펴보았다.

구리가 표면각인된 poly(ethyleneimine) (PEI)가 접목된 메조포러스 실리카 SBA-15 (Cu-imprinted PEI-SBA-15)를 합성하였다. 이때 Cu-imprinted PEI-SBA-15 의 준비과정에서 구리가 PEI-SBA-15 에 부하되는 양을 증진시키기 위하여 염소이온과 구리간의 몰비를 증진시켜 부하를 수행하였다. 그 후 구리가 흡착된 지점에 대한 가교와 흡착된 구리의 탈착을 통하여 Cu-loaded PEI-SBA-15 를 준비하였다. $[Cl^-]/[Cu(II)]$가 2 에서 1000 인 조건에서 합성한 Cu-loaded PEI-SBA-15 를 활용하여 구리에 대한 선택성 실험을 수행하였다. Cu(II), Pb(II), Zn(II), Ni(II), Co(II)와 같은 2 가의 이온들이 동시에 존재하는 조건에서 선택성 실험을 수행한 결과 Cu(II)에 대한 선택도는 $[Cl^-]/[Cu(II)]$가 500 인 조건에서 최대였으며, 79.62 의 값을 보였다. PEI-SBA-15 대비하여 Cu-imprinted PEI-SBA-15 의 Cu(II)에 대한 상대적 선택도는 29.24 이었다. Cu(II), Al(III), Cr(III), Zr(IV)와 같은 구리와 다른 3, 4 가의 이온들이 동시에 존재하는 조건에서 선택성

실험을 수행한 결과 Cu(II)에 대한 선택도는 [Cl^-]/[Cu(II)]가 500 인 조건에서 최대였으며, 3.40 의 값을 보였다. PEI-SBA-15 대비하여 Cu-imprinted PEI-SBA-15 의 Cu(II)에 대한 상대적 선택도는 3.96 이었다. 이를 통하여 구리 각인된 SBA-15 의 준비과정에서 높은 [Cl^-]/[Cu(II)] 조건하에서 수행됨에 따라 의 구리에 대한 선택성이 증진될 수 있음을 확인하였다.

구리가 표면 각인된 PEI 피복 실리카 겔 (Cu-PEI-silica gel)을 합성하였다. Cu-PEI-silica gel 은 PEI 피복 실리카 겔(PEI-silica gel)의 합성과정에서 구리의 부하과정을 추가하는 간단한 방법을 통하여 수행하였다. 배치실험을 통하여 구리에 대한 흡착능을 확인해본 결과 Cu-PEI-silica gel 이 352.540 mg/g 의 흡착능을 보였으며 PEI-silica gel 의 경우 30.727 mg/g 의 흡착능을 보였다. Cu(II), Pb(II), Zn(II), Ni(II), Co(II)와 같은 2 가의 이온들이 동시에 존재하는 조건에서 선택성 실험을 수행한 결과, 5.17 의 Cu(II)에 대한 상대적 선택도를 보였다. Cu(II), Al(III), Cr(III), Zr(IV)와 같은 구리와 다른 3, 4 가의 이온들이 동시에 존재하는 조건에서 선택성 실험을 수행한 결과 3.06 의 Cu(II)에 대한 상대적 선택도를 보였다. 이를 통하여, PEI-silica gel 의 합성과정에서 구리의 부하과정을 추가하는 간단한 방법을 바탕으로 구리에 대한 흡착능과 선택성이 증진된 Cu-PEI-silica gel 을 합성할 수 있음을 확인하였다.

다양한 알킬사슬 길이를 지닌 사급 암모늄 기능화된 SBA-15 를 합성하고 이의 물리화학적 특성을 살펴보았다. 또한 이를 활용하여 질산이온에 대한 흡착특성을 살펴보았다. 배치실험을 통한 실험결과 더 긴 길이의 알킬사슬을 지닐수록 질산이온에 대한

흡착속도가 느려지나 흡착능과는 큰 관계를 보이지 않았다. 경쟁이온 실험 결과, 알킬사슬이 길수록 질산이온을 더욱 선택적으로 제거하였다. 이는 질산이온이 다른 경쟁이온에 비하여 가장 큰 값의 수화 에너지를 가지고 있으며, 알킬사슬이 길수록 덜 수화되는 경향에서 기인한다. 따라서 알킬사슬이 긴 사급 암모늄 기능화된 SBA-15 가 질산이온을 선택적으로 제거할 수 있다. 또한 질산이온의 선택적 제거에 있어 인산이온의 영향이 가장 컸으며 염소이온의 영향이 가장 적었다. 이를 통하여 다양한 알킬사슬 길이를 지닌 사급 암모늄 기능화된 메조다공성 실리카가 잘 합성되었음을 확인하였으며 알킬사슬 길이에 의한 질산이온에 대한 선택적 제거특성을 확인 할 수 있었다.

dimethyloctyl alkyl chain 과 dimehtyldodecyl alkyl chain 의 사급암모늄으로 기능화된 실리카겔 (C8Q-silica gel, C12Q-slica gel)을 합성하고 이의 물리화학적 특성을 살펴보았다. 또한 배치실험과 칼럼실험을 통하여 질산이온에 대한 흡착특성을 살펴보았다. 실험 결과 C12Q-slica gel 이 질산이온을 선택적으로 제거하는데 더 적합한 흡착제로 판단하였다. 칼럼실험에서, 초기 질산이온 농도, 유량, 칼럼의 길이 등의 영향을 살펴보았다. 그 결과, Bohart-Adams 와 bed depth service time 모델이 흐름조건에서 질산이온을 제거하는 것을 표현하는데 적합한 모델로 판단되었다. 인공지하수를 바탕용액으로 하여 칼럼실험을 수행한 결과, 중탄산이온이 추가된 경우에도 C12Q-silica gel 를 통하여 질산이온을 선택적으로 제거할 수 있었다. 2 회의 재생후에도 파과곡선이 유지됨을 확인할 수 있었다. 이를 통하여

사급암모늄으로 기능화된 실리카 겔이 잘 합성되었음을 확인하였으며 흐름 조건에서의 질산이온에 대한 제거특성을 확인하였다.

본 연구에서는 다양한 실험들을 통하여 수중 오염물질의 선택성이 증진된 흡착제를 개발하여 이의 선택적 흡착특성을 살펴보았다. 또한 개발된 흡착제의 수처리에 대한 적용 가능성을 확인하였다. 본 연구 결과를 통해 선택성이 증진된 흡착제의 제조 및 이를 통해 선택적 제어가 증진된 수처리에 활용할 수 있을 것으로 기대된다.

주요어: 선택적 흡착제, 이온 각인, 표면 이온 각인, 사급암모늄 기능화, 알킬사슬 길이, 선택적 제거, 구리, 질산이온

학번: 2013-30343